Improving estimates of net ecosystem CO_2 exchange between the Arctic land surface and the atmosphere

by

Kristina A. Luus

A thesis
presented to the University of Waterloo
in fulfillment of the
thesis requirement for the degree of
Doctor of Philosophy
in
Geography and Earth Sciences

Waterloo, Ontario, Canada, 2013

I hereby declare that I am the sole author of this thesis. This is a true copy of the thesis, including any required final revisions, as accepted by my examiners.

I understand that my thesis may be made electronically available to the public.

Abstract

Feedbacks between the climate system and the high-latitude carbon cycle will substantially influence the intensity of future climate change. It is therefore crucial that the net ecosystem exchange of CO_2 (NEE) between the high-latitude land surface and the atmosphere is accurately quantified, where NEE refers to the difference between ecosystem respiration (R) and photosynthesis (gross ecosystem exchange, GEE): $NEE = -GEE + R$ in μmol/m^2/s. NEE can only be directly measured over areas of $\approx$1 km^2 through eddy covariance, and modeling approaches such as the Vegetation Photosynthesis Respiration Model (VPRM) are required to upscale NEE. VPRM is a remote sensing based model that calculates R as a linear function of air temperature (T_a) when air temperature is above a given threshold (T_{low}), and sets respiration to a constant value when $T_a < T_{low}$. GEE is estimated according to remote sensing observations of vegetation indices, shortwave radiation, air temperature, and soil moisture. Although *in situ* findings have shown that snow and Arctic species composition have a substantial influence on high-latitude NEE, model estimates of high-latitude NEE have typically been generated without Arctic-specific vegetation classes, and without using remote sensing observations to represent the effects of snow on NEE. The hypothesis driving this work was therefore that uncertainty in estimates of high-latitude NEE could be reduced by representing the influences of Arctic vegetation classes and snow. The central objectives were to determine feasible approaches for reducing uncertainty in VPRM estimates of NEE by representing the influences of snow and Arctic vegetation, create PolarVPRM accordingly, and analyze inter-annual variability in PolarVPRM estimates of high-latitude North American NEE (2001–2012).

The associations between snow and NEE, and the potential to describe these influences on NEE using remote sensing observations, were examined using time lapse camera observations of snow cover area (SCA) and eddy covariance measurements of NEE from Daring Lake, Northwest Territories, Canada. Analyses indicated good agreement between SCA derived from camera, Landsat and Moderate Resolution Imaging Spectroradiometer (MODIS) observations. SCA was also found to influence the timing and magnitude of NEE. MODIS SCA was therefore incorporated into VPRM, and VPRM was calibrated using eddy covariance and meteorological observations collected in 2005 at Daring Lake. VPRM was run through years 2004–2007 over both Daring Lake and Ivotuk, Alaska, USA, using four model formulations, three of which represented the effects of SCA on respiration and/or photosynthesis, and another which did not use MODIS SCA. Comparisons against eddy covariance observations indicated that uncertainty was reduced in VPRM estimates of NEE when respiration was calculated as a linear function of soil temperature when SCA$\geq$50%, and as a linear function of air temperature when SCA$<$50%, thereby reflecting the influence of snow on decoupling soil/air temperatures. Representing the effect of SCA on NEE therefore reduced uncertainty in VPRM estimates of NEE.

In order to represent spatial variability in high-latitude estimates of NEE due to vegetation type, Arctic-specific vegetation classes were created for PolarVPRM by combining and aggregating two existing vegetation classifications: the Synergetic Land Cover Product and the Circumpolar Arctic Vegetation Map. Levene's test indicated that the PolarVPRM vegetation classes divided the pan-Arctic region into heterogeneous distributions in terms of net primary productivity, and passive microwave derived estimates of snow and growing season influences on NEE. A non-parametric statistical approach of Alternating Conditional Expectations found significant, non-linear associations to exist between passive microwave derived estimates of snow and growing season drivers of NEE. Furthermore, the shape of these associations varied according to the vegetation class over which they were examined. Further support was therefore provided to the idea that uncertainty in model estimates of NEE could be reduced by calculating snow and growing season NEE separately within each vegetation class.

PolarVPRM estimates of NEE in 2001–2012 were generated at a three hourly and $\frac{1}{6}^{\circ} \times \frac{1}{4}^{\circ}$ resolution across polar North America (55–170°W, 55–83°N). Model calibration was conducted over three sites: Daring Lake, Ivotuk, and Atqasuk, Alaska, USA. Model validation was then conducted by comparing PolarVPRM estimates of year-round daily average NEE to non-gap-filled eddy covariance observations of daily average NEE acquired over the three calibration sites, as well as six other Arctic sites. PolarVPRM performed well over all sites, with an average mean absolute error (MAE) of 0.20 μmol/m^2/s, and had diminished error rates when the influence of SCA on respiration was explicitly represented. Error analysis indicated that peak growing season GEE was underestimated at Barrow because GEE at this site showed a stronger response to the amount of incoming shortwave radiation than at the calibration site, suggesting that PolarVPRM may underestimate GEE over wetland and barren vegetated regions. Despite these uncertainties, PolarVPRM was found to generate more accurate estimates of mean monthly and daily NEE relative to eddy covariance observations than two established models, FLUXNET Model-Tree Ensemble (MTE) and CarbonTracker. Relative to eddy covariance observations and PolarVPRM estimates, MTE tended to overestimate snow season respiration, and CarbonTracker tended to overestimate the amount of midday photosynthesis. Analysis of PolarVPRM output across North America (north of 55° N) found an increase in net annual carbon efflux over over time (2001–2012). Specifically, increased rates of respiration are estimated when soil and air temperatures are warmer. Although increases in growing season vegetation indices and air temperature enable greater photosynthetic uptake by Arctic vegetation, forests and shrublands uptake less CO_2 in the middle of the growing season when air temperatures rise above the physiological optima for photosynthesis. As a result, PolarVPRM estimated a decline in net photosynthetic uptake over time. Overall, PolarVPRM output indicates that North American regions north of 55°N are losing strength as a carbon sink in response to rising air temperatures.

Acknowledgements

First and foremost, I would like to thank my incredible co-supervisors, Drs. John Lin and Richard Kelly, for sharing their passion for research with me, and for helping me learn to become a researcher. Thank you for supporting me through every challenge with wisdom and enthusiasm. Thank you also to my amazing committee members, Drs. Claude Duguay and Yulia Gel, for providing insightful suggestions throughout my PhD. Thank you to Dr. Sharon Cowling for being a wonderful external examiner. Thank you also to my generous collaborators, Drs. Elyn Humphreys, Peter Lafleur and Walter Oechel, and professors Drs. Alexander Brenning, Michael English and Roland Hall for their greatly valued input and assistance.

I would like to acknowledge the many researchers and field assistants of the Canadian Carbon Program, Ameriflux and Fluxnet for providing valuable eddy covariance and meteorological measurements. Similarly, thank you to the researchers who created and allowed access to the following remote sensing products: AMSR-E land surface parameter, CAVM, CarbonTracker, FLUXNET Model-Tree Ensemble, GlobSnow, GloPEM, Landsat, MOD09A1, MOD10A1, MOD13A1, and NARR. Thank you also to the creators and developers of R and R libraries.

I would like to thank the employees at SHARCNET, IST and the ENV MAD lab for maintaining reliable computing resources on campus. Funding from NSERC in the form of a Vanier Canadian Graduate Scholarship is also gratefully acknowledged. Finally, I would like to thank my friends and family for encouraging me throughout my graduate studies.

Table of Contents

List of Tables

List of Figures

Preface

The thesis presented here has been formatted according to the University of Waterloo's Guidelines for the Manuscript Option, PhD in Geography. Chapters 2, 3, 4 and 5 therefore represent four distinct manuscripts, three of which have been published or submitted to refereed journals. All four papers build sequentially on the central objective of improving estimates of net ecosystem CO_2 exchange between the high-latitude land surface and atmosphere.

- KA Luus, JC Lin, REJ Kelly and CR Duguay (2013). Subnivean Arctic & sub-Arctic net ecosystem exchange (NEE): Towards representing snow season processes in models of NEE using cryospheric remote sensing. *Progress in Physical Geography*. [Chapter 2].
- KA Luus, REJ Kelly, JC Lin, ER Humphreys, P Lafleur and WC Oechel (In Review). Modeling the influence of snow cover on low Arctic net ecosystem exchange. *Environmental Research Letters Special Issue on Cryospheric Ecosystems*. [Chapter 3].
- KA Luus, Y Gel, JC Lin, REJ Kelly and CR Duguay (2013). Pan-Arctic linkages between snow accumulation and growing season air temperature, soil moisture & vegetation. *Biogeosciences Discussions*, 10, 1747-1791. Under review for publication in *Biogeosciences*. [Chapter 4].
- KA Luus, JC Lin, REJ Kelly, et al. (In Preparation). PolarVPRM: A remote sensing based model for estimating high-latitude net ecosystem CO_2 exchange. [Chapter 5].

The research presented here was conducted and written primarily by K.A. Luus, and was made possible by the guidance and assistance of Professors C.R. Duguay, Y. Gel, E.R. Humphreys, R.E.J. Kelly, P. Lafleur, J.C. Lin and W.C. Oechel. Preliminary versions of Chapters 3, 4 and 5 were presented at three refereed conferences: *Luus et al.* (2011), *Luus et al.* (2010a) and (*Luus et al.*, 2012), respectively.

Plain language summary

Rising atmospheric concentrations of carbon dioxide (CO_2) are causing the Earth's temperature to rise. Presently, enormous amounts (1.4×10^15 kg) of carbon are stored below-ground in Arctic regions, and it is likely that future atmospheric concentrations of CO_2 and global temperatures will rise due to the natural releases of carbon from below-ground into the atmosphere. It is therefore important to keep track of the net ecosystem exchange (NEE) of CO_2 between the Arctic land surface and the atmosphere, and understand its responses to climate change. Researchers can measure atmospheric concentrations of CO_2 across the entire Arctic using satellite observations, but NEE can only be measured directly using towers which are expensive and time consuming to keep running. Models are therefore needed to generate estimates of NEE across regions, but these models tend to have large uncertainties. The objective of this thesis was to reduce uncertainty in model estimates of Arctic NEE.

Recent studies have shown that snow influences the rate and timing of soil respiration in Arctic regions, and that satellite observations can provide good estimates of the timing of snowfall and snowmelt. Satellite observations of snow were therefore included in a model of NEE, and these observations were used to help reduce error in snow season estimates of respiration. Representing these influences therefore means that we might get better estimates of NEE, and we might also get new insights into the Arctic carbon cycle. We were therefore curious about what linkages exist between snow and growing season influences on NEE. In other words, do areas that tend to have conditions more conducive to photosynthesis also receive more snow, which is conducive to greater rates of respiration? We studied these non-linear associations and found highly variable associations which varied by vegetation class. For example, forested sites with more vegetation and colder summer temperatures tend to accumulate more snow, whereas the opposite is true over tundra regions. It is clear, then, that including both snow and growing season influences on NEE is likely to improve model estimates.

PolarVPRM was then developed to estimate NEE in northern regions, using Arctic-specific vegetation classes and representing the influences of both snow and growing season processes on NEE. We checked how well this model fit against tower observations of NEE, carried out a mathematical analysis of model errors, and looked at how PolarVPRM estimates of NEE compared against other models. Since these indicated that PolarVPRM performed well, we then looked at what PolarVPRM could tell us about how NEE had changed over time between 2001–2012. Over time, it appears that regions north of the treeline are releasing more CO_2, and that forested regions are uptaking less CO_2 through photosynthesis.

Chapter 1

Introduction

1.1 Motivation

Carbon dioxide (CO_2) is a long-lived greenhouse gas whose global emissions have increased by 80% (21 to 38 Gt CO_2/yr) between 1970-2004 (*Solomon et al.*, 2007). Climate change has been found to both increase photosynthetic uptake of carbon by vegetation due to northward movements of the shrub and treelines (*Hinzman et al.*, 2005; *Tape et al.*, 2006), and to increase the amount of CO_2 and CH_4 released through soil respiration and permafrost thaw (*Tarnocai*, 2006). Pan-Arctic analyses of trends over time in vegetation and temperature indicated significant rises in air temperature, the normalized difference vegetation index (NDVI), and net uptake of carbon by vegetation (net primary productivity, NPP) Figure 1.1.

As noted by *Lafleur and Humphreys* (2008): "the extent to which winter CO_2 emissions may offset increased summer sequestration is not presently known. This is probably one of the most critical issues in arctic C balance research today". Not only is this issue critical within carbon balance research, but the carbon balance of northern ecosystems has widespread scientific and policy implications. High-latitude cryospheric soils presently contain between 1400 to 1850 Gt of organic carbon (*McGuire et al.*, 2010). To put this number in perspective, if 1400-1850 Gt C were theoretically to be instantaneously released into the atmosphere as CO_2, this would cause global concentrations of CO_2 to immediately triple, from ≈397 ppm (as of 03/12) to between 1060-1274 ppm. In the more realistic IPCC A1B emission scenario for 2200, permafrost thaw alone is predicted to cause a rise in atmospheric CO_2 concentrations of 87±29 ppm (*Schaefer et al.*, 2011).

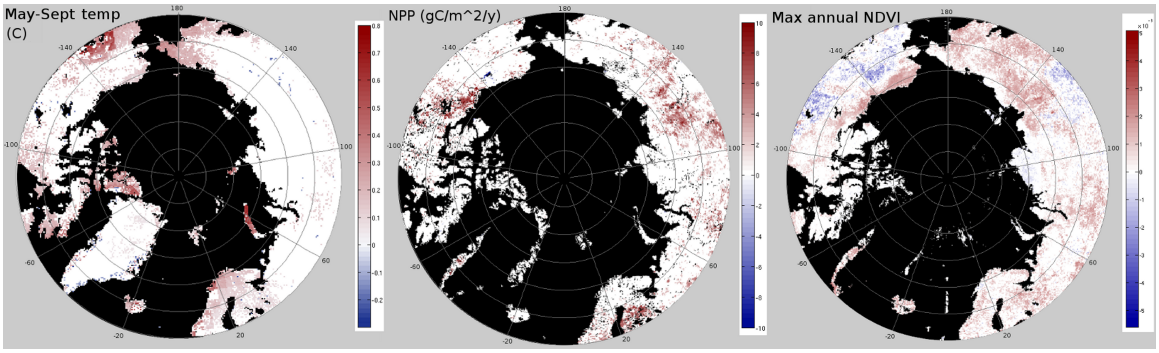

Figure 1.1: Trends over time (1982–2000) in pan-Arctic May–September APP-x temperature (left), GloPEM net primary productivity (centre) and GIMMS normalized difference vegetation index (right). The Sen's slope values are indicated only at locations showing significant (p-value<0.05) change over time. This figure represents an extension of the analysis provided in *Luus* (2009).

Accurate estimates of the land-atmosphere exchange of CO_2 through photosynthesis and respiration (net ecosystem exchange, or NEE) are therefore crucial, especially at high-latitudes. Substantial uncertainties exist regarding NEE across the Arctic and sub-Arctic land surfaces. Model estimates of Arctic and sub-Arctic NEE are poorly constrained, due to the scarcity of high-latitude observations of CO_2 exchange, and due to the fact that models do not represent Arctic-specific drivers of NEE. The question therefore arises: Could uncertainty in estimates of Arctic and sub-Arctic NEE be reduced through the development of a model that uses a remote sensing approach to explicitly represent Arctic vegetation classes and Arctic snow season drivers of NEE? If so, what might the implications of the model outputs be for our present understanding of the northern carbon cycle and its response to climate change?

1.2 Objectives

The central objective of this research was to improve scientific understanding of the high-latitude North American carbon cycle in terms of its present-day magnitude and drivers (2001–2012). This objective was accomplished by first reviewing recent literature to identify sources of uncertainty in high-latitude measurements and regional estimates of NEE, and suggesting strategies which could be used to reduce uncertainty in model estimates of NEE. Investigations indicated that over half of annual CO_2 efflux occurs during the

long snow season, but that no models to date had employed remote sensing observations to represent snow season influences on NEE. The motivation was therefore provided for improving model estimates accordingly.

The second objective was to reduce uncertainty in model estimates of high-latitude net ecosystem CO_2 exchange by representing snow season influences on NEE. The third objective was to examine the spatial associations between snow and growing season influences on NEE across Arctic vegetation classes, which provided the context and motivation necessary to represent Arctic vegetation and snow in a new model of NEE (PolarVPRM). The fourth objective was to generate improved model estimates of the North American carbon budget using PolarVPRM. PolarVPRM was first evaluated over two validation sites along with two established models, and findings indicated that PolarVPRM had the lowest errors over these sites. Since these model estimates showed reduced uncertainty relative to field observations, trends over time in PolarVPRM output and drivers (2001–2012) were analyzed to understand the recent response of the high-latitude North American carbon cycle to changing climate conditions.

1.3 Organization

Chapter 2 examines the suitability of various cryospheric remote sensing observations and products for inclusion in models of NEE, and provides recommendations of how carbon models might incorporate remote sensing observations of snow. One direction which is described as especially promising is the use of visible and infrared observations of fractional snow cover to determine the start and end of the snow season, and the rate of snow onset and depletion. Another promising research direction involved estimating snow season respiration as a function of snow accumulation. Although preliminary analysis indicated that this strategy might be feasible, it also revealed that this approach might introduce substantial uncertainties into model estimates due to the coarse resolution of remote sensing observations of snow accumulation (25 km) and the lack of snow accumulation measurements at eddy covariance sites (*Luus et al.*, 2010b).

The potential for remote sensing observations of fractional snow cover to be incorporated into models of NEE is therefore assessed in Chapter 3. Analyses indicated that associations existed between NEE and snow cover area which could be well described using remote sensing observations. Uncertainty in VPRM estimates of NEE at paired calibration and validation sites was reduced by including remote sensing observations of fractional snow cover, and estimating growing season and snow season respiration as functions of air and soil temperature, respectively.

These results therefore indicated the possibility that regional estimates of polar NEE may be improved by representing fractional snow cover area, and underscored a common finding in published studies [Chapter 2] that the carbon balance itself is altered by inter-connected changes in snowpack dynamics and in the factors determining growing season uptake of CO_2 (quantity of vegetation, soil moisture and air temperature). A non-parametric statistical technique was used to assess the non-linear linkages between satellite passive microwave observations of pan-Arctic snow accumulation and growing season land surface properties (air temperature, soil moisture and vegetation) [Chapter 4]. These linkages were analyzed within seven pan-Arctic vegetation classes, defined by combining two established vegetation classifications and aggregating similar vegetation types.

Briefly, within each vegetation class, regions with greater aboveground biomass, wetter soils and warmer air temperature tend to have less snow at the start and end of the snow season, likely due to the effects of interception, sublimation and melt. Mean growing season air temperature and biomass are both inversely associated with snow accumulation in forested sites, but directly associated with snow accumulation over Arctic tundra regions with $<$75 mm of snow water equivalent. Interconnections between the drivers of snow and growing season NEE, and the possibility of observing linkages in coarse, pan-Arctic observations that agree with locally observed thresholds and interactions underlines the complexity of the cryosphere-atmosphere-biosphere system. As a result of this complexity, it is likely that model estimates of high-latitude NEE could be improved by calculating snow and growing season NEE separately within each vegetation class.

PolarVPRM estimates of pan-Arctic NEE were therefore generated using the vegetation classes established in Chapter 4, and the influences of snow on NEE described in Chapter 3. Model evaluation indicated that PolarVPRM generated estimates of NEE with good agreement against eddy covariance derived observations of NEE, and against previous modeling approaches[1]. PolarVPRM estimates of high-latitude North American NEE (55–83°N) showed increases over time (2001–2012) in respiration over tundra regions, and declines in the rate of photosynthetic uptake by vegetation over forested regions. These changes in NEE occurred due to warming air/soil temperatures and declines in vegetation indices, and account for a substantial decline in the net uptake of carbon by northern ecosystems. The main contributions of this thesis were therefore in reviewing snow season influences on NEE, describing the non-linear linkages between snow and growing season

[1]The eddy covariance technique is an established approach for collecting representative observations of land-atmosphere NEE at a high temporal resolution over $\approx$1 km^2 areas. Although noise and uncertainty exist in eddy covariance derived calculations of of NEE (as discussed in section 2.3), these are commonly used as standard estimates of NEE. Likewise, in this thesis, eddy covariance observations represent the standard against which model uncertainty and improvements are described.

drivers of NEE, establishing and implementing a remote sensing based approach for representing the influence of snow on NEE, and analyzing the implications of this model output for our current understanding of the high latitude North American carbon budget and its responses to recent climate change.

Chapter 2

Subnivean Arctic & sub-Arctic net ecosystem exchange (NEE): Towards representing snow season processes in models of NEE using cryospheric remote sensing

Overview

In the Arctic and sub-Arctic, up to half of annual net ecosystem exchange (NEE) occurs during the snow season. Subnivean soil respiration can persist at a greater rate when the overlying snowpack has a lower thermal conductivity, and the rate of photosynthetic uptake at the start and end of the snow season can be diminished by fractional snow cover. Although recent studies have indicated that uncertainty in model estimates of NEE can be reduced by representing the influence of a modeled snowpack on soil respiration, models of NEE have not represented the influence of snowpack dynamics on processes such subnivean photosynthesis or CO_2 diffusivity, and have not used remote sensing observations to characterize snow season processes. We therefore: 1) review snow season processes and their effects on NEE; 2) assess the suitability of cryospheric remote sensing approaches for models of NEE; and 3) suggest strategies for representing snow season processes in models of NEE. Satellite visible and infrared remote sensing observations of fractional snow cover in spring and fall could be used to restrict estimates of photosynthetic uptake in models of NEE while snow is present. Passive and active microwave observations of snow accumulation and soil freeze/thaw from satellites could be combined with observations of air temperature to generate more realistic estimates of soil temperature and soil respiration. Satellite altimeter or airborne LiDAR observations of snow depth could be used to estimate the influence of snow accumulation and tree wells on soil respiration. Including remote sensing observations of snow properties in models of NEE could therefore reduce uncertainty in snow season estimates of NEE, resulting in a better understanding of the northern carbon cycle. Furthermore, process-based simulations of snow season NEE could enable an improved understanding of how the northern carbon cycle is responding to climate driven changes in the interconnected biospheric, atmospheric and cryospheric systems.

2.1 Introduction

Anthropogenic emissions have the potential to increase global atmospheric concentrations of CO_2 to twice the preindustrial level by approximately 2100, which is predicted to cause warming of high-latitude regions (*Christensen et al.*, 2012). Concern exists that climate change is likely to be amplified through positive climate-carbon-cycle feedbacks (*Cox et al.*, 2000; *Friedlingstein et al.*, 2001), such as the biospheric release of CO_2 and CH_4 from thawing permafrost (*Tarnocai*, 2006). Northern cryospheric soils currently contain 1400-1850 Pg stores of organic carbon (*McGuire et al.*, 2010) which, if all released into the atmosphere as CO_2, would theoretically equate to an increase of 666-880 ppm in global atmospheric concentrations. Simulations using the Intergovernmental Panel on Climate Change A1B emission scenario for 2200 indicate that permafrost thaw could increase atmospheric concentrations of CO_2 by 87 ± 29 ppm (*Schaefer et al.*, 2011). As permafrost thaws, a portion of the increase in CO_2 efflux is predicted to be offset by greater uptake of carbon by vegetation, although uncertainty exists regarding the magnitude of the biospheric response to warming and the time period over which it will persist (*Cramer et al.*, 2001; *Euskirchen et al.*, 2006), partially due to the complexity of the predicted response of high-latitude net ecosystem exchange to rising atmospheric concentrations of CO_2 [Figure 2.1].

Models provide local to global scale estimates of the land-atmosphere exchange of carbon based on locally observed associations between carbon cycling, meteorological conditions and land surface characteristics. The modeling approach used to generate estimates of carbon cycling can be described as either process-based or remote sensing based, where process based models predominantly represent interacting physical processes and remote sensing based models rely on spatial observations of the land surface (*Cramer et al.*, 1999). Several components of the land-atmosphere exchange of carbon can be estimated using these models, including Net Primary Productivity (NPP), Net Ecosystem Exchange (NEE) and Net Ecosystem Productivity (NEP) (*Cramer et al.*, 1999). NPP refers to the net carbon uptake by vegetation in , and is equal to the total carbon fixed by photosynthesis (Gross Primary Productivity, GPP) minus the carbon returned as CO_2 to the atmosphere during vegetation growth and maintenance respiration (Autotrophic Respiration, R) (*Bonan*, 2002):

$$NPP = GPP - R_{\mathrm{a}} \tag{2.1}$$

In terrestrial ecosystems, NEE refers to the instantaneous vertical flux of CO into and out of an ecosystem in which occurs primarily through processes such as photosynthesis and respiration. Terrestrial NEE is equal to total carbon fixed by photosynthesis

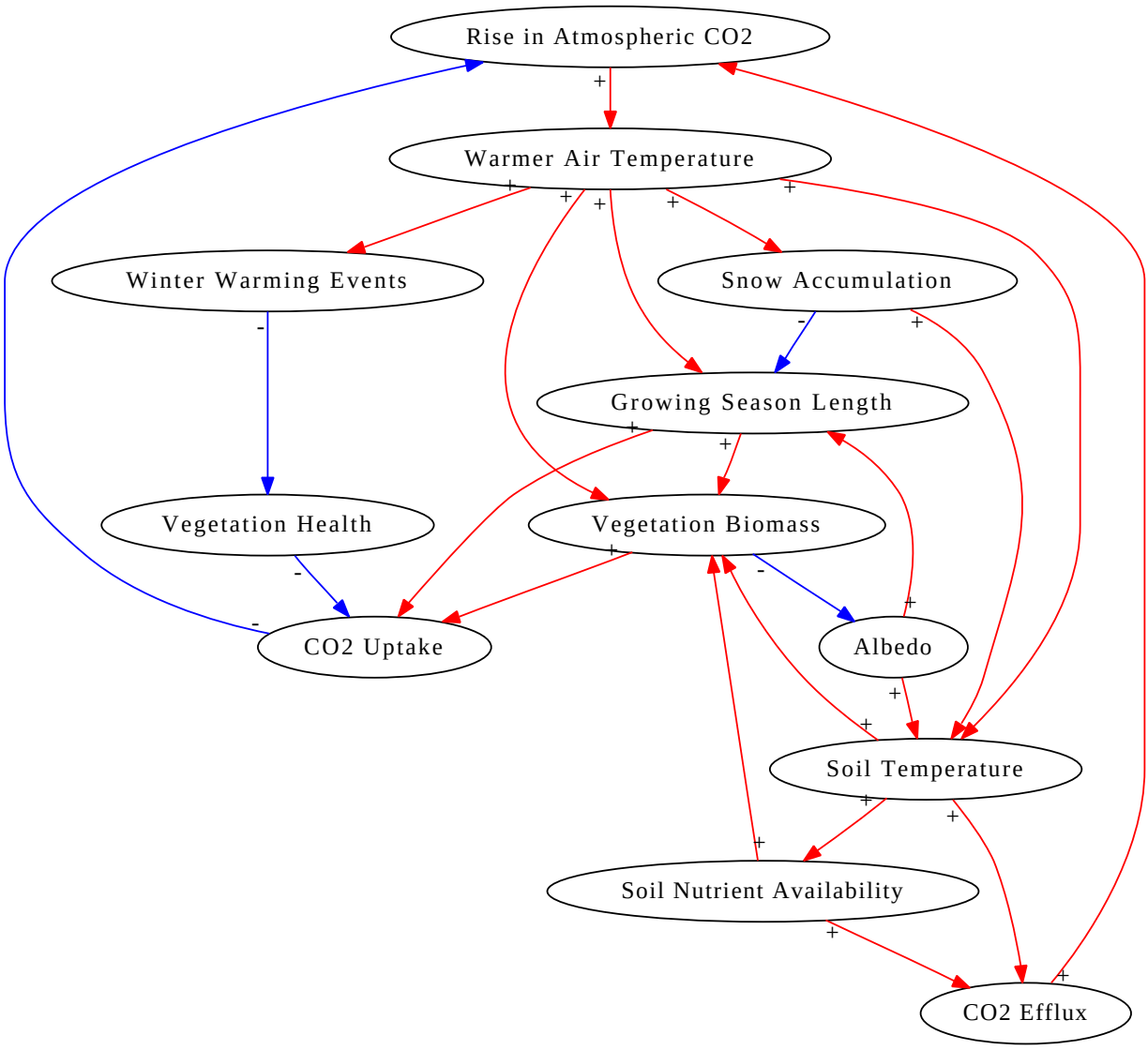

Figure 2.1: Flowchart representing how polar net ecosystem exchange is predicted to respond to rising levels of atmospheric CO_2 and subsequent warming. Warming-induced increases are indicated in red (+), and decreases are indicated in blue (-).

minus autotrophic respiration and carbon loss through soil organic matter decomposition by microorganisms (Heterotrophic Respiration, H_R). Calculations of NEE do not include

inorganic sources and sinks of CO_2 (e.g., precipitation and weathering) which can be substantial in aquatic ecosystems but are minimal in terrestrial ecosystems. Therefore, when gaseous fluxes of CH_4, lateral fluxes of dissolved organic carbon and dissolved inorganic carbon are minimal, terrestrial NEE is equal in magnitude to NEP, but with a sign reversal to reflect the fact that NEE is negative when CO_2 is removed from the atmosphere (*Lovett et al.*, 2006):

$$-NEE = NEP = GPP - R_{\mathrm{a}} - R_{\mathrm{h}} = NPP - R_{\mathrm{h}} \tag{2.2}$$

Recent Arctic and sub-Arctic field studies of NEE have indicated that the snow season accounts for up to 50% of annual CO_2 efflux at sub-Arctic (*Aurela et al.*, 2004; *Zimov et al.*, 1996), low Arctic (*Mikan et al.*, 2002; *Sullivan et al.*, 2008) and high Arctic (*Elberling and Brandt*, 2003) sites. Studies have also indicated that greater snow accumulation can encourage greater releases of CO_2 at sub-Arctic (*Larsen et al.*, 2007a), low Arctic (*Walker et al.*, 1999), and high Arctic (*Morgner et al.*, 2010) sites. The focus of this paper is on exploring the possibility that incorporating remote sensing observations of snow properties and their influence on NEE could reduce uncertainty in model estimates of Arctic and sub-Arctic NEE.

We begin by reviewing model estimates of snow season NEE [Section 2.2], and the sources of uncertainties in local and regional estimates of high-latitude NEE [Section 2.3]. Within this context, recent findings regarding the influence of snow on spatial [Section 2.4] and seasonal [Section 2.5] patterns in Arctic and sub-Arctic CO_2 fluxes are discussed, as well as the implications of these findings for modeling high-latitude NEE. Established approaches for remote sensing of snow are then reviewed. The advantages and limitations of each remote sensing approach are described in the context of how useful they may be for estimating the influence of snowpack dynamics on NEE [Section 2.6]. Suggestions are then provided on how to incorporate remote sensing observations into models of NEE [Section 2.6.6], followed by an outline of how the resulting models could be applied to assess the influence of climate-driven shifts in snow regimes on NEE [Section 2.7].

The central contribution of this paper is therefore in synthesizing recent findings regarding the influence of snow on spatial and temporal patterns in high-latitude NEE, and in providing a framework through which an appropriate remote sensing strategy can be selected for representing these processes when generating model estimates of Arctic and sub-Arctic NEE. The locations at which key *in situ* studies of Arctic and sub-Arctic snow season NEE were conducted are summarized in Table 2.1, and mapped in Figure 2.2.

Table 2.1: Locations of selected key in situ studies of snow-CO_2 interactions, classified as sub-Arctic, low Arctic and high Arctic according to (*Walker et al.*, 2005). Sub-Arctic sites indicated as transitional are considered to be south of the treeline by (*Walker et al.*, 2005), but are characterized by environmental conditions typical of low Arctic regions.

Site	Region	Latitude	Longitude	Snow-CO_2 research
S1	Sub-Arctic	61°08-10'N	149°38-49'W	(*Sullivan*, 2010)
S2	Sub-Arctic	68°20-21'N	18-19°E	(*Grogan et al.*, 2004; *Grogan and Jonasson*, 2005) (*Grogan and Jonasson*, 2006; *Larsen et al.*, 2007a) (*Björkman et al.*, 2010; *Bokhorst et al.*, 2010)
S3	Sub-Arctic	67°29'N	162°12'W	(*Sullivan*, 2010)
S4	Sub-Arctic	69°08'N	27°17'E	(*Aurela et al.*, 2004)
T1	Transitional	58°45'N	94°04'W	(*Lafleur et al.*, 2001)
T2	Transitional	63°52'N	149°15'W	(*Schuur et al.*, 2009)
T3	Transitional	64°75'N	148°25'W	(*Grogan and Chapin III*, 1999)
T4	Transitional	68°N	134°W	(*Jones et al.*, 1999)
T5	Transitional	68°18'N	18°51'E	(*Fox et al.*, 2008)
T6	Transitional	68°30'N	161°24'E	(*Zimov et al.*, 1993, 1996)
L1	Low Arctic	64°50-52'N	111°34-38'W	(*Nobrega and Grogan*, 2007; *Oelbermann et al.*, 2008) (*Buckeridge and Grogan*, 2010; *Buckeridge et al.*, 2010) (*Humphreys and Lafleur*, 2011)
L2	Low Arctic	68°37-38'N	149°18-38'W	(*Oberbauer et al.*, 1998; *Walker et al.*, 1999) (*Mikan et al.*, 2002; *Olsson et al.*, 2003) (*Oberbauer et al.*, 1998; *Sullivan et al.*, 2008) (*Nowinski et al.*, 2010; *Euskirchen et al.*, 2012)
L3	Low Arctic	68°28'N	155°44'W	(*Olsson et al.*, 2003)
L4	Low Arctic	71°19'N	156°36'W	(*Tieszen*, 1974; *Panikov et al.*, 2006)
H1	High Arctic	74°30'N	20°30'-21°W	(*Elberling and Brandt*, 2003; *Elberling et al.*, 2008) (*Christensen et al.*, 2012)
H2	High Arctic	78°10'N	16°04'E	(*Morgner et al.*, 2010; *Björkman et al.*, 2010)
H3	High Arctic	78°N	19°E	(*Elberling*, 2007)

2.2 Modeling snow season NEE

In situ observations of NEE can be upscaled to generate estimates over larger areas of the Arctic using either 1) meteorological inputs and physiological relationships between temperature, radiation, hydrology, phenology and respiration (*Vourlitis et al.*, 2000); 2) direct observations of NEE (*McGuire et al.*, 2012); or 3) a combination of observed NEE and remote sensing estimates of leaf area index and land cover (*Marushchak et al.*, 2012). However, due to the size and spatial heterogeneity of landscapes in the Arctic and sub-Arctic (*Lantz et al.*, 2010; *Nobrega and Grogan*, 2008), errors can arise when upscaling is used to generate circumpolar estimates of NEE (*La Puma et al.*, 2007). Challenges in upscaling NEE are worsened by the sparse and uneven distribution of eddy covariance

towers at high-latitudes (*Baldocchi*, 2008).

Estimates of biospheric carbon cycle variables such as GPP, respiration, NEE and NPP are typically modeled from a variety of remotely sensed, meteorological, and eddy covariance-derived inputs, in addition to measured or optimized region-specific parameters (*Cramer et al.*, 1999; *Krinner et al.*, 2005; *Sitch et al.*, 2007; *Bondeau et al.*, 2007; *Baker et al.*, 2008; *Randerson et al.*, 2009). Biospheric models vary greatly in terms of the approach used (remote sensing vs. process based), inherent simplifying assumptions, initial conditions, complexity with which various processes are represented, representation of land-use change and whether or not they can be applied prognostically. Generally, however, models must be capable of describing how land surface characteristics (e.g. vegetation, soil) and meteorological conditions (e.g. temperature, photosynthetically active radiation) result in given levels of NEE. These model relationships must be adequately generalized so as to yield estimates over regions where *in situ* observations are unavailable (*Cramer et al.*, 1999; *Sitch et al.*, 2007; *Dietze et al.*, 2011; *Huntzinger et al.*, 2012).

The Simple Biosphere Model (SiB) is a process-based model that calculates the regional land-atmosphere exchange of energy, mass and momentum by representing small-scale physical processes (e.g. transpiration, runoff, respiration, photosynthesis) using equations with a physical or biological basis (*Sellers et al.*, 1986). Models such as SiB are highly useful for simulating the land surface energy balance in a biophysically accurate manner, and can be used alone or in combination with general circulation models for predictive and simulation purposes. In a full description of the SiB3 numerical scheme, (*Baker*, 2005) indicates that although growing season processes are comprehensively described, and snow properties are calculated according to the Common Land Model (CLM) formulation by (*Dai et al.*, 2003), grid cells could only be described as either snow-covered or snow-free. Including a representation of fractional snow cover may therefore improve estimates of snow season photosynthesis and respiration by SiB3.

The Vegetation Photosynthesis and Respiration Model (VPRM) is a remote sensing based model that estimates NEE according to a simple mathematical structure (*Mahadevan et al.*, 2008). Respiration is described as a linear function of air temperature, and photosynthetic uptake is calculated as a function of air temperature, incoming shortwave radiation, and estimates of vegetation biomass and land surface moisture from visible and infrared remote sensing derived indices. Whereas process-based models contain complex representations of processes, VPRM contains only four parameters per vegetation class (*Mahadevan et al.*, 2008). Therefore, although VPRM cannot be used for biophysical simulation of processes, the resulting estimates of NEE have shown good agreement against observational data, and the errors and uncertainties can be traced to specific inputs (*Lin et al.*, 2011), and the utility of these models is therefore in generating regional estimates of

NEE. Remote sensing based models of NEE such as VPRM have not explicitly represented the influence of snowpack parameters on NEE.

Recently, several process-based models have represented the influence of a model snowpack on soil temperature and respiration. For example, process-based simulations of soil CO_2 efflux by (*Kucharik et al.*, 2000) and (*Pumpanen et al.*, 2003) made use of land surface temperature, including snow surface temperature when available; however, no mention is made of specific adaptations made to the model for describing subnivean production or diffusion of CO_2. (*McGuire et al.*, 2000) generated estimates of heterotrophic respiration both with and without a representation of the insulation provided by snow using the following three process-based models: Century, Terrestrial Ecosystem Model (TEM) and the Carnegie-Ames-Stratford Approach (CASA). When the model deemed snow to be present, soil temperature was set to 0°C. Evaluations of the resulting models indicated that models showed better agreement against observational data when the influence of a snowpack was explicitly represented, and that this prevents heterotrophic respiration from being underestimated during the snow season.

Modifications have been made to several process-based models to allow them to better simulate the physical processes driving Arctic NEE such as snow and vegetation. For example, (*Wania et al.*, 2009) modified the Lund-Potsdam-Jena Dynamic Global Vegetation Model (LPJ-DGVM, by (*Sitch et al.*, 2003)) so that it would include snow densification over time, permafrost, northern hydrology and peatland vegetation. Snow was simulated as a homogeneous layer that increased in density from 150 to 500 kg/m^3 during the snow season, with snow season length assumed to be the same length as the previous snow season and thermal conductivity calculated as a function of density according to parameters developed by (*Sturm et al.*, 1997). Similarly, snow is modeled as a homogeneous layer in ORCHIDEE, which changes over time through melt, sublimation and snowfall, all of which are calculated according to the surface energy balance. The thermal conductivity of the snowpack is typically fixed, but more realistic estimates of soil carbon have been generated by incorporating field-based observations of snow properties (*Gouttevin et al.*, 2012).

Therefore, although several models have benefited from including a simple representation of snow processes or field-based observations of snow characteristics, the influence of snow on soil respiration is not usually represented in models of NEE, and processes such as subnivean photosynthesis are not represented in existing models. Furthermore, when models of NEE do simulate snow accumulation, they do so in a relatively simple manner, such that snow metamorphism and the formation of ice lenses or depth hoar do not occur, although these influence snowpack thermal conductivity and diffusivity. Site characteristics, such as vegetation and topography, also may not have a realistic influence on snowpack development in existing models. Due to the challenges in accurately simulating snowpack

dynamics, and due to the spatial dependence of snow and NEE, we suggest that remote sensing observations of snow may provide an optimal approach for characterizing snow season influences on NEE throughout the Arctic and sub-Arctic. Remote sensing observations could either be directly included as inputs into remote sensing based or process-based models of NEE, or incorporated into process-based simulations in order to constrain estimates of snow accumulation. Remote sensing observations of snow season characteristics could thereby enable models of NEE to simulate the complex responses of subnivean respiration and photosynthesis to snowpack properties, and may allow uncertainty to be reduced in Arctic and sub-Arctic estimates of snow season NEE.

2.3 Uncertainties in Arctic and sub-Arctic NEE

The following section explores uncertainties in local and regional scale observations of NEE in order to provide a context for later discussion of strategies which may reduce uncertainty in snow season estimates of high latitude NEE. Uncertainties in observations of Arctic site scale NEE ($< 10^5$ m) exist due to a number of factors involved in acquiring accurate observations (*Björkman et al.*, 2010) and quantifying the portion of subnivean NEE that was produced during the snow season (*Panikov*, 2009). Regional scale ($> 10^5$ m) estimates of the carbon budget can be generated using a variety of approaches such as atmospheric inversion, process-based modeling, spatial upscaling of local observations, and remote sensing based modeling (*Cramer et al.*, 1999; *Sitch et al.*, 2007; *McGuire et al.*, 2012). Recent syntheses by (*McGuire et al.*, 2012) and (*Huntzinger et al.*, 2012) have indicated that although convergence exists regarding decadal trends in the Arctic carbon cycle, substantial uncertainties exist in estimates of circumpolar Arctic NEE.

2.3.1 Uncertainties in measurements of NEE

Regional surface CO_2 fluxes can be estimated using observations from Lagrangian, "airmass-following" aircraft observations (*Lin et al.*, 2004) and satellites such as the Greenhouse gases Observing Satellite (GOSAT) (*Chevallier et al.*, 2010). However, satellites are limited in yielding accurate observations of CO_2 over Arctic and sub-Arctic regions due to the uncertainties introduced by snow/ice covered surfaces, limited availability of cloud-free observations, and a large solar zenith angle at high-latitudes (*Boesch et al.*, 2011). Observations from aircrafts are, by necessity, limited in their temporal resolution. Year round observations of CO_2 fluxes and net carbon uptake can therefore be accurately and directly

measured only at local scales ($< 10^5$ m), especially at high-latitude sites (*Bréon and Ciais*, 2010).

Local measurements of NEE can be acquired at the plot scale (10-100 m) using chambers, or at the patch scale (10-10^5 m) using eddy covariance measurements (*Fox et al.*, 2008), which measure the land-atmosphere turbulent exchange of CO_2 (*Baldocchi et al.*, 1988). Although the accuracy of eddy covariance observations can be compromised by cold season heat transfer in open path eddy covariance systems (*Amiro*, 2010), uncertainty can arise in point measurements due to landscape heterogeneity and site selection bias. Previously, these factors have resulted in 60% overestimates of chamber measured NEE compared to footprint modeled eddy covariance NEE, as observed at site S2 by (*Fox et al.*, 2008). Financial and logistical challenges associated with gathering field measurements limit the collection process itself, the types of measurements that can be taken, and the locations at which they can be acquired (*Campbell et al.*, 2005; *Bäckstrand et al.*, 2010), resulting in a bias towards data collection during the growing season. Recently, however, the eddy covariance technique has been used to characterize high-latitude NEE year-round at site L2 by (*Euskirchen et al.*, 2012).

A majority of snow season observations of NEE have been collected using point measurement techniques. Point observations of snow season NEE are collected using chambers connected to infrared gas analyzers either at the top of the snow surface or over a patch of ground surface from which snow has very recently been cleared. Alternatively, a trace gas technique can be used to create a time series of CO_2 efflux based on multiple sampling within the snowpack. NEE can also be measured using air sampling of CO_2 concentrations at two points above and below the snowpack then estimating CO_2 efflux based on an assumption of Fickian diffusion. However, the accuracy of these estimates may be compromised by deviations from simple Fickian diffusion approaches due to non-steady-state convection (*Jones et al.*, 1999).

A comparison of the aforementioned CO_2 sampling techniques by (*Björkman et al.*, 2010) at a sub-Arctic (S2) and a High Arctic (H2) site showed that the trace gas and diffusion based methods found little difference in CO_2 between high and low snow accumulation conditions whereas chamber sampling found greater effluxes of CO_2 arising from the sites with greater accumulation of snow. The application of chamber based techniques may be especially prone to errors since chambers at the top of the snowpack measure only fluxes from the snow surface (*Morgner et al.*, 2010), and chamber measurements taken at the soil surface immediately after snow removal can initially show very large fluxes of CO_2 before leveling off (*Grogan and Jonasson*, 2005). As a result, different techniques have yielded observations of NEE that vary by up to two orders of magnitude at a single site (*Björkman et al.*, 2010). The discrepancies found between observations collected using

different techniques limits the potential for comparisons to be made between sites.

The aforementioned *in situ* approaches are also prone to errors because they sample CO_2 at a very small scale and are therefore influenced by small-scale heterogeneities. Furthermore, snowpack stratigraphy and diffusion are altered in the process of acquiring non-automated observations of NEE, such that the manual collection of NEE observations during the snow season may be biased. As a result of discrepancies in the spatial scale and magnitude of observed NEE from different techniques, as well as the overall shortage in snow season observations at high-latitude sites, it is not possible at this point to conduct a thorough inter-site comparison of relationships between snow and NEE. However, it is still possible to rely on findings from individual sites regarding NEE and its association with snow accumulation. Future improvements in automated measurement techniques and greater generalization of sampling strategies would also allow an improved understanding of how associations between snow and NEE vary across study sites. Furthermore, the greater application of snow sampling strategies to characterize the density, grain characteristics and total accumulation of snow relative to its snow water equivalent (SWE) could further assist researchers in understanding the relationship between snow dynamics and NEE and how it varies between study sites.

2.3.2 Uncertainties in the partitioning of snow season NEE

Uncertainty exists regarding how much of the NEE released during the snow season is being produced through subnivean respiration and what portion of CO_2 released throughout the snow season was produced during the antecedent growing season. Although the exact ratio varies by season and site, it is important to evaluate the relative contributions of production and release as these define the main mechanisms and snowpack characteristics that affect snow season NEE, as snow influences both the rate of production and diffusion of CO_2.

Using laboratory testing of soil from L4, (*Panikov et al.*, 2006) found that a majority of snow season effluxes of CO_2 occurs due to microbial activity, and that variation in CO_2 release (v) can be estimated in a laboratory setting based on incubation temperature (T), the unfrozen soil water content (W), and three constants (A, λ and k): $v = A^{\lambda T + kW}$ ($R^2 > 0.98$). This study indicated that a smaller portion of CO_2 arises from abiotic releases of accumulated CO_2. However, in regions such as T2 that are undergoing permafrost thaw, abiotic releases of CO_2 can form an important portion of net carbon exchange (*Schuur et al.*, 2009). The exact portion of apparent CO_2 flux that arises from abiotic releases and microbial activity therefore varies according to site conditions. (*Elberling and Brandt*,

2003) found that 40% of total annual soil respiration in a Greenland heath (H1) arose from subnivean respiration, and that 80% of subnivean respiration between 0 to -9°C became trapped in soil. Although abiotic releases of CO account for a more substantial portion of efflux during the snow season than during the growing season, most of the CO_2 annually released by soil tends to arise from soil respiration (*Zimov et al.*, 1993; *Pumpanen et al.*, 2003; *Panikov et al.*, 2006).

The main limitation on snow season respiration relates to the influence of sub-zero soil temperatures on reducing availability of unfrozen water (*Panikov*, 2009). In loam soils at site T5, free water has been observed at temperatures of -10°C (*Zimov et al.*, 1993). Unfrozen water has even been detected in clayey permafrost soil at temperatures of -60°C (*Ananyan*, 1970) (in Russian, cited by (*Wagner*, 2008)). In a laboratory setting, subsoil microbial activity has been observed to occur at temperatures of -39°C in an Arctic soil sample acquired from site L4 (*Panikov et al.*, 2006). Subnivean temperatures are typically much warmer than -39°C, and the amount of unfrozen water in soil has been observed to decline only marginally at temperatures below -5°C at a high Arctic site (H1) (*Elberling and Brandt*, 2003), thereby enabling substantial subnivean production of CO_2. Furthermore, as respiration is an exothermic reaction, greater rates of respiration during the snow season also induce elevated soil temperatures and rates of decomposition (*Zimov et al.*, 1993; *Khvorostyanov et al.*, 2008; *Koven et al.*, 2011).

Snow accumulation influences both the rate of diffusion and rate of production of CO_2 through respiration, and so it is difficult to quantify the exact contribution of snow accumulation to the release and production of CO_2 while uncertainty remains regarding the partitioning of snow season NEE. Field studies have indicated greater effluxes of CO_2 and warmer soil temperatures in regions with greater snow accumulation using measurement approaches that observe both instantaneous diffusion through a snowpack (e.g. (*Sullivan*, 2010)) as well as net accumulated effluxes of accumulated CO_2 throughout the snow season (e.g. (*Nobrega and Grogan*, 2007)). Likewise, field studies employing experimental winter warming (e.g. (*Bokhorst et al.*, 2010)) and experimental nutrient enrichment (e.g. (*Zimov et al.*, 1996)) have found increases in snow season CO_2 effluxes relative to control plots. Since snow season changes in temperature, nutrient enrichment and snow accumulation alter the total release of CO_2, it is clear that a substantial portion of snow season NEE arises from subnivean respiration.

Furthermore, as more CO_2 is released from sites with greater snow accumulation, snow has a more important role in encouraging greater rates of respiration by insulating the soil from cold temperatures than in limiting diffusion of CO_2. Therefore, despite uncertainties regarding the exact portion of NEE that arises through biotic production and abiotic releases, it is clear that snow season production of CO_2 accounts for a substantial portion

of snow season NEE (*Elberling and Brandt*, 2003; *Panikov et al.*, 2006) and that subnivean NEE is sensitive to soil temperature and snow accumulation (*Bokhorst et al.*, 2010).

2.3.3 Uncertainties in regional estimates of NEE

Recently, the North American Carbon Program conducted an inter-comparison of nineteen terrestrial biospheric models (*Huntzinger et al.*, 2012), including Can-IBIS (*Wang et al.*, 2011), CLM-CASA (*Randerson et al.*, 2009), LPJ-wsl (*Bondeau et al.*, 2007), ORCHIDEE (*Krinner et al.*, 2005), SiB3 (*Baker et al.*, 2008) and MODIS (*Running et al.*, 2004). These models vary in terms of how photosynthesis is calculated, which assumptions are made, which driver datasets are used, as well as which processes and land surface characteristics are represented, and at what level of complexity, as described in detail by (*Huntzinger et al.*, 2012). Overall, model estimates of North American NEP ranged from -0.7 to 2.2 PgC/yr, indicating uncertainty regarding whether North America was a net carbon source or sink (*Huntzinger et al.*, 2012). Estimates of NEE are complicated by the non-linearity of processes influencing CO_2 exchange at various scales (*Levy et al.*, 1999), inherent challenges in optimizing numerous parameters (*Prihodko et al.*, 2008), and innate challenges in complex representations of processes (*Abramowitz et al.*, 2007).

Physiological models are used to model NEE over a variety of landscapes, including temperate rainforests (*Coops et al.*, 2007), evergreen needleleaf forests (*Xiao et al.*, 2004a) and temperate grasslands (*Wu et al.*, 2008). However, a process-based approach can be more challenging to implement in Arctic and sub-Arctic regions due to challenges in representing processes that drive northern NEE such as fire regimes and soil characteristics, as well as challenges in accurately representing a highly heterogeneous landscape (*La Puma et al.*, 2007). Model calibration and validation are further complicated in high-latitude regions due to the limited number of Arctic and sub-Arctic sites at which eddy flux observations are acquired, and the clustering of northern field studies in Alaska and Scandinavia [Figure 2.2].

Furthermore, as eddy covariance observations are collected preferentially during the growing season in high-latitude regions, it can be difficult to calibrate and evaluate the accuracy of snow season estimates. In light of the many challenges faced in the process of collecting and analyzing observations of snow season NEE, and in generating regional estimates of Arctic NEE, we suggest that uncertainty in model estimates of snow season NEE may be reduced by incorporating objective, regional scale, remote sensing derived observations of snow properties. A review of the spatial and temporal associations between snow and NEE is therefore provided in sections 4 and 5, followed by recommendations of

how these processes can be represented in models of NEE using remote sensing observations of snow properties. These snow season processes and the suggestions of how they may be represented in models of NEE also appear in Table 2.3.

2.4 Spatial associations between snow and NEE

Snow season NEE has been observed to vary according to the thickness of snow, soil temperature and vegetation composition at site H3 (*Elberling*, 2007). The strength of the associations between air temperature, soil temperature and NEE depends in part on the duration of snow cover and the physiological activity of vegetation during winter thaws (*Starr and Oberbauer*, 2003; *Sullivan et al.*, 2008). Furthermore, the timing and magnitude of winter CO_2 transport depend on snow conditions, CO_2 production, site characteristics and weather conditions (*Jones et al.*, 1999).

The acquisition of regional estimates of NEE is complicated by the scale dependence of NEE as well as the spatial variability of the various controlling influences on NEE such as snow, soil, vegetation and microclimate status. Arctic transect studies have indicated that macro scale ($>10^4$ m) vegetation spatial patterns are influenced by latitudinal climatic gradients, topography, precipitation and active layer depth (*Gould et al.*, 2003; *McGuire et al.*, 2002). At the site scale (10–10^4 m), vegetation varies according to micro-topography and soil type, which both influence soil moisture (*Svensson and Callaghan*, 1988). Similarly, spatio-temporal variability of snow is scale dependent. At the micro (10–10^2 m) scale, transport and surface roughness influence distributions of snow. At the macro scale, variations in snow are controlled by elevation, orography and latitude, as well as distance from barriers and water, at the meso (10^2–10^3 m) scale, variations tend to be influenced by slope, elevation, aspect, and vegetation (height, extent, density, etc.) (*Bonan*, 2002). Therefore, both vegetation and snow vary across the landscape and both are scale dependant. Likewise, a portion of the spatial variability in NEE is likely due to the influence of snow and vegetation.

Due to the spatial variability of the factors controlling snow season NEE, it is important that attempts to reduce uncertainty in sub-Arctic and Arctic NEE estimates during the snow season be founded upon the current state of knowledge regarding the influence of snow on the uptake and efflux of COat Arctic and sub-Arctic study sites.The following section therefore provides a synthesis of recent *in situ* findings regarding the site-scale associations between snow, vegetation and snow season NEE. Implications of these findings for representing the influence of snow on winter NEE are then discussed based on the physical processes driving these interactions [Table 2.3].

2.4.1 Greater efflux of CO_2 from sites with greater snow accumulation

Snow acts as an insulator because it has a small volumetric heat capacity, undergoes little heat loss by convection, and has a low thermal conductivity. The thermal conductivity of snow has been observed to range from 0.025-1.61 W/-m^{-1}-deg-C^{-1} in snowpacks with densities of 100-800 kg/m^3 (*Gray and Male*, 1981). Generally, low values of thermal conductivity (e.g. 0.06 W-m^{-1}-deg-C^{-1}) are observed in the Arctic and sub-Arctic (*Sturm*, 1992). The thermal conductivity of a snowpack is influenced by factors such as snowpack depth, bonding, temperature, porosity, ventilation, and grain characteristics, but can be can be estimated as a simple, positive function of snow density (*Sturm et al.*, 1997). A greater accumulation of snow is generally associated with diminished thermal conductivity of the land-atmosphere interface (*Gray and Male*, 1981). Snowpacks can therefore decouple air and soil temperatures (*Olsson et al.*, 2003) since less heat is transferred from the soil when an overlying layer of snow is present (*Bonan*, 2002). As a result, the frozen soil at 40-120 cm depth from which CO_2 is emitted has been observed to be 10-40°C warmer than the surface air temperature at a Siberian sub-Arctic site T6 (*Zimov et al.*, 1993). For example, at two low Arctic sites located at L3, minimum 16 cm soil temperatures in the -10 to -5°C range were observed with minimum air temperatures of -30°C (*Olsson et al.*, 2003).

Microbial fluxes have been observed to increase as a function of temperature over both organic and mineral soils at site L1 (*Oelbermann et al.*, 2008). The association between soil respiration and temperature is driven by intracellular desiccation or extracellular barriers to diffusion in frozen soils, and by soil organic matter in thawed soils (*Mikan et al.*, 2002). The influence of snow accumulation on CO_2 flux has been detected experimentally at a variety of sites using snow fences, which cause a local increase in snow accumulation through wind deposition. Across a sub-Arctic gradient in Sweden (S2), comparisons of treatment and control plots indicated that snow accumulation had an important influence on soil temperature. Between 41 to 75% of the variation in respiration could be explained as a function of soil temperature at site S2 (*Grogan and Jonasson*, 2006). Near the Arctic treeline in Alaska (S3), CO_2 flux varied significantly (p-value<0.01) between sites and years, and according to both snow depth and soil surface temperature. Soil surface temperature and snow depth were correlated (r=0.73, p-value<0.01). Soil temperature and snow depth were greater in forested regions than at the treeline, and both increased in forests with greater stand density (*Sullivan*, 2010).

At a low Arctic site in northern Alaska (L2), warmer soil temperatures and greater rates of respiration were observed at plots that had received a greater accumulation of snow due

to the installation of snow fences (*Walker et al.*, 1999). At low Arctic site L1, observations of net seasonal CO_2 flux were collected using soda lime traps, which accumulate mass as CO_2 is released throughout the season. These measurements indicated a 60% increase in total snow season CO_2 efflux in snow accumulation plots (1 m of snow) relative to control plots (0.3 m of snow) (*Nobrega and Grogan*, 2007). At an Alaskan tussock tundra site (L2), snow accumulation acted as a stronger control on CO_2 distributions than air temperature (*Sullivan et al.*, 2008). Experimental snow accumulation (30-150 cm) at a high Arctic site in Svalbard (H2) led to significant increases in both soil temperature and ecosystem respiration, leading to a doubling of CO_2 efflux at both heath and meadow sites (*Morgner et al.*, 2010). Greater snow accumulation over several varied Arctic and sub-Arctic ecosystems therefore induced increased CO efflux.

2.4.2 Influence of vegetation on snow and snow season NEE

Interactions between snow and vegetation have been observed to alter snow season photosynthesis (*Larsen et al.*, 2007a) and respiration (*Grogan and Jonasson*, 2006) at site S2. In regions where tree wells form, the size of tree wells and the resulting soil heat loss depend on micro-scale (10–10^2 m) vegetation distributions (*Sturm*, 1992). The species distributions of vegetation at a site can therefore influence the soil temperature and respiration. At the meso scale (10^2–10^3 m), groupings of trees act as windbreaks, causing an increase in snow deposition nearby (*Gray and Male*, 1981), which could potentially increase the rate of soil respiration.

Vegetation species composition also has an influence on subnivean photosynthesis and respiration. Shrub stems encourage the growth of large faceted crystals via metamorphism under strong temperature gradients. Faceted crystals have one fifth to one twentieth of the effective thermal conductivity of a high density wind slab (*Zhang et al.*, 1996), resulting in the release of greater effluxes of CO_2 from areas containing shrubs, as observed at site S2 (*Sullivan*, 2010). Also, although cold temperatures and diminished light availability reduce photosynthetic assimilation of CO_2 (*Billings and Mooney*, 1968), the species present at a site influence the resulting rate of photosynthesis. While in a dormant state, evergreen vegetation protects itself from light stress through non-photochemical dissipation of absorbed light (*Öquist and Huner*, 2003). Following frost hardening, evergreen trees have been observed to undergo no growth and "no measurable net photosynthesis" as long as subzero air temperatures persist (*Öquist and Huner*, 2003). Although vascular plants cannot conduct photosynthesis when their tissues are frozen, evidence exists that lichens can perform photosynthesis at temperatures below -10°C (*Kappen*, 1993). Furthermore, indications exist that low Arctic tundra vegetation, especially mosses and evergreens, may

be capable of performing photosynthesis at greatly diminished rates under thin snow cover, as long as conditions are suitably warm (*Tieszen*, 1974).

(*Larsen et al.*, 2007a) reported that cold season (October to May) photosynthesis accounted for up to 19% of annual photosynthesis in a mesic, moss-dominated sub-Arctic heath with little (30-40 cm) snow (site S2). Similarly, (*Starr and Oberbauer*, 2003) found evidence of subnivean photosynthesis by Arctic evergreens on the north slope of Alaska (site L2) during a two to four week period at the end of the snow season in the presence of air temperatures above 0°C and encouraged by elevated subnivean concentrations of CO_2. At a High Arctic site in Zackenberg (H1), (*Christensen et al.*, 2012) observed low levels of photosynthesis to continue to occur at the start of the snow season. Vegetation therefore shows greatly reduced rates of photosynthesis in the presence of snow, even in Arctic species which are adapted to perform photosynthesis in sub-zero conditions.

2.4.3 Implications for models of NEE

Remote sensing observations of snow water equivalent (SWE) or snow depth could be used in combination with observations of air temperature to gain more accurate estimates of subnivean temperatures. The influence of greater snow accumulation on increased rates of soil respiration observed at many high, low and sub-Arctic sites (e.g. S2- (*Grogan and Jonasson*, 2006); S1- (*Sullivan*, 2010); L1- (*Nobrega and Grogan*, 2007); H2- (*Morgner et al.*, 2010)) could therefore be represented in models of NEE. This influence could be represented using remote sensing observations of SWE or snow depth to determine more accurate estimates of soil respiration, or by assimilating remote sensing observations of SWE into model estimates of snowpack accumulation to better constrain estimates of soil respiration.

The initial appearance of snow and concurrent drops in air and soil temperatures greatly limit the rate of photosynthetic uptake in Arctic vegetation (*Billings and Mooney*, 1968; *Carstairs and Oechel*, 1978; *Öquist and Huner*, 2003). The influence of snow on limiting the rate of snow season photosynthesis could be represented in models of NEE using observations of fractional snow cover area, and then diminishing the rate of photosynthesis in regions where snow is accumulating by an appropriate quantity given the vegetation distribution. The differing abilities of vascular and non-vascular plants to conduct photosynthesis in sub-zero conditions could therefore be represented. Greater benefits may be accrued by representing fractional snow cover in autumn than spring as photosynthesis is more heavily influenced by air temperature and photoperiod at the start of the snow season than at the end of the snow season, as described by (*Euskirchen et al.*, 2012).

The influence of vegetation on snowpack properties such as the formation of tree wells (*Sturm*, 1992) and faceted crystals in shrub-dominated regions (*Zhang et al.*, 1996), and their influences on increasing and diminishing local snow thermal conductivities, respectively, could be represented using vegetation species-specific expressions to determine soil respiration as a function of snow accumulation. Another option may be to incorporate field observations of grain characteristics to represent the growth of faceted crystals, or high resolution LiDAR observations to detect the formation of tree wells.

2.5 Seasonal responses of NEE to snow fall, metamorphism and melt

Observations of seasonal changes in the relationships between snow cover/accumulation and CO_2 are summarized below according to three time periods: initial snow fall, midwinter and final snow melt. The implications of seasonal transitions in snow-CO_2 associations for incorporating remote sensing estimates of snow into models NEE are then described. These associations and their implications are also summarized in Table 2.3.

2.5.1 Initial snow fall

The timing of initial snowfall represents a transition to the snow season, which is accompanied by greatly diminished rates of photosynthesis and cooler soil temperatures (*Olsson et al.*, 2003). The initial accumulation of snow at the start of the snow season cools the ground surface due to the high emissivity and high surface albedo of snow, which results in diminished absorption of solar radiation (*Zhang et al.*, 1996). Prior to initial snow fall, the soil active layer depth is at an annual maximum but starts to diminish as soil cooling occurs, thereby diminishing the rates of microbial activity (*Elberling*, 2007) due to indirect effects such as intercellular desiccation and extracellular barriers to diffusion (*Mikan et al.*, 2002). Near the end of the growing season, plant productivity becomes limited by the availability of daylight. Initial snowfall in autumn limits light penetration to vegetation, thereby reducing photosynthetic uptake (*Euskirchen et al.*, 2012).

Litter loss in autumn occurs mostly due to leaching of organic compounds (*Bokhorst et al.*, 2010), and is influenced by both temperature and nutrient availability. Nutrient enrichment with a labile carbon source was found to quadruple September to November CO_2 effluxes at a Siberian sub-Arctic site (T5) (*Zimov et al.*, 1996). (*Bokhorst et al.*, 2010) found that 90% of winter litter mass decomposition at sub-Arctic site S2 occurred within

the first month of initial snow fall in autumn. Therefore, the nutrient, soil temperature and snow conditions present during the short time period immediately following initial snow fall can have an important effect on net snow season NEE.

2.5.2 Snow metamorphism

Due to soil nutrient and temperature limitations, the rate of CO_2 production is greater during snow fall and snow melt than during the intermediate portion of the snow season when metamorphism is the dominant process, as observed by (*Elberling*, 2007) at H3. However, the middle of the snow season has a long duration and therefore accounts for a large portion of the annual CO_2 budget. In the middle of the snow season, the snowpack is transformed over time through destructive and constructive metamorphism. Destructive metamorphism refers to the process through which dendritic crystals are broken into rounded ice grains that become joined through sintering as snow crystals move to an equilibrium state, resulting in a minimum ratio of surface area to volume. Destructive metamorphism is controlled by vapour transfer within the accumulating pack, and is the dominant process following snow fall (*Colbeck*, 1980). Constructive metamorphism refers to the formation of temperature and vapor pressure gradients within snowpacks resulting in the diffusion of water vapor upwards, from warm to cold regions of the snowpack. Once the vapor has risen to a $<0^{\circ}$C area of the snowpack, it refreezes in the form of faceted crystals. Cycles of freeze and melt within snowpacks cause the formation of large, irregular grains that grow upwards from the bottom of the snowpack (*Gray and Male*, 1981).

In terrestrial Arctic or sub-Arctic snowpacks unaffected by melt or strong wind activity, the top layer will remain less dense, weak and contain relatively unchanged snow crystals that have had their dendrites broken off. The middle layer will be dense and strong with small ice crystals due to destructive metamorphism, where air space and crystal size are diminished under densification processes. The bottom layer is generally weak, with low thermal conductivity. It will typically contain faceted crystals, or depth hoar (*Gray and Male*, 1981) [Table 2.2]. The structure and low density of depth hoar cause it to have a very low thermal conductivity relative to other layers of snow (*Zhang et al.*, 1996). Arctic and sub-Arctic snowpacks often contain wind slabs or ice lenses; when present, multiple layers of depth hoar can be formed (*Sturm et al.*, 1995).

Steady state soil heat flux is influenced by the thermal conductivity, temperature and thickness of the snowpack (*Gray and Male*, 1981). In other words, the influence of mid-season snow on CO_2 flux depends on the thermal conductivity of snow (in $Wm^{-1} \circ C^{-1}$) as greater water availability with warmer soil temperatures leads to greater rates of CO_2

Table 2.2: Description of general snowpack characteristics, arranged in their order of placement in the snowpack, with fresh snow at the top and depth hoar forming closest to the ground. *In situ* snow characteristics, however, are highly spatially and temporally variable, and are heavily influenced by site characteristics. Multiple layers of depth hoar interspersed by layers of ice can often be observed in Arctic and sub-Arctic snowpacks.

	Density	Grain size	Grain shape	Primary process	Thermal cond.
Fresh snow	Low	Medium	Various	Precipitation event	Low
Rounded	High	Small	Round	Destructive metamorphism	Medium
Depth hoar	Low	Large	Faceted	Constructive metamorphism	Very Low

production (*Panikov et al.*, 2006). In general, the thermal conductivity of a snowpack increases as the quantity of air relative to ice/water decreases. Packed, dense snowpacks therefore tend to transfer heat from soil at the greatest rate (*Slaymaker and Kelly*, 2007). Thermal conductivity (k_t) can be estimated according to snowpack density (ρ) using a quadratic expression or logarithmic expression (*Sturm et al.*, 1997). For example, (*Jeffries et al.*, 1999) estimated thermal conductivity of snow on the Alaskan North Slope as $k_t = 0.138 - 1.01\rho + 3.233\rho^2$. The development of new sampling strategies has also allowed direct measurement of thermal conductivity, enabling analysis into the influence of snowpack stratigraphy on thermal conductivity (*Sturm et al.*, 2002). Surface melt, freezing rain and wet snow refreezing at night cause the formation of ice layers and crusts. Rain can fall in temperatures as low as -10°C when ice nucleation is not present, resulting in ice crusts (*Gray and Male*, 1981). When ice lenses and wind crusts form, the porosity of the snowpack decreases while the pathways through which air could travel become increasingly tortuous, resulting in diminished permeability and air flow. Under these conditions, larger CO_2 concentration gradients form between the bottom of the snow pack and ambient air (*Jones et al.*, 1999). Ice cover also limits exchange of gas with the atmosphere, but is not thought to limit seasonal total gas exchange (*Gray and Male*, 1981). Ice lenses within the snowpack can also influence the accuracy of diffusion-based measurements, since they defy the assumption of a linear CO_2 gradient within the snowpack (*Sullivan*, 2010). The use of snow pits to examine the presence of ice lenses can, therefore, improve the reliability of measurements (*Sullivan*, 2010). Erosion and windpacking in tundra snowpacks cause slabs to form, and blizzards cause massive hard drifts.

Air temperature also influences snow-CO_2 relationships, even though this influence is limited by the insulating properties of the snowpack. At a low Arctic tundra site (L1), a cold front was observed to cause a temporary drop in soil temperature at 2 cm below the surface and produced diminished fluxes of CO_2 (*Buckeridge and Grogan*, 2010). Extreme

winter warming events initially encourage microbial activity and soil respiration. Following warming, however, soil refreezes more deeply as the insulation provided by snow is lost (*Bokhorst et al.*, 2010), which can cause damage to vegetation that will substantially diminish net primary productivity over the following growing season (*Bokhorst et al.*, 2009). Meteorological influences during the snow season can therefore alter snowpack properties as well as NEE.

2.5.3 End of season snow melt

Snow melt occurs due to a combination of rainfall, absorption of solar radiation and sensible heat exchange from the air to ground (*Gray and Male*, 1981). The process of snowmelt is accelerated by albedo effects as the snowpack water content increases, snow depth decreases and low albedo vegetation is uncovered (*Bonan*, 2002). Due to the higher thermal conductivity of water relative to air, wet snow cannot maintain temperature gradients or insulate soil as well as dry snow (*Gray and Male*, 1981). The high thermal conductivity of the snowpack at the end of the snow season therefore limits the influence of snow on soil temperature (*Zimov et al.*, 1996). As a result, changes in snowpack stratigraphy in a wet snowpack are therefore likely to have little influence on CO_2 production during snow melt. However, in regions characterized by low Arctic vegetation, the diffusivity of the snowpack may continue to influence the rate of soil CO_2 release during snow melt (S2- (*Björkman et al.*, 2010)) and warmer temperatures can increase the rate of soil respiration at the end of the snow season (T5- (*Zimov et al.*, 1996)).

Effluxes of CO_2 at the end of the snow season occur due to an increase in CO_2 production as nutrients and moisture are released through soil thaw, and due to snowmelt, which allows CO_2 trapped beneath the snowpack to be released (*Elberling et al.*, 2008). An increase in snow accumulation has been associated with diminished growing season photosynthesis due to delayed onset of the growing season at site H2 (*Morgner et al.*, 2010). Thicker snow cover and later timing of snowmelt have been found to increase the magnitude and delay the timing of CO_2 released in late winter and early spring in mesic low Arctic tundra at site L1 (*Buckeridge and Grogan*, 2010). Conversely, in upland tundra and sedge fen locations at site L1, variations in the timing of snowmelt did not substantially alter early season or total NEP (*Humphreys and Lafleur*, 2011). Springtime freeze-thaw cycles have likewise been observed not to significantly influence total springtime CO_2 efflux rates in a sub-Arctic heath (S2) (*Grogan et al.*, 2004). Springtime variations in air temperature at a low Arctic mesic birch hummock site (L1) did not bring about freeze-thaw cycles in soil, and also did not cause pulses of CO_2 (*Buckeridge and Grogan*, 2010). The timing

of snowmelt onset and end therefore appears to have a more important influence on NEE than concurrent fluctuations in air temperature.

2.5.4 Implications for modeling snow season NEE

Following the first snowfall of the snow season, soil cooling limits the rate of respiration and the rate of photosynthesis declines due to cold air temperatures and diminished light availability under snow (*Olsson et al.*, 2003). The timing of these transitions could be represented in models of NEE using remote sensing observations of fractional snow cover [Table 2.3]. Similarly, as nutrient availability declines following initial snow fall (*Bokhorst et al.*, 2010), the limiting influence of nutrients following litter loss could be described according to a time period following initial snowfall.

In midwinter, snow metamorphic processes act as a dominant influence on the thermal conductivity of the snowpack (*Gray and Male*, 1981). However, little NEE occurs during the middle of the snow season (*Elberling*, 2007). Mid-winter fluxes of CO_2 have been observed to vary little between sites (*Zimov et al.*, 1993) and are minimal due to nutrient limitation (*Mikan et al.*, 2002). Existing process-based model and inversion approaches simulate diminished midwinter NEE, even when the influence of snow on NEE is not explicitly represented (*McGuire et al.*, 2012). Models of NEE are therefore more likely to benefit from improved characterizations of early and late snow season NEE than of midwinter NEE, especially due to the lack of operational remote sensing estimates of snow thermal conductivity or microphysical structure [Table 2.4], and existing challenges in accurately modeling snowpack thermal conductivity and density, as described by (*Saito et al.*, 2012). However, if snowpack metamorphism was to be included in models of NEE, it may be best to use a process-based approach to simulating snowpack dynamics, and assimilating remote sensing observations of SWE to ensure accuracy in snowpack accumulation.

Extreme winter warming events (*Bokhorst et al.*, 2010) could be identified by tracking fractional snow cover and snow wetness throughout the cold season. At sites where extreme winter warming events occur, the resulting damage to the photosynthetic capacity of vegetation could be examined using satellite observations of mid-growing season vegetation health via the Normalized Difference Vegetation Index (NDVI). In DGVMs, the influence of extreme winter warming events on hindering NPP could therefore be simulated using remote sensing observations of both the snow and growing seasons. Representing these processes in models could allow insights into the complex responses of the carbon cycle to warmer snow and growing season air temperatures. During snowmelt, CO_2 stored within the snowpack is released, and CO_2 production also increases due to warmer temperatures

and the release of nutrients as soil thaws (*Elberling et al.*, 2008; *Buckeridge and Grogan*, 2010). Delayed timing of snowmelt can also lead to a later start of the growing season at certain sites (*Morgner et al.*, 2010). Incorporating remote sensing estimates of fractional snow cover at the end of the snow season, or the snow state as wet or dry, may therefore prove beneficial for representing snow season processes that drive NEE [Table 2.3]. The following section provides a summary of recent approaches used to collect remote sensing observations of snow, and provides an assessment of which strategies may be most useful for reducing uncertainty in snow season estimates of Arctic and sub-Arctic NEE.

2.6 Remote sensing of influences on snow season NEE

Ideally, remote sensing observations incorporated into models of NEE would be at an appropriate resolution, with reasonable accuracy and would have the ability to characterize aspects of the land surface with the greatest influence on NEE, as described in Table 2.3. The advantages and limitations of visible/infrared, altimeter, passive microwave and active microwave approaches for observing snow characteristics are evaluated below in light of their potential contribution to models of NEE. A brief summary of these remote sensing products and their relevance to models of NEE can be found in Table 2.4.

2.6.1 Visible and infrared observations of snow cover area

Fractional snow cover area can be estimated from visible and infrared remote sensing observations using the Normalized Difference Snow Index (NDSI) to differentiate snow from clouds. Although both clouds and snow strongly reflect visible radiation, snow has a much lower reflectance in the mid-infrared range than clouds (*Crane and Anderson*, 1984). On this basis, estimates of snow cover area from Earth Observing System (EOS) Moderate Resolution Imaging Spectroradiometer (MODIS) observations can be generated using the ratio of (green (r_{GREEN}=0.545-0.565 μm) to mid-infrared (r_{MIDIR}=1.628-1.652 μm) reflectance (*Hall et al.*, 1995):

$$NDSI = \frac{r_{GREEN} - r_{MIDIR}}{r_{GREEN} + r_{MIDIR}} \tag{2.3}$$

In regions where low illumination, surface water or vegetation complicate retrievals, thresholds can be set to further differentiate snow covered surfaces (*Hall and Riggs*, 2007; *Riggs and Hall*, 2004). For example, snow and water can have similar values of NDSI but

water has a lower r_{NIR} (0.841-0.876 μm) reflectance than snow. Therefore, non-forested regions with NDSI$\geq$0.4 and where $\geq$10% and r_NIR $\geq$10% can be designated as snow covered (*Foster et al.*, 2011). Similarly, in regions with dense forest cover, observations of NDVI can be used to set lower NDSI thresholds in order to detect sub-canopy snow cover area (*Hall et al.*, 1998).

MOD10 daily, 8-day and monthly composites of snow cover are generated at 500 m to 0.25° grid resolutions using MODIS surface reflectance and masks for cloud cover and land/water (*Hall and Riggs*, 2007). Surface temperature is also incorporated in order to mask out regions with temperatures of >283°K (*Riggs and Hall*, 2011). Validation of MOD10 snow cover has shown an accuracy of 93% relative to *in situ* observations and other operational snow cover products, with the main source of error arising from snow/cloud discrimination (*Hall and Riggs*, 2007). The NDSI has also been used to estimate fractional snow cover from a variety of other platforms ranging from 1-25 km in resolution (*Xiao et al.*, 2004b). For example, the NSDI in SPOT VEGETATION images (1 km) has shown good agreement with ground observations of snow cover (*Dankers and De Jong*, 2004).

A major limitation of visible and infrared observations is that they cannot be used to estimate the quantity of snow because of the short penetration depth of light due to scattering (*Dozier and Painter*, 2004). Furthermore, the acquisition of visible and infrared observations is limited at high-latitudes due to cloud cover and polar darkness. The most suitable applications for optical remotely sensed images of snow are therefore in characterizing the snow cover area at the start and end of the snow season (e.g. (*Vikhamar and Solberg*, 2003; *Paudel and Andersen*, 2011)).

Year-round estimates of snow cover extent are therefore often generated using a combination of visible and infrared derived observations with remote sensing observations from a variety of other sensors. For example, the U.S. National Oceanic and Atmospheric Administration (NOAA) has been generating weekly estimates of Northern Hemisphere snow cover extent since 1966, and have been producing interactive multisensor snow and ice mapping system (IMS) estimates of snow and ice cover since 1999 at 24 km from a variety of inputs (*Ramsay*, 1998). Since 2004, IMS estimates of snow cover extent have additionally been generated at a daily, 4 km resolution (*Helfrich et al.*, 2007) using visible and infrared observations from MODIS and the Advanced Very High Resolution Radiometer (AVHRR) in additional to several non-optical sources of imagery.

The main difference between the IMS and MOD10 products is that MOD10 is produced in a fully automated manner, whereas IMS requires human intervention (*Frei and Lee*, 2010). Relative to higher resolution optical data and passive microwave observations of snow, NOAA snow charts have had a late season bias by up to four weeks (*Wang et al.*,

2005). Conversely, the MODIS snow cover area product tends not to identify snow in autumn over Eurasian deciduous needleleaf forest when this is observed by IMS (*Frei et al.*, 2012). Since autumn snow cover influences the photoperiod and photosynthetic uptake by vegetation more than spring snow cover, it may be best to use IMS products for modeling NEE over Eurasia. However, if the influence of fractional snow cover on NEE is represented in either process-based or remote sensing based models of NEE, and estimates of pan-Arctic fractional snow cover are required after 2000, it may be beneficial to use the MODIS snow cover area product.

2.6.2 Altimeter observations of snow depth

Light detection and ranging (LiDAR), or laser altimetry, measures the time between emission and reception of a laser pulse in order to map the three dimensional aspects of topography. LiDAR has been used for a variety of applications ranging from biophysical canopy mapping (*Lefsky et al.*, 2002) to sea level height (*Lemoine et al.*, 2010). Estimates of snow depth can be made by subtracting measurements of the topography at a time when snow is not present from measurements of topography during the snow season (*Fassnacht and Deems*, 2006; *Deems et al.*, 2006; *Hopkinson et al.*, 2004).

However, LiDAR based techniques for accurately estimating snow depth (<10 cm) may also be compromised by snowfall, fog or large grain size within the snowpack (*Prokop*, 2008) and the acquisition of high-resolution LiDAR observations by aircraft is expensive. An alternative may therefore be to use observations from NASAs Geoscience Laser Altimeter System (GLAS) carried on the Ice, Cloud and land Elevation Satellite (ICESat). ICESat/GLAS collects topographic measurements every eight days over regions with a 70 m diameter every 175 m, and these observations have previously been used to generate daily estimates of snow depth over sea ice (*Kwok and Cunningham*, 2008), Arctic land cover (*Ranson et al.*, 2004) and topography of land (*Atwood et al.*, 2007). One of the stated potential applications of ICESat was to estimate terrestrial snow depth (*Zwally et al.*, 2002); however, no studies to date have applied ICESat for characterizing terrestrial snow depth. Radar altimeter measurements from Topex-Poseidon have been used to characterize terrestrial snow depth (*Papa et al.*, 2002). Terrestrial snow depth could therefore potentially be characterized using ICESat/GLAS or Topex-Poseidon altimeter observations, and to apply these estimates of snow depth to reduce uncertainty in models of NEE. The low spatial resolution of satellite altimeter observations or the high cost of airborne observations may limit the utility of LiDAR estimates in models of NEE. With the development of ICESat-2, this exploration may be possible.

Although field studies focusing on snow-NEE associations have tended to quantify snow in terms of its depth (e.g. (*Grogan and Jonasson*, 2006; *Sullivan*, 2010)), the regional scale thermodynamic properties of snow cannot be well estimated as a direct function of snowpack thickness alone (*Slaymaker and Kelly*, 2007). Altimeter observations are likely to be most useful in situations where estimates of NEE are required for a small homogeneous region where the site-scale association between snow depth and NEE has already been characterized from *in situ* observations. Airborne LiDAR estimates of local snowpack depth and vegetation may also be of use in characterizing local snow microtopography and features such as tree wells, which can alter soil temperature and respiration.

2.6.3 Passive microwave observations of SWE

Passive microwave sensors measure the Earths brightness temperature (T_b) at frequencies ranging from 1 to 18 GHz. T_b represents the amount of radiation emitted by an object at a given wavelength, as expressed by the radiation emitted by a hypothetical blackbody at the same physical temperature (T). Since real objects emit less energy radiation than perfect (blackbody) emitters, brightness temperature at a given wavelength is a function of the physical temperature and emissivity (ϵ <1) of a material (*Chang et al.*, 1976):

$$T_b = \epsilon T \tag{2.4}$$

Passive microwave observation can be used to estimate the timing of freeze/thaw cycles (*Zhang and Armstrong*, 2001; *Smith et al.*, 2004) and to detect ice lenses (*Rees et al.*, 2010). The state of the soil as frozen or thawed influences soil respiration, and ice lenses alter the diffusion of CO_2 through the snow pack (*Elberling*, 2007; *Sullivan*, 2010). The quantity of snow accumulation in terms of its snow water equivalent (SWE) can also be estimated from passive microwave observations. SWE is more useful than snow cover area for many hydrological and climatological applications as it relates directly to the amount of water accumulated in the snow cover, rather than the simple presence of snow (*Foster et al.*, 2005).

SWE can be estimated from passive microwave observations using site-specific regression values or inversion modeling approaches. Typically, SWE is estimated according to the amount of volume scatter of microwave radiation through the snowpack, which increases with the depth and density of the snowpack (*Ulaby and Stiles*, 1980). Estimates of SWE are usually generated according to the difference between brightness temperature at two frequencies, such as 19 and 37 GHz observations from AMSR-E (e.g. (*Pulliainen*

and Hallikainen, 2001)), since 37 GHz observations display greater scatter than 19 GHz observations with greater snow accumulation. However, several aspects of the Arctic and sub-Arctic environment such as microwave emission from dense snowpacks and high lake fractional coverage necessitate the use of tundra-specific algorithms for SWE using observations at 37 GHz (*Derksen et al.*, 2010). Currently, a leading product containing estimates of SWE across the northern hemisphere is GlobSnow, which shows strong agreement against ground-based measurements (*Takala et al.*, 2011).

A drawback of using passive microwave observations of SWE in models of NEE is that estimates of the SWE from deep (>0.5 m) snowpacks may not be accurate since the scattering signal at 37 GHz loses sensitivity at these snow depths (*Shi*, 2008). Another drawback is that SWE can only be estimated from dry snowpacks using passive microwave observations. Wet snow mainly emits passive microwave radiation, and the influence of volume scattering on the passive microwave signal is therefore difficult to discern (*Stiles and Ulaby*, 1980). However, this may not be a great concern in representing the influence of snow accumulation on NEE since only dry snowpacks maintain air-soil temperature differentials that affect the production of CO_2 (*Zimov et al.*, 1996). The main drawback of incorporating passive microwave observations into models of NEE is that the resolution at which observations are collected (25 km) may not be fine enough for characterizing variability in cryospheric influences on NEE over heterogeneous Arctic landscapes. The main advantage of passive microwave observations is that they can be collected throughout the snow season over high latitudes, and are not hindered by polar darkness or non-precipitating cloud cover (*Foster et al.*, 2011). Furthermore, the thermal conductivity of the snowpack, which influences soil respiration, is determined through a combination of snowpack density, grain characteristics and accumulation (*Gray and Male*, 1981).

Although thermal conductivity is not a direct function of SWE, strategies do exist for estimating snow temperature using passive microwave derived observations of SWE, when combined with a land surface model and atmospheric forcing (e.g. (*Sun et al.*, 2004). The influence of snow accumulation on soil respiration could therefore be estimated by including observations of SWE. Furthermore, in regions where moisture resulting from snowmelt influences soil moisture, estimates of water availability upon snowmelt could be improved by incorporating estimates of SWE at the end of the snow season into hydrological estimates by process-based models.

2.6.4 Active microwave observations of snow characteristics

Active microwave observations of backscatter can be used to estimate snow wetness, thermal resistance and snow water equivalent (SWE) (*Shi*, 2008; *Rott et al.*, 2010). The timing

of snowmelt can also be estimated from active microwave observations (*Royer et al.*, 2010; *Wang et al.*, 2008) since backscatter diminishes as the snowpack liquid moisture increases (*Chang et al.*, 1985). Presently, active microwave observations are being collected at the C-band, and these observations can, be used to characterize snow liquid water content (*Niang et al.*, 2007).

Measuring the amplitude and phase of polarization state and interferometry from repeat pass observations could also be used to characterize other snow characteristics such as grain size, snow depth, structure and density (*Shi*, 2008). However, to date, current approaches to estimate SWE and snow characteristics from existing space-borne synthetic aperture radar (SAR) observations have been complicated by the dependence of these algorithms on the study site location and the year. The active microwave signal is influenced by a number of different characteristics of the snowpack that alter the snowpack geometry, composition and volume. Efforts to estimate specific characteristics of the snowpack are therefore complicated by the need to decompose this signal. Ground-based and airborne active microwave observations are currently being collected to assess the potential for snowpack properties to be estimated from twin frequency observations at 9.6 and 17.2 GHz (*Rott et al.*, 2010).

Several products are being developed to make use of active microwave observations in combination with other sensors. For example, daily estimates of the state of the land surface as frozen or thawed will be available at a 3 km resolution from the Soil Moisture Active-Passive (SMAP) mission (*Entekhabi et al.*, 2010; *Kim et al.*, 2010). Similarly, the Air Force Weather Agency/NASA Snow Algorithm (ANSA) combines MODIS visible and infrared observations with active and passive microwave observations in order to generate estimates of SWE, fractional snow cover, snowmelt onset and regions of active melt (*Foster et al.*, 2011). Unfortunately, the active microwave observations were acquired by NASAs QuickSCAT, which was in operation from 1999-2009. Presently, no established products of SWE or snowmelt onset/end exist that use active microwave observations alone. In future, it may be advantageous to use a combined product in models of NEE if estimates of a variety of snow season characteristics are desired.

2.6.5 Suitability of different remote sensing approaches for models of NEE

The suitability of various remote sensing approaches in estimating snowpack characteristics that alter snow season NEE are summarized in Table 2.4. Visible and infrared remote sensing data are most useful in situations where high resolution estimates (weekly, >30

m) of snow cover area are desired at the start or end of the snow season. Laser altimeter estimates of snow depth may be useful where the association between snowpack depth and NEE is known, and where snow cover is adequately consistent and homogeneous so that point observations could adequately characterize regional snow depth. High resolution observations (<20 cm) by airborne LiDAR could likewise assist in characterizing the snowpack depth, but are unlikely to be collected routinely or regionally for scientific studies due to the high financial cost. Although a majority of field studies have investigated the influence of snow accumulation on NEE in terms of snow depth, the stratigraphy, SWE and snow grain characteristics are more important for the thermal conductivity and gas diffusivity of a snowpack. Therefore, estimates of SWE are likely to be of greater use in models of NEE than altimeter observations of snow depth, as SWE has a more important influence on soil respiration and soil moisture availability than snow depth.

The inclusion of passive microwave observations in models of NEE would be most likely to be beneficial in regions that are sufficiently homogeneous so as to not be hindered by the coarse ($\approx$ 25 km) resolution of these products. Presently, active microwave observations can be used to assess snowmelt timing, but existing systems cannot be used to generate regional estimates of SWE or other snow characteristics due to challenges in decomposing the active microwave signal, as the relationships between SWE, snowpack stratigraphy and the active microwave signal vary across study sites and years. Established products exist for passive microwave observations of SWE from GlobSnow, and visible and infrared observations of fractional snow cover area from MODIS 10. Synergistic products indicating soil freeze/thaw such as SMAP and ANSA estimates of SWE and fractional snow cover which are currently in development may prove helpful in future studies involving NEE.

2.6.6 Incorporating remote sensing of snow into models of NEE

Remote sensing observations could be incorporated into models of Arctic and sub-Arctic NEE in several ways. Firstly, these observations could be brought in as model inputs in remote sensing or process-based models of NEE in order to represent snowpack properties relevant to NEE [Table 2.3]. Another option is that model calibration or evaluation could consist of comparing remote sensing observations of factors such as the dates of initial snow fall and snow melt against estimates of NEE for portions of the year when observations of NEE are unavailable in order to better understand model performance. This approach could be used both for models that explicitly represent snow processes, and for those which do not. A final option is for models of NEE to explicitly represent physical processes during the snow season, and to incorporate remote sensing observations of snowpack properties into model representations of snowpacks in order to better constrain estimates of NEE.

The optimal strategy depends largely on the model class (prognostic or diagnostic), its formulation (remote sensing or process based), and the intended purpose of the model.

Incorporating remote sensing observations directly into models of NEE is advantageous when model output is required over large regions or many years, as a comparison of 33 snow models by (*Rutter et al.*, 2009) indicated that model performance in estimates of SWE and snow depth varied by site and year. It may therefore be more difficult to examine the sources of uncertainty in models of NEE if these models make use of process-based representations of snowpack properties which are unconstrained by *in situ* or remote sensing observations.

Certainly, representing the influence of fractional snow cover area on photosynthesis and respiration could be conducted by directly incorporating remote sensing based estimates of snow cover area [Tables 2.3 & 2.4]. Due to the scale dependence of NEE, snow and vegetation, it is important that model representations of interactions between snow, vegetation and NEE consider whether discrepancies exist in the spatial scales at which these interactions are observed and modeled, and how uncertainties due to this effect can be mitigated. Remote sensing observations are acquired at a coarse resolution that is more similar to typical model resolutions than the scale at which field observations are acquired, and this may prove beneficial in characterizing snow at an appropriate resolution.

The combination of a process-based model of snow and NEE, and remote sensing observations of snow, would be optimal for representing the response of NEE to changes in snowpack characteristics (e.g. timing of snow on/off, ice layers, metamorphism, changes due to warming events). A process-based approach may also be beneficial in estimating light penetration and its influence on subnivean photosynthesis, and in representing the influence of ice lenses on altering the portion of CO_2 which results from biotic and abiotic releases. The effects of snow metamorphism, snow cover and snow-vegetation interactions on albedo could likewise be simulated using a process-based approach. Representing these snow season processes in models of NEE, as well as interactions between vegetation, meteorological conditions, permafrost, soil carbon content, snow albedo, soil respiration, and photosynthesis, could contribute to an improved understanding of the drivers of Arctic and sub-Arctic NEE.

2.7 Conclusions

In situ studies have indicated that a substantial portion of NEE in the Arctic and sub-Arctic occurs during the snow season (*Zimov et al.*, 1996; *Sullivan et al.*, 2008; *Aurela*

et al., 2004), and that the spatiotemporal dynamics of NEE are influenced by the timing of initial snow fall in autumn (*Euskirchen et al.*, 2012), the timing of final snowmelt in spring (*Buckeridge and Grogan*, 2010; *Morgner et al.*, 2010), and the quantity of snow accumulated (*Sullivan et al.*, 2008; *Nobrega and Grogan*, 2007). The main contribution of this paper has been to provide a summary of the physical processes driving NEE, and in providing strategies for representing these processes in models of NEE [Table 2.3] and selecting an optimal remote sensing approach for characterizing snow season properties [Table 2.4]. Incorporating remote sensing observations of snow season properties of the land surface may assist in both reducing uncertainty in model estimates of Arctic and sub-Arctic NEE, and in providing insights into the complex physical interactions that occur between snow and NEE throughout the snow season.

Understanding the interactions between snow, vegetation and the northern carbon cycle is especially important due to the complex and interconnected reactions of biological, cryospheric, hydrological and atmospheric systems to climate change and rising levels of atmospheric CO_2 [Figure 2.1]. Uncertainty regarding the response of Arctic systems to predicted changes in climate remains one of the most critical issues in Arctic carbon balance research today (*Lafleur and Humphreys*, 2008). Climate change is predicted to cause a rise in temperature and an increase in precipitation (*Christensen et al.*, 2007), which is predicted to result in diminished snow cover extent and greater snow accumulation across the Arctic (*AMAP*, 2011). Deeper snowpacks could accelerate the rate of winter respiration, but a longer growing season may result in greater photosynthetic uptake by vegetation. Changes in vegetation composition are likely to increase the uptake of carbon in short-lived tissues as temperature constraints on productivity are relaxed (*Schlesinger and Lichter*, 2001), but species change may also lead to larger effluxes of CO_2 at Arctic sites since greater shrub prevalence is associated with diminished thermal conductivity of snow (*Sturm et al.*, 2001a). The net influence of climate change on the northern carbon balance therefore depends on the relative magnitude of changes in CO_2 uptake and efflux by soil microbial communities resulting from changes in snow, temperature and vegetation [Figure 2.1]. Model estimates of NEE are thus important for quantifying and understanding the net effect of these cumulative changes.

Predictions for the year 2050 indicate that climate change may bring about an increase in maximum snow depth and a 20% decline in average pan-Arctic snow cover duration, which could increase the rate of both subnivean respiration and photosynthetic uptake in spring and fall (*AMAP*, 2011). The timing of initial snow fall alters the photosynthetic uptake of carbon by vegetation at the end of the growing season (*Euskirchen et al.*, 2012) and changes in the timing of snowmelt can alter the carbon balance of a site (*Morgner et al.*, 2010). Furthermore, permafrost thaw may be accelerated by increased accumulation of

snow or warming temperatures, which can result in effluxes of CO (*Nowinski et al.*, 2010; *Schuur et al.*, 2009). Over the next century, thawing permafrost is predicted to release 16-20%, of soil organic carbon, resulting in large effluxes of CO_2 and CH_4 through aerobic and anaerobic decomposition (*Zhang et al.*, 2008). An increase in snow accumulation would therefore be likely to bring about greater effluxes of CO_2 both through more extensive permafrost thaw and greater rates of soil respiration. Including observations of fractional snow cover at the start and end of season, as well as snow accumulation, could therefore assist in determining how climate driven shifts in precipitation, temperature, snow accumulation and snow duration alter the timing and magnitude of the northern carbon budget.

Extreme winter warming events have already begun to be observed regionally in the Mackenzie Basin (*Cao et al.*, 2007), and these events are predicted to increase in prevalence over time due to climate change (*AMAP*, 2011), which may result in damaged vegetation and diminished photosynthetic uptake during the following growing seasons (*Bokhorst et al.*, 2009). Conversely, diminished snow duration has been observed to increase the uptake of CO_2 at the start and end of the growing season as well as the rate of respiration at an Alaskan tundra site (*Oberbauer et al.*, 1998). Identifying mid-winter melt events, and quantifying the subsequent change in soil temperature, could therefore prove crucial in understanding the response of the carbon cycle to warming winter temperatures.

Previously, studies have assessed the response of the biosphere-atmosphere system to changes in snowcover using a combination of longitudinal field studies (e.g. (*Aurela et al.*, 2004)) and biosphere-atmosphere transfer models (e.g. (*Yang et al.*, 1997)). Process-based ecosystem models have been applied in order to estimate past (*McGuire et al.*, 2001) and future (*Cramer et al.*, 2001) changes in the global carbon balance resulting from climate change and shifts in atmospheric levels of CO_2. As climate change continues to alter northern ecosystems and the relationships between cryospheric and biospheric components of the Earth system, the ability to accurately quantify the Arctic carbon budget and its response to climate change will be crucial. Including remote sensing observations of the cryosphere in models of NEE will allow these models to simulate snow season NEE, and its response to regional cryospheric changes.

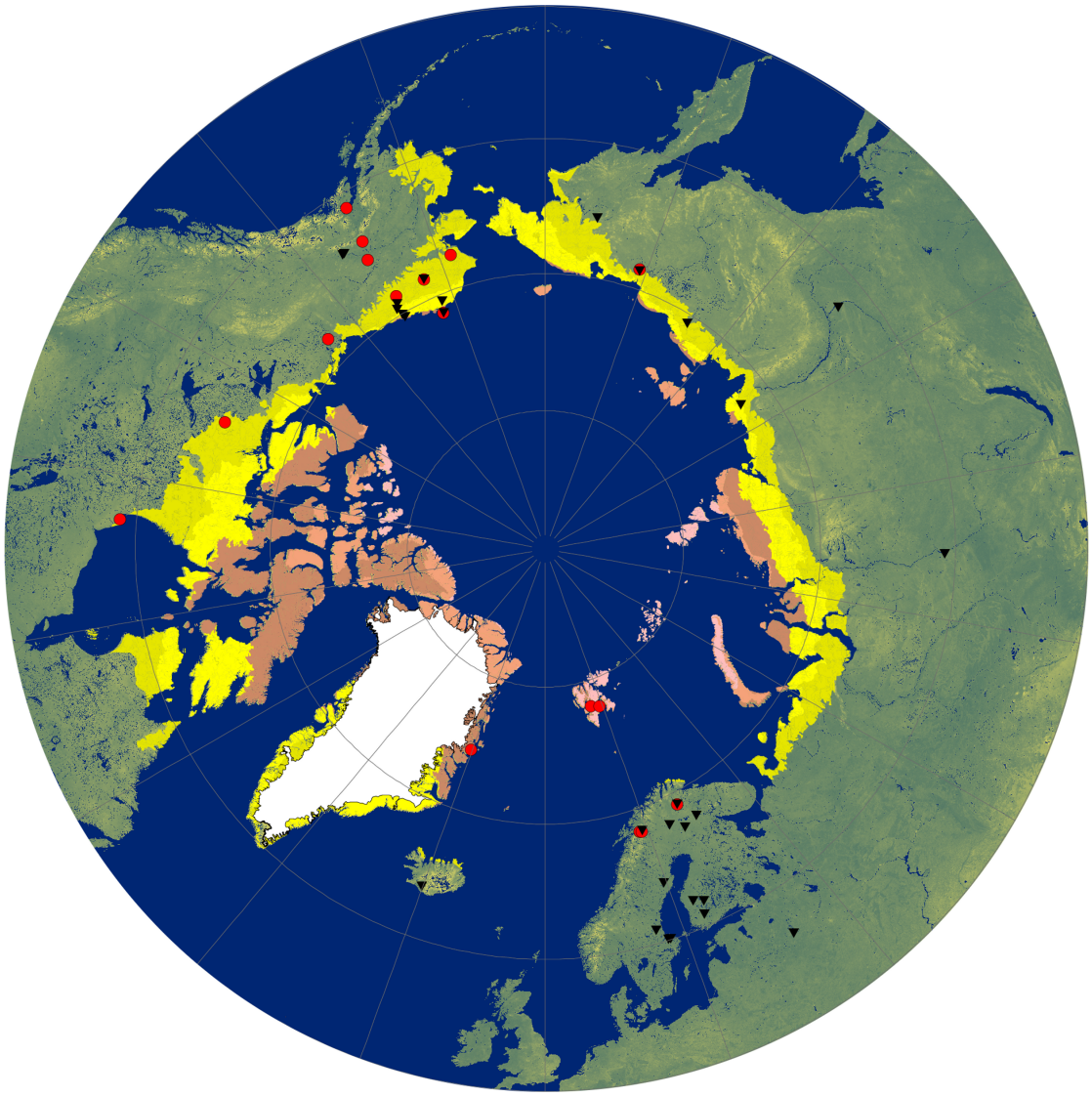

Figure 2.2: Pan-Arctic locations at which field studies of snow season NEE were conducted (red points) and locations of northern Fluxnet stations (black triangles). Regions are defined as low Arctic (yellow), high Arctic (red) and below the treeline (green) according to the Circumpolar Arctic Vegetation Map (*Walker et al.*, 2005). Mean AVHRR NDVI values from the CAVM are shown for regions south of the treeline, where darker shades of green correspond to larger values of NDVI.

Table 2.3: Influences of fractional snow cover area (SCA), snow water equivalent (SWE), soil state as frozen/unfrozen, snow state as wet/dry, ice lenses and snow depth (SD) on NEE, and how remote sensing observations (R.S. Obs.) of the aforementioned snow characteristics can be incorporated into models of NEE in order to represent snow season processes, and thereby reduce uncertainty in estimates of snow season NEE. The Normalized Difference Vegetation Index (NDVI) is suggested as a manner to estimate vegetation biomass from visible and infrared remote sensing observations in order to represent snow-vegetation interactions, where appropriate. Please not that the numbers indicated in brackets refer to sub-sections within Chapter 2.

Processes	Influences on NEE (relevant section)	R.S. Obs.	How to represent processes in models using R.S. Obs.
Soil cooling by snowfall	Diminished respiration and photosynthetic uptake (5.1).	SCA or soil freeze	Soil temperatures could be reduced upon initial appearance of snow or initial soil freezing.
Snow limits photosynth.	Less photosynthetic uptake, especially by trees (4.2).	SCA	Photosynthesis could be reduced in accordance with the fractional snow cover observed.
Litter loss at start of snow season	Respiration in mid to late winter limited by low levels of soil nutrients (5.1).	SCA	Model soil nutrient levels could be initially elevated for the first ~30 days following initial snowfall, then diminished for the rest of the snow season.
Snow limits soil heat loss	Subnivean respiration persists in soils, as these remain warmer than the air (4.1).	SWE or SD	Estimate soil respiration as a function of snow accumulation (SWE or SD) and air temperature.
Snowpack metamorph.	Metamorphism (5.2) and the formation of faceted crystals (4.2) alter subnivean temperature.	SWE and SD	Incorporate observations of snowpack properties (using SWE, SD, vegetation maps, and fieldwork) in estimates of soil respiration.
Formation of tree wells	Tree wells increase the rate of heat loss from soil, which can diminish rates of soil respiration (4.2).	NDVI or LiDAR	Soil respiration could be diminished in regions with dense forest cover (according to growing season NDVI) or where LiDAR observations indicate tree wells.
Extreme winter warming events	Warming first increases rates of soil respiration. Loss of snow thermal gradient. Resulting frost damage to vegetation can limit their photosynthetic capacity (5.2).	Snow state, SCA or NDVI	Mid-winter declines in fractional snow cover area can be indicative of winter warming events. Declines in photosynthetic capacity can be monitored with NDVI, and changes in NPP can be simulated in DGVMs.
Wind/ice layers form	Ice layers limit snow diffusivity, and allow CO_2 to be stored within the snowpack (5.2).	Ice lenses	Ice lenses can be observed using passive microwave observations.
Onset of snowmelt	Respiration increased by warmer temperatures and nutrient availability (5.3). Release of CO_2 from snowpack.	Snow wetness or SCA	Releases of CO_2 and increased rates of respiration following snowmelt can be simulated according to the timing of snow wetness and diminished snow cover.
End of snowmelt	Diminished snow cover and warmer air temperatures allow photosynthesis (4.3).	SCA	Photosynthetic uptake at the end of the snow season can be reduced according to fractional snow cover area.

Table 2.4: Summary of which snow characteristics can be acquired using each remote sensing approach (*Jensen*, 2007). Products which make use of two or more categories of remote sensing observations include IMS (snow cover extent), ANSA (fractional snow cover, SWE & snowmelt) and SMAP (soil freeze/thaw). The main advantages and limitations of each approach are briefly described in terms of their potential for being applied in models of NEE.

Image mode	Active/ passive	Reso-lution	Wavelength	Satellites/ products	Snow/soil characteristics	Advantages	Limitations
Imaging	**passive**	30m - 1 km	Visible (0.4-0.7 µm) and infrared (0.7-15 µm)	**Satellites:** AVHRR MODIS SPOT **Product:** MOD10	Fractional snow cover area, or the timing of snow on/off at the start and end of the snow season	Moderate spatial and temporal (daily-weekly) resolution estimates available of fractional snow cover.	Arctic observations can only be collected during the start and end of the snow season due to polar darkness. Observations of fractional snow cover in spring and fall can be limited by cloud cover, which is especially prevalent at high latitude sites.
		5 - 60 km	Passive microwave (1-200 GHz or 0.15-30cm)	**Satellites:** AMSR-E SSM/I **Product:** GlobSnow SWE	Snow water equivalent (SWE), snow state (wet/dry) and soil freeze/thaw state	Daily observations of SWE are available across the pan-Arctic, and are unhindered by cloud cover or polar darkness.	Coarse spatial resolution (10s of km) inadequate for local scale applications. Accurate estimates of SWE are complicated by wet snow, deep snowpacks and vegetation.
	active	10m-1 km	Active microwave (L, C, X & Ku bands, or 1-2, 4-8, 8-12.5 and 12.5-18 GHz)	**Satellites:** Quick-SCAT ENVISAT /ASAR	Snowmelt onset timing and soil freeze-thaw status	Daily to weekly coverage. Ku scatterometers can estimate regional SWE and snowmelt onset at a coarse resolution. Active and passive microwave observations can be combined to generate estimates of soil freeze/thaw, which affects NEE.	Existing SAR systems (C- and X-band) are not generally applicable for SWE estimation.
		<30 cm	Airborne LiDAR (1.064 & 0.532 µm)	**Satellites:** ICESat/GLAS	Snow depth	Very fine spatial resolution and high spatial sampling frequency can characterize snow and land microtopography.	Prohibitively expensive. Observations are therefore limited to individual study sites, with few observations per snow season.
Non-imaging		70 m (laser) – 10 km (radar)	Satellite altimetry (laser: 1.064 & 0.532 µm, radar: Ku (12-18GHz) & Ka (26.5-40 GHz) bands)	**Satellites:** Topex-Poseidon	Snow depth	Moderate to low spatial and temporal (weekly) resolution. Field studies have described the influence of snow depth on NEE.	Sampling along nadir tracks only. Satellite altimetry is typically used for oceans and ice sheet science applications, rather than terrestrial operational applications.

Chapter 3

Modeling the influence of snow cover on low Arctic net ecosystem exchange

Overview

Arctic net ecosystem exchange (NEE) of CO_2 between the land surface and atmosphere is influenced by the timing of snow onset and melt. Snowpacks influence the rate of respiration by decoupling soil and air temperatures, and hinder the rate of photosynthetic uptake by vegetation at the start and end of the snow season by inducing dormancy and limiting light availability. The objective of this study was therefore to examine whether uncertainty in model estimates of NEE could be reduced by representing the influence of snow on NEE using remote sensing observations of snow cover area (SCA). Observations of NEE and time-lapse images of fractional snow cover collected at a low Arctic site (Daring Lake, NWT) in May–June 2010 were first analyzed in relation to Landsat and MODIS estimates of SCA. As findings indicated good agreement between local and satellite observations of SCA, MODIS estimates of SCA were incorporated into the Vegetation Photosynthesis Respiration Model (VPRM). VPRM was calibrated at Daring Lake using 2005 observations of NEE, shortwave radiation and temperature acquired from eddy covariance and meteorological stations. Estimates of NEE were then generated using model formulations with and without explicit representations of the influence of SCA on respiration and/or photosynthesis. Model performance was assessed relative to unfilled eddy covariance observations from Daring Lake and Ivotuk, AK for years 2004–2007. Uncertainty in VPRM estimates of NEE was reduced when respiration was estimated as a function of air temperature during the growing season, and as a function of soil temperature during the snow season, when soil and air temperatures are decoupled by an overlying snowpack.

3.1 Introduction

In low Arctic regions, the initial onset and final melt of snow mark important transitions in net ecosystem exchange (NEE) (*Olsson et al.*, 2003; *Grogan et al.*, 2004; *Bokhorst et al.*, 2010; *Buckeridge and Grogan*, 2010), where NEE is defined as the biospheric flux of CO_2 into and out of the land surface (*Lovett et al.*, 2006). NEE can be described as the sum of photosynthetic uptake by vegetation (GEE, or gross ecosystem exchange) and ecosystem respiration (R): $NEE = -GEE + R$. According to the sign convention used in this study, uptake of CO_2 from the atmosphere is represented as negative NEE, and release of CO_2 into the atmosphere is shown as positive NEE.

Photosynthetic uptake by vegetation is maximized during the growing season, when above-freezing air temperatures and sunny conditions support plant growth. During snow onset in autumn, the land surface is cooling (*Zhang et al.*, 1996), light availability is limited, and most plants are in senescence, resulting in diminished rates of photosynthesis and respiration (*Billings and Mooney*, 1968; *Carstairs and Oechel*, 1978; *Öquist and Huner*, 2003; *Olsson et al.*, 2003; *Euskirchen et al.*, 2012). Snowpack development decouples soil temperatures (T_{soil}) and air temperatures (T_{air}) (*Bonan*, 2002), allowing subnivean respiration to persist at low T_{air} (*Zimov et al.*, 1993; *Olsson et al.*, 2003). Snow melt in the Arctic normally takes place within a month of the solstice. Light availability is therefore high, and melt is accompanied by warmer T_{air}, soil thaw and greater availability of nutrients. As a result, snowmelt is accompanied by rapid increases in rates of respiration (*Zimov et al.*, 1996; *Mikan et al.*, 2002; *Oelbermann et al.*, 2008; *Elberling et al.*, 2008). Although the length of time between snowmelt and green-up varies by species (*Humphreys and Lafleur*, 2011), the timing of snowmelt at a site influences the timing of photosynthetic uptake by vegetation (*Morgner et al.*, 2010; *Buckeridge and Grogan*, 2010).

Landscape rates of photosynthesis and respiration during snow onset and snow melt are also influenced by the proportion of the land surface which is snow covered at any given point in time (snow cover area, or SCA). Comparisons of NEE at plots with differing quantities of snow have found diminished rates of photosynthesis and respiration during snow onset/melt at plots with greater SCA (e.g. *Buckeridge and Grogan* (2010) and *Morgner et al.* (2010)). Representing SCA in biospheric carbon flux models could therefore allow the snow, transitional and growing seasons to be clearly delimited. Model estimates of NEE during these time periods could therefore be generated by simulating the differing seasonal drivers of NEE for each period. Hence, uncertainty in model estimates of Arctic NEE might be reduced by explicitly representing the influence of SCA on NEE.

Although most model estimates of Arctic NEE do not simulate snow season influences on NEE, several process-based approaches (e.g. (*McGuire et al.*, 2000; *Wania et al.*, 2009;

Gouttevin et al., 2012)) have represented snowpack properties (e.g. density, diffusivity) mechanistically, and have then generated estimates of subnivean respiration in light of these snowpack properties. Findings from such studies indicate that model approaches which represented snowpack properties had lower error rates compared to model approaches which did not explicitly represent snowpack properties. Since >50% of annual low Arctic CO_2 efflux can occur during the snow season (*Mikan et al.*, 2002; *Sullivan et al.*, 2008), the resulting improvements in model performance can have important implications for accuracy in estimates of the Arctic carbon cycle.

To date, model estimates of NEE have not made use of remote sensing observations of snowpack characteristics, although many established approaches exist which would be suitable for inclusion in models of NEE (*Luus et al.*, In press). Specifically, estimates of SCA can be made from visible and infrared remote sensing observations from satellites such as Landsat (*Dozier*, 1989; *Rosenthal and Dozier*, 1996) and MODIS (Moderate Resolution Imaging Spectroradiometer) (*Hall et al.*, 2002; *Hall and Riggs*, 2007; *Riggs and Hall*, 2011). Applying a remote sensing approach to estimating snowpack properties for inclusion in model estimates of NEE offers several advantages over a process-based approach. Incorporating remote sensing observations of snow characteristics in a model of NEE limits the propagation of meteorological biases into estimates of snow characteristics, and allows spatially variability in snow distributions to be captured without having to simulate the many land surface influences on snow accumulation and melt (e.g. topography, aerodynamic roughness).

Estimates of SCA from satellites such as Landsat and MODIS could therefore be incorporated into models of biospheric CO_2 fluxes, potentially improving the representation of respiration and photosynthesis processes. For example, when the land surface is partially snow covered (0% <SCA< 100%) at the start and end of the snow season, photosynthesis could be suppressed according to the percentage of the land surface which is snow-covered, in recognition of the influence of snow on hindering photosynthesis. Incorporating remote sensing observations of SCA could also allow the snow and growing seasons to be delineated clearly and accurately, such that variations in model formulations for respiration and photosynthesis specifically related to snow and no-snow conditions could be simulated. The goal of this research was to explore the potential for incorporating SCA and its effects on biospheric carbon fluxes into the Vegetation Photosynthesis Respiration Model (VPRM), a diagnostic, remote sensing based model designed to provide regional estimates of NEE (*Mahadevan et al.*, 2008). The specific objectives were to examine the feasibility of assimilating MODIS SCA into a model of biospheric carbon fluxes, and to examine whether uncertainty in VPRM estimates of NEE could subsequently be reduced by simulating the influences of SCA on photosynthesis and/or respiration.

3.2 Methodology

Preliminary analysis was conducted using eddy covariance observations of NEE, meteorological observations, and time-lapse camera images acquired in May-June 2010 from Daring Lake, NWT, Canada. The four parameters in the VPRM were then calibrated using 2005 NEE and meteorological observations from the mixed tundra site at Daring Lake. Evaluation of VPRM performance with and without the representation of snow season processes was conducted by running VPRM over years 2004–2007 at two low Arctic sites: Daring Lake and Ivotuk. Model evaluation then consisted of comparing outputs to unfilled eddy covariance observations of NEE from these two sites. Field observations of NEE were filtered only to remove periods of time with low frictional velocity.

3.2.1 Study sites

The Daring Lake site is located in the southern portion of the Northwest Territories at 64°52N, 111 °34'W, ≈200 km northeast of Yellowknife. Daring Lake receives an average of 200-300 mm in precipitation annually, and has a mean annual temperature of -12.5 to -10.5 °C (*Lafleur and Humphreys*, 2008). At this study site, four time-lapse cameras were set to capture thrice daily images of the land surface in May–June 2010 from towers overlooking mixed tundra (MT), fen (FN), lakeside mixed tundra (LK), and tall shrub (SB) vegetation. Observations of NEE were simultaneously acquired from eddy covariance towers at MT and FN in May–June 2010. Measurements of NEE and meteorological variables have been collected at the Daring Lake MT site since 2004. The MT site is underlain by sand to loamy sand textured soil and is composed of shrub tussock tundra and mesic heath. The FN site is a wet sedge meadow with 40 cm of peat soil overlying silt loam textured soil. The dominant vegetation is sedges, with minor amounts of dwarf birch and a moss understory (*Humphreys and Lafleur*, 2011; *Lafleur and Humphreys*, 2008).

Ivotuk is an Ameriflux site located on the North Slope of Alaska at 68°29N, 155°44′, ≈300 km south of Barrow. Eddy covariance observations of NEE and meteorological measurements were collected at Ivotuk from 10/03–10/07. The average temperature and liquid precipitation at Ivotuk are reported within the range of -8.9 to -14.6 °C and 123–221 mm by *Laskowski* (2010). The site is classified as a moist, acidic, tussock tundra site dominated by *Eriphorum vaginatum* and containing shrubs, mosses and lichen (*Thompson et al.*, 2006; *Laskowski*, 2010).

Figure 3.1: Camera images of fractional snow cover over four vegetation types at Daring Lake (from top to bottom: mixed tundra, fen, lakeside mixed tundra and tall shrub) on May 9 (DOY 129), May 31 (DOY 151) and June 3 (DOY 154) 2010.

3.2.2 Calculating snow cover area

Snow cover area was estimated from visible or infrared observations available at three resolutions, from three different sources: time-lapse camera (<10 m), Landsat (30 m) and MODIS (500 m). Although images from both May 1–June 30 2010 and August 30 – December 7 2010 were examined, we focus the analysis of snow-NEE associations on the time period when camera images were acquired simultaneously with meteorological and eddy covariance observations: May 1–June 30 2010. All camera images acquired during this two month time period were individually classified in ENVI/IDL using a combination of supervised parallelepiped and unsupervised isodata classifiers in ENVI. The accuracy of these estimates was assessed visually, and supervised classifications were used in situations where isodata did not perform well. Figure 3.1 shows a selection of time-lapse images from the four locations at Daring Lake at the start, middle and end of snow melt in 2010. From these analyses, a percentage of fractional snow cover was calculated.

Landsat images were collected over the 2004-2007 and 2010 periods in May–June. These images were classified in terms of snow presence/absence using the Normalized Difference Snow Index (NDSI). The NDSI is used to identify snow on the basis that snow reflects less middle-infrared (r_{MIDIR}, 1.55-1.75 μm) than visible (r_{GREEN}, 0.52-0.60 μm) radiation relative to other land surface covers:

$$NDSI = \frac{r_{\mathrm{GREEN}} - r_{\mathrm{MIDIR}}}{r_{\mathrm{GREEN}} + r_{\mathrm{MIDIR}}} \tag{3.1}$$

Regions with NDSI> 0.4 and $r_{0.76-0.90\mu m} > 11\%$ were classified as snow covered, whereas other regions were classified as non-snow covered, as according to *Hall et al.* (1995). The MODIS MOD10A1 fractional SCA product was used as the 500 m estimate of SCA. As Landsat is available on 7-9 day intervals, interpolation was used to generate half-hourly estimates of snow cover. Furthermore, as MOD10A1 daily estimates of SCA were very noisy, the date at which <50% was first achieved was set as the initial date of snow off, and snow depletion was then linearly interpolated.

3.2.3 Incorporating the influence of snow cover in VPRM

VPRM has previously been used to simulate NEE over mid-latitude (south of 56°N) sites in North America (*Mahadevan et al.*, 2008; *Hilton et al.*, 2012). Photosynthetic uptake by vegetation (gross ecosystem exchange, GEE) is calculated according to incoming photosynthetically active radiation (PAR), the fraction of PAR which can be absorbed by photosynthetically active vegetation ($FAPAR_{\mathrm{PAV}}$) and scalar values representing the limiting influences of air temperature (T_{scale}), land surface water (W_{scale}), and phenology (P_{scale}). PAR and T_scale are derived from North American Regional Reanalysis (NARR) downward shortwave radiation and $\mathrm{T_{air}}$ at 2m datasets, whereas $\mathrm{W_{scale}}$, $\mathrm{P_{scale}}$ and $\mathrm{FAPAR_{PAV}}$ are derived from MODIS. $\mathrm{PAR_0}$ and λ are empirically calibrated parameters representing light use efficiency (*Mahadevan et al.*, 2008).

$$GEE = (\lambda T_{\mathrm{scale}} W_{\mathrm{scale}} P_{\mathrm{scale}}) FAPAR_{\mathrm{PAV}} \frac{1}{1 + \frac{PAR}{PAR_0}} PAR \tag{3.2}$$

Respiration is calculated using a piecewise approach. When air temperatures ($\mathrm{T_{air}}$) are warmer than a threshold temperature ($\mathrm{T_{low}}$), respiration is calculated as a linear function of air temperature ($\mathrm{RESP}=\alpha \times \mathrm{T_{air}} + \beta$). When $\mathrm{T_{air}} < \mathrm{T_{low}}$, respiration is set to a low, baseline value that is independent of temperature. $\mathrm{T_{low}}$, α, and β are calculated according to the

relationships observed between NEE and T_{air} in tower observations. NEE is calculated according to the sum of GEE and respiration: $NEE = -GEE + RESP$.

VPRM does not explicitly include the effects of snow cover on respiration and photosynthesis. Instead, respiration is assumed to remain at a constant rate throughout the time period when $T_{air}<T_{low}$, regardless of fluctuations over time in subnivean temperatures. Photosynthesis is diminished under conditions of low T_{air}, EVI or shortwave radiation. MOD10A1 SCA (SCA, 0-100%) was incorporated as a driver dataset into VPRM, and daily estimates of NEE in 2004–2007 at Daring Lake and Ivotuk were then generated using four model formulations, some of which include NARR T_{soil} (at 0-10cm). The α, β, T_{low}, α_{soil}, and β_{soil} parameters were all individually calibrated to eddy covariance observations collected at Daring Lake in 2005. In all of the model formulations below, GEE_0 is used to refer to GEE as calculated in equation 3.2, and $NEE = GEE + RESP$.

i. $\texttt{RESP}_0$ & $\texttt{GEE}_0$:

$$GEE = GEE_0$$

$$R = \begin{cases} T_{air} \geq T_{low} : \alpha T_{air} + \beta \\ T_{air} < T_{low} : RESP_{low} \end{cases}$$

ii. $\texttt{RESP}_0$ & $\texttt{GEE}_s$:

$$GEE = GEE_0(100\% - SCA)$$

$$R = \begin{cases} T_{air} \geq T_{low} : \alpha T_{air} + \beta \\ T_{air} < T_{low} : RESP_{low} \end{cases}$$

iii. $\texttt{RESP}_s$ & $\texttt{GEE}_0$:

$$GEE = GEE_0$$

$$R = \begin{cases} SCA < 50\% : \alpha T_{air} + \beta \\ SCA \geq 50\% : \alpha_s T_{soil} + \beta_{soil} \end{cases}$$

iv. $\texttt{RESP}_s$ & $\texttt{GEE}_s$:

$$GEE = GEE_0(100\% - SCA)$$

$$R = \begin{cases} SCA < 50\% : \alpha T_{air} + \beta \\ SCA \geq 50\% : \alpha_s T_{soil} + \beta_{soil} \end{cases}$$

VPRM performance under these four model formulations was assessed both qualitatively, and statistically. The error ϵ, or difference between predicted (VPRM) and observed (eddy covariance) daily average values of NEE ($\epsilon_i = \text{pred}_i - \text{obs}_i$), was evaluated using two metrics:

the Mean Absolute Error (MAE) and Root Mean Squared Error (RMSE) (*Willmott and Matsuura*, 2005):

$$MAE = n^{-1} \sum_{i=1}^{n} |\epsilon_i| \tag{3.3}$$

$$RMSE = \left[n^{-1} \sum_{i=1}^{n} |\epsilon_i|^2 \right]^{\frac{1}{2}} \tag{3.4}$$

Results were evaluated over two time periods: May 1–June 7 of 2004–2007 (MJ), and the portion of years 2004–2007 when MOD10A1 reported >0% SCA (snow season, or SS).

3.3 Results and Discussion

The feasibility of representing snow season processes in VPRM was addressed by comparing ground-mounted camera observations of SCA to satellite estimates of SCA. Subsequently, reductions in model uncertainty arising from explicitly representing the effects of SCA on NEE are described.

3.3.1 Landsat and MODIS estimates of local snow cover

Time-lapse camera observations of fractional SCA agree well with linearly interpolated Landsat NDSI observations of whether the pixel containing each camera was snow-covered or snow-free [Figure 3.2]. Both Landsat and time-lapse cameras showed snow depletion to occur within a seven day period, with no substantial melts before snow depletion and no snow accumulation following depletion. To assess the agreement between Landsat and MODIS with time-lapse images of fractional snow cover, the timing of 50% snow cover was linearly interpolated from the camera, MODIS and Landsat observations. There was a slight advance or delay of two to five days in MODIS Landsat estimates of depletion relative to the cameras, depending on the site [Table 3.1]. This slight discrepancy is likely due to the coarser resolution of MODIS and Landsat relative to time-lapse camera images. Since lakes melt more gradually than land surfaces, this results in a bias towards late estimates of SCA. However, this slight discrepancy appears reasonably small.

Examination of MODIS SCA tiles containing Daring Lake and Ivotuk found that <10% of each mid-winter scene had false negatives, and <10% of each growing season scene contained false positives. These errors are likely due to low solar angles and cloud edges, respectively, and will be fixed in upcoming versions of MOD10A1 (*Riggs and Hall*, 2011).

	FN	LK	MT	SB
Camera	150	151	151	150
Landsat	155	155	155	148
MODIS	155	155	155	155

Table 3.1: The ordinal date at which SCA is first below 50% according to time-lapse camera observations and interpolated estimates of SCA derived from Landsat and MODIS over four vegetation types at Daring Lake.

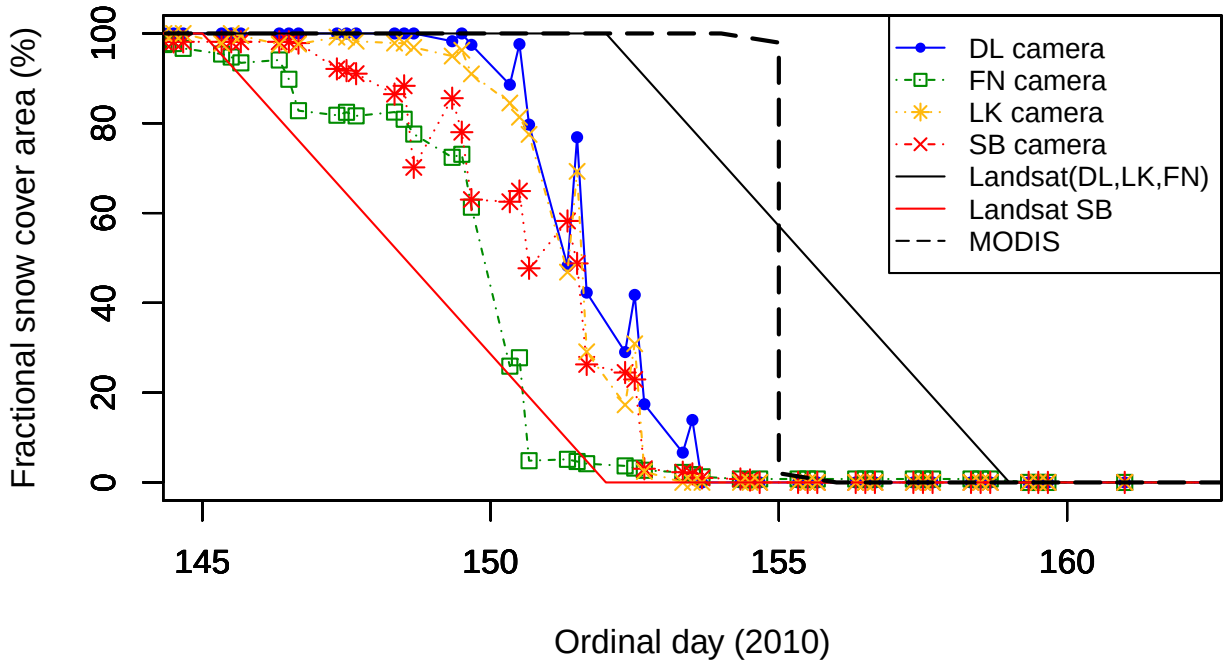

Figure 3.2: Fractional snow cover % over time (May 25–June 11 2010) from classified, thrice daily camera images from four sites Daring Lake, NWT: MT (blue), FN (green), LK (yellow), and SB (red). Landsat derived estimates of SCA appear as straight undotted lines. Landsat SCA for the pixel containing SB is shown in red. Landsat SCA for the pixels containing MT, FN and LK are all indicated in black, as weekly Landsat estimates of snow on/off showed identical values at these three sites.

As snow melt was observed to occur as a single snow depletion event at Daring Lake [Figure 3.2], a locally weighted least squares smoothing algorithm was applied to the MODIS observations to ensure that false negatives or false positives would not appear in mode inputs, and to ensure good agreement between local and coarse (500 m) resolution estimates

of fractional snow cover.

3.3.2 Associations between NEE and SCA

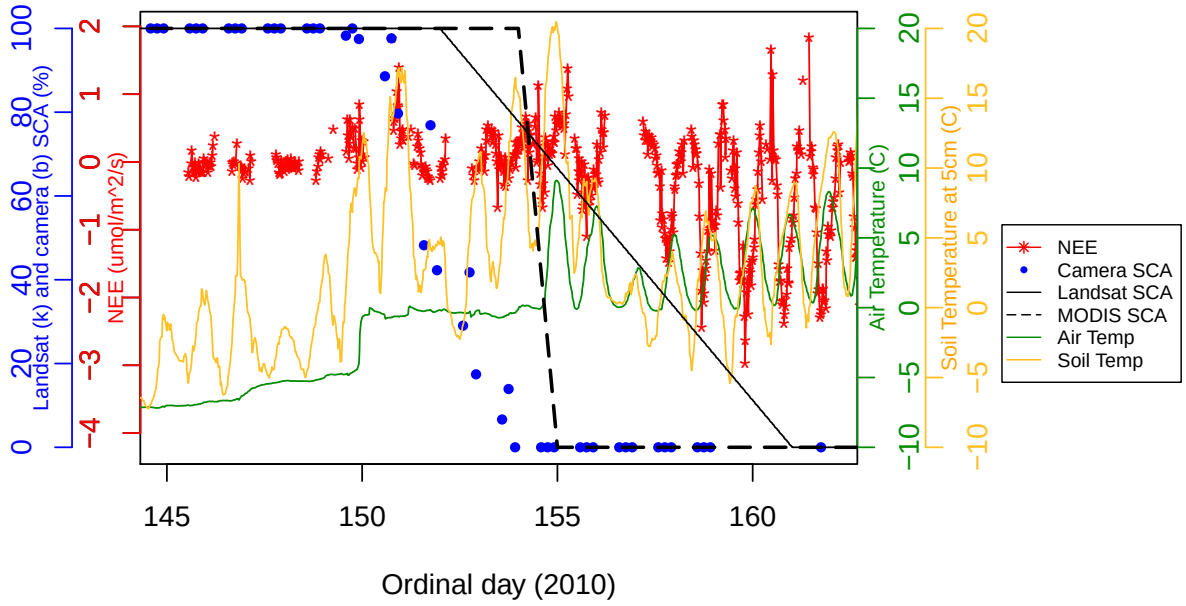

Figure 3.3: Landsat SCA, MODIS SCA, time-lapse camera SCA, NEE, 5 cm soil temperature and air temperature from May 25 – June 11 2010 at the Daring Lake mixed tundra (MT) site.

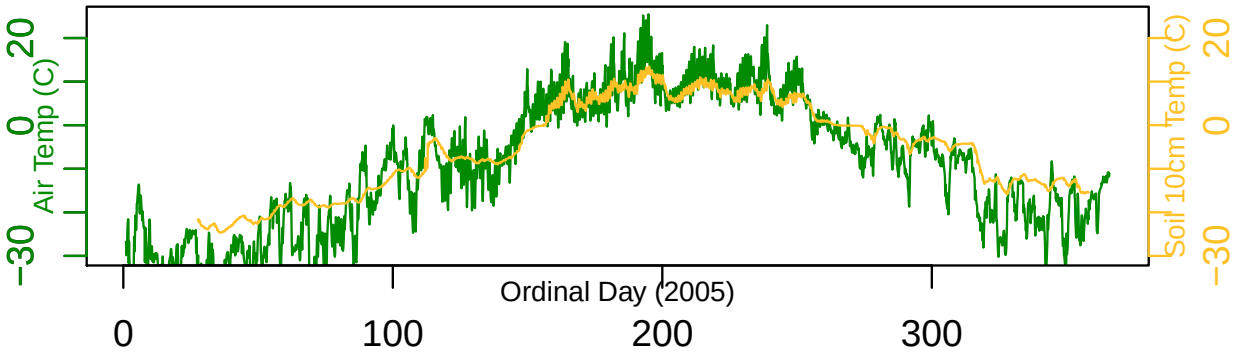

Figure 3.4: Air temperature (green) and 10 cm soil temperature (yellow) over time at Daring Lake MT (2005).

Preliminary investigation of SCA, T_{soil}, air temperature and NEE over time at the Daring Lake MT site indicated several important effects of snow cover area on NEE [Figure 3.3]. Although the low thermal conductivity of snow maintains warmer T_{soil} than T_{air} throughout the middle of winter [Figure 3.4], in the time period immediately preceding snow melt, air temperatures are warmer than T_{soil}. As T_{air} rises, T_{soil} slowly follows to reach a temperature of 0°C, at which point snow melt begins.

A decline in SCA initially increases the rate of CO_2 efflux, leading to greater respiration. T_{air} and T_{soil} become more closely synchronized following snow melt. Once snow melt is complete, vegetation begins to green-up, leading to an increase in the rate of photosynthetic uptake of CO_2. It is therefore possible that model uncertainty may be reduced by representing the influence of snow on hindering photosynthetic uptake by vegetation. Furthermore, as respiration depends on T_{soil} (*Mikan et al.*, 2002; *Oelbermann et al.*, 2008), it is reasonable that subnivean respiration should be estimated as a function of T_{soil} when T_{air} and T_{soil} are decoupled.

3.3.3 VPRM estimates of NEE with and without MOD10A1 SCA

All four VPRM formulations generated reasonable estimates of NEE over Ivotuk and Daring Lake MT in years 2004–2007 (MAE=0.2-0.5 μmol/m^2/s and RMSE=0.6-1.8 μmol/m^2/s). MAEs were similar between the DL-MT and IV sites. RMSE values tend to be greater at the IV site because a greater portion of observations were collected in mid-winter, a time of year in which uncertainty in measurements of NEE is greatest (*Amiro*, 2010).

Uncertainty in VPRM estimates of NEE was reduced when snow season respiration was calculated as a function of T_{soil}, and when snow season photosynthesis was simulated using the original VPRM formulation [Table 3.2]. When considering May–June estimates of NEE, the improved VPRM formulation ($RESP_s$ & GEE_0) had mean MAEs and RMSEs of 0.20 and 0.75 μmol/m^2/s, whereas the original VPRM formulation ($RESP_0$ & GEE_0) had mean MAEs and RMSEs of 0.31 and 0.80 μmol/m^2/s. Likewise, MAEs and RMSEs were diminished throughout the snow season with the improved ($RESP_s$ & GEE_0) VPRM formulation.

These reductions in model uncertainty are important because the extended duration of the winter period in the Arctic means that even small biases in daily average NEE can have a substantial effect on annual estimates of net carbon exchange. Comparisons of the cumulative carbon exchange for each site indicated that the $RESP_0$ & GEE_0 formulation

consistently estimated greater quantities of net carbon efflux than the $RESP_s$ & GEE_0 formulation [Table 3.3].

Time	Site	VPRM form	2004	2005	2006	2007
MJ	DL	$RESP_0$ & GEE_0	0.320 (0.366)	0.408 (0.587)	0.415 (0.742)	0.212 (0.405)
MJ	DL	$RESP_0$ & GEE_s	0.356 (0.417)	0.594 (0.850)	0.422 (0.748)	0.566 (0.727)
MJ	DL	$RESP_s$ & GEE_0	0.223 (0.278)	0.122 (0.392)	0.404 (0.737)	0.083 (0.501)
MJ	DL	$RESP_s$ & GEE_s	0.240 (0.288)	0.303 (0.428)	0.413 (0.740)	0.209 (0.354)
MJ	IV	$RESP_0$ & GEE_0	0.201 (0.968)	0.194 (0.627)	0.517 (0.826)	0.228 (1.845)
MJ	IV	$RESP_0$ & GEE_s	0.247 (1.042)	0.315 (0.623)	0.502 (0.824)	0.103 (1.658)
MJ	IV	$RESP_s$ & GEE_0	0.085 (0.913)	0.045 (0.589)	0.415 (0.741)	0.194 (1.832)
MJ	IV	$RESP_s$ & GEE_s	0.141 (0.935)	0.137 (0.595)	0.417 (0.743)	0.195 (1.832)
SS	DL	$RESP_0$ & GEE_0	0.475 (0.672)	0.307 (0.791)	0.283 (0.603)	0.295 (0.597)
SS	DL	$RESP_0$ & GEE_s	0.517 (0.723)	0.341 (0.837)	0.350 (0.618)	0.364 (0.717)
SS	DL	$RESP_s$ & GEE_0	0.425 (0.649)	0.251 (0.767)	0.258 (0.610)	0.206 (0.613)
SS	DL	$RESP_s$ & GEE_s	0.433 (0.652)	0.286 (0.771)	0.260 (0.611)	0.269 (0.591)
SS	IV	$RESP_0$ & GEE_0	0.270 (0.722)	0.063 (1.163)	0.244 (0.789)	0.045 (1.840)
SS	IV	$RESP_0$ & GEE_s	0.207 (0.775)	0.269 (1.37)	0.229 (0.832)	0.139 (1.801)
SS	IV	$RESP_s$ & GEE_0	0.179 (0.656)	0.185 (1.198)	0.178 (0.808)	0.055 (1.837)
SS	IV	$RESP_s$ & GEE_s	0.193 (0.664)	0.175 (1.199)	0.179 (0.809)	0.055 (1.836)

Table 3.2: Uncertainty in May 1–June 30 (MJ) and snow season (SS) estimates of NEE by VPRM both with ($_s$) and without ($_0$) representations of the influences of snow on respiration and GEE. Results are indicated for the Daring Lake MT calibration site, as well as the Ivotuk validation site, for years 2004–2007. Mean absolute error (MAE) values are indicated first, followed by root mean squared error (RMSE) values in brackets. All error rates were calculated by comparing daily average eddy covariance NEE to daily average model NEE.

Site	VPRM form	2004	2005	2006	2007
DL	$RESP_0$ & GEE_0	0.08	1.61	4.27	-0.86
DL	$RESP_s$ & GEE_0	-3.52	-2.37	0.57	-3.49
IV	$RESP_0$ & GEE_0	5.37	5.22	4.19	4.89
IV	$RESP_s$ & GEE_0	1.36	1.49	0.63	1.03

Table 3.3: Estimates of annual net carbon exchange ($gC/m^2/y$) by different VPRM formulations.

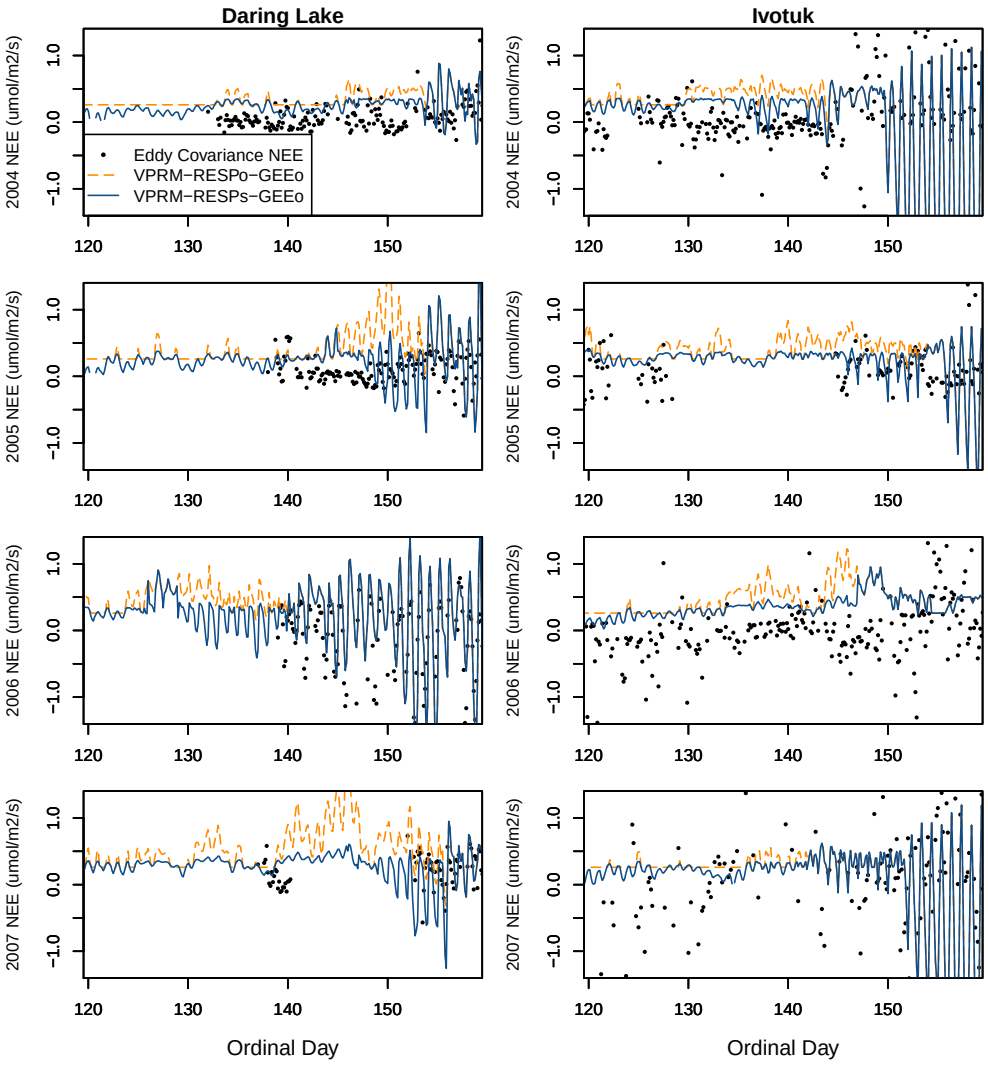

Figure 3.5: NEE from May 1-June 7 of years 2004–2007 at Daring Lake MT (left) and Ivotuk (right) as observed using the eddy covariance technique (black), and as estimated by VPRM both with (blue) and without (orange) a representation of the influence of snow on soil respiration. Within each plot, the date where the model estimates appear to merge represents the day at which SCA initially decreases below 50%. Within each plot, the date where estimates from the two models appear to merge represents the day at which SCA initially decreases below 50%.

Time	Site	VPRM form	2004	2005	2006	2007
MJ	DL	$\texttt{RESP}_{\texttt{Tsoil}}$ Linear	0.662 (1.042)	0.558 (0.830)	0.806 (1.126)	0.583 (0.800)
MJ	DL	$\texttt{RESP}_{\texttt{Tsoil}}$ PWL	0.623 (0.991)	0.520 (0.754)	0.736 (1.021)	0.532 (0.732)
MJ	IV	$\texttt{RESP}_{\texttt{Tsoil}}$ Linear	1.161 (1.753)	1.550 (2.310)	0.619 (0.874)	1.510 (2.073)
MJ	IV	$\texttt{RESP}_{\texttt{Tsoil}}$ PWL	1.110 (1.714)	1.536 (2.293)	0.598 (0.864)	1.512 (2.076)
SS	DL	$\texttt{RESP}_{\texttt{Tsoil}}$ Linear	0.329 (0.476)	0.650 (0.883)	0.367 (0.532)	0.457 (0.659)
SS	DL	$\texttt{RESP}_{\texttt{Tsoil}}$ PWL	0.309 (0.475)	0.605 (0.820)	0.371 (0.528)	0.423(0.609)
SS	IV	$\texttt{RESP}_{\texttt{Tsoil}}$ Linear	0.438 (0.717)	0.802 (1.393)	0.527 (0.819)	1.390 (2.000)
SS	IV	$\texttt{RESP}_{\texttt{Tsoil}}$ PWL	0.422 (0.718)	0.785 (1.378)	0.512 (0.809)	1.379 (1.993)

Table 3.4: Uncertainty in May 1–June 30 (MJ) and snow season (SS) estimates of NEE by VPRM at Daring Lake and Ivotuk, using the alternate formulations through which respiration is calculated year-round as a linear or piecewise linear (PWL) function of T_{soil}. Mean absolute error (MAE) values are indicated first, followed by root mean squared error (RMSE) values in brackets. MAE and RMSE were calculated from daily average observations.

Modeling subnivean respiration as a function of T_{soil} rather than T_{air} prevented the magnitude of respiration from being overestimated at the end of the snow season, when T_{air} was consistently warmer than T_{soil} [Figures 3.3 & 3.5]. This is consistent with previous findings that freeze-thaw temperature fluctuations accompanying snow melt do not substantially influence effluxes of CO_2 (*Grogan et al.*, 2004; *Buckeridge et al.*, 2010). Calculating subnivean respiration as a function of T_{soil} allowed VPRM to simulate both the gradual, steady increase in respiration accompanying snowmelt, and mid-winter declines in soil respiration (*Bokhorst et al.*, 2010).

A natural question, then, is whether uncertainty in estimates of NEE could be similarly reduced by calculating respiration year-round as a function of T_{soil}, without an explicit representation of SCA. VPRM was therefore run under two alternate scenarios, both of which calculated respiration as a function of T_{soil} throughout the snow and growing seasons, and neither of which explicitly represented SCA [Table 3.4]. In the linear formulation, respiration was calculated year-round as a function of soil temperature. In the piece-wise linear formulation, respiration was calculated as a function of T_{soil} when $T_{soil} > T_{low}$, T_{low}=-2.59°C, and was otherwise set to a constant value. Parameters describing the year-round associations between respiration and T_{soil} were set according to observations collected in 2005 at Daring Lake.

VPRM estimates of NEE were then generated for years 2004–2007 over Daring Lake and Ivotuk [Table 3.4]. The RMSE and MAE error rates from the T_{soil} formulations of VPRM

are greater than the error rates from the T_{air} or combined T_{air}/T_{soil} formulations. Both T_{soil} formulations of VPRM underestimate respiration substantially, especially at the start and end of the snow season (SCA$<$ 50%), when T_{air} is substantially warmer and displays greater diurnal variation than T_{soil} [Figures 3.3 & 3.4]. These model formulations then estimate unrealistically large rates of annual net carbon uptake by both sites. Therefore, although estimates of subnivean respiration can be improved by calculating respiration as a function of soil temperature, uncertainty in VPRM estimates of NEE near the start and end of the growing season is reduced when respiration is calculated as a function of T_{air}.

Although snow melt is accompanied by an increase in photosynthesis [Figure 3.3], the subsequent green-up was best captured by the original formulation of VPRM, where snow season photosynthesis is limited implicitly by darkness, cold T_{air} and vegetation senescence. Simulating further reductions in photosynthesis when SCA$>$0% caused VPRM to underestimate GEE. This finding is consistent with *in situ* observations of subnivean photosynthesis in Arctic regions (*Larsen et al.*, 2007b). The RMSEs and MAEs from the $RESP_0$ & GEE_s and $RESP_s$ & GEE_s formulations therefore exceeded those from the formulations which did not further suppress GEE as a linear function of SCA. Overall, the lowest errors were found when the model was run with the $\texttt{RESP}_s$ `&` $\texttt{GEE}_0$ formulation [Figure 3.6]. Although the reductions in error appear minor, these substantially change estimates of net C exchange due to the long duration of the winter season [Figure 3.7].

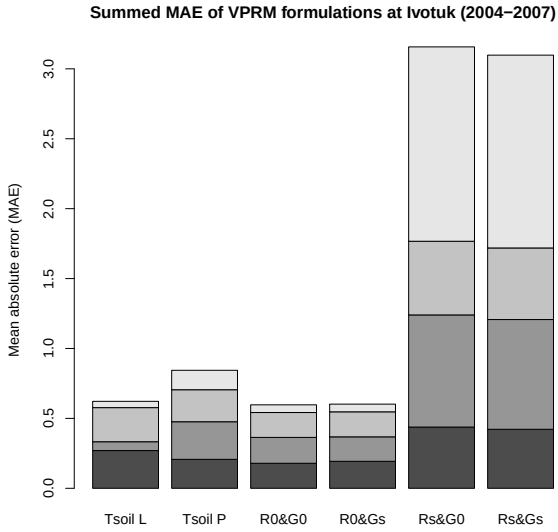

Figure 3.6: Mean absolute error of all model formulations at Ivotuk for the snow seasons of years 2004 (dark grey) to 2007 (light grey).

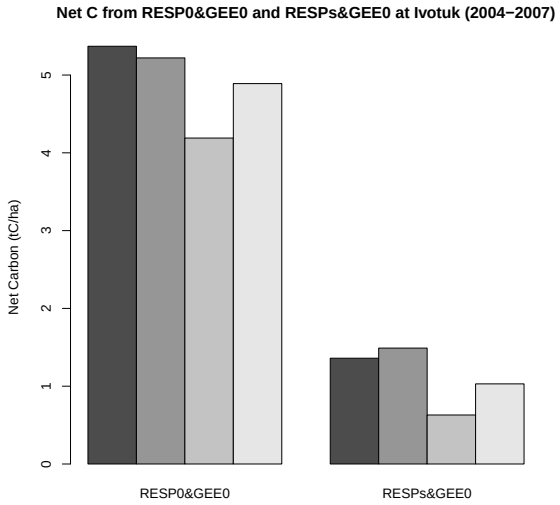

Figure 3.7: Net carbon (tC/ha) predicted in years 2004 (dark grey) to 2007 (light grey) by $\texttt{RESP}_0$ & $\texttt{GEE}_0$ and $\texttt{RESP}_s$ & $\texttt{GEE}_0$.

Climate change is predicted to both increase Arctic snow accumulation and diminish the length of the Arctic snow season (*AMAP*, 2011). Previous studies at Daring Lake have found that natural inter-annual variability in snow melt timing did not markedly affect early or total growing season CO_2 flux (*Humphreys and Lafleur*, 2011), but that plots with artificially increased snow depth and duration showed altered CO_2 fluxes upon snow melt (*Buckeridge and Grogan*, 2010). Incorporating satellite observations of SCA into biospheric carbon flux models could therefore allow the snow and growing seasons to be delineated, enable snow season influences on respiration to be represented, and permit reduced uncertainty in estimates of the Arctic carbon cycle. Insights could therefore be gained into the regional response of the Arctic carbon cycle to altered biological, meteorological and cryospheric conditions.

3.4 Conclusions

In Arctic regions, the timing of snow onset and melt influence the rates of photosynthesis and respiration. The importance of the snow on/off transition suggests that insights into the northern carbon cycle and its response to changing snow conditions may be gained by representing the influence of snow on NEE. The feasibility of incorporating remote sensing observations of snow into models of NEE was demonstrated by findings showing: 1) good

agreement between time-lapse camera (<10 m) and remote sensing estimates of SCA from Landsat (30 m) and MODIS (500 m); and 2) associations between *in situ* NEE and SCA at Daring Lake, NWT.

Uncertainty in VPRM estimates of NEE at two low Arctic sites was reduced by representing the decoupling effects of a snowpack on T_{soil} and T_{air}. Estimating subnivean respiration as a function of T_{soil} prevented respiration from being overestimated when it was limited by cool T_{soil} at the start/end of the snow season, and enabled variability in cold season NEE to be simulated. The timing and magnitude of photosynthesis at the start and end of the snow season were best captured by the original VPRM formulation, which used an indirect approach to simulate the influence of cold temperature, senescent vegetation and diminished sunlight on hindering photosynthesis. The resulting VPRM formulation, containing an implicit representation of the effects of SCA on photosynthesis and an explicit representation of the influence of SCA on respiration, had diminished RMSEs and MAEs across both sites and all years (2004–2007).

Incorporating remote sensing observations of snow cover into VPRM also allowed the snow and growing season to be objectively partitioned, and could enable the model to continue performing in conditions of changing snow regimes. Insights into the response of the Arctic carbon cycle to climate-driven shifts in snow and growing season land surface properties could therefore be gained. Future work will consist of applying the snow season formulation to a variety of sub-Arctic, low Arctic and high Arctic sites in order to determine if model error may be reduced in all cases.

3.5 Acknowledgements

We thank Michael Treberg for assistance in setting up Moultrie I-65 cameras, and gathering *in situ* observations of NEE and snow cover. Logistical assistance from Steve Matthews at Daring Lake was greatly appreciated. We also wish to thank all researchers and field assistants involved in the collection of the valuable datasets at Ivotuk and Daring Lake. Funding from NSERC through a Discovery Grant and a Vanier Canada Graduate Scholarship is gratefully acknowledged.

Chapter 4

Pan-Arctic linkages between snow accumulation and growing season air temperature, soil moisture & vegetation

Overview

Arctic field studies have indicated that the air temperature, soil moisture and vegetation at a site influence the quantity of snow accumulated, and that snow accumulation can alter growing season soil moisture and vegetation. Climate change is predicted to bring about warmer air temperatures, greater snow accumulation and northward movements of the shrub and tree lines. Understanding the response of northern environments to changes in snow and growing season land surface characteristics requires: (1) insights into the present-day linkages between snow and growing season land surface characteristics; and (2) the ability to continue to monitor these associations over time across the vast pan-Arctic. The objective of this study was therefore to examine the pan-Arctic (north of 60° N) linkages between two temporally distinct data products created from AMSR-E satellite passive microwave observations: GlobSnow snow water equivalent, and NTSG AMSR-E Land Parameter (growing season air temperature, soil moisture and vegetation transmissivity). Due to the complex and interconnected nature of processes determining snow and growing season land surface characteristics, these associations were analyzed using the modern non-parametric technique of Alternating Conditional Expectations (ACE), as this approach does not impose a predefined analytic form. Findings indicate that regions with lower vegetation transmissivity (more biomass) at the start and end of the growing season tend to accumulate less snow at the start and end of the snow season, possibly due to interception and shading. Warmer air temperatures at the start and end of the growing season were associated with diminished snow accumulation at the start and end of the snow season. High latitude sites with warmer mean annual growing season temperatures tended to accumulate more snow, probably due to the greater availability of water vapor for snow season precipitation at warmer locations. Regions with drier soils preceding snow onset tended to accumulate greater quantities of snow, likely because drier soils freeze faster and more thoroughly than wetter soils. Understanding and continuing to monitor these linkages at the regional scale using the ACE approach can allow insights to be gained into the complex response of Arctic ecosystems to climate-driven shifts in air temperature, vegetation, soil moisture and snow accumulation.

4.1 Introduction

Interactions between cryospheric, biological and atmospheric components play an important role in the Arctic climate system (*Serreze and Barry*, 2005), and linkages between snow water equivalent (SWE), soil moisture, air temperature and the quantity of vegetation determine the carbon balance of northern regions (*Sitch et al.*, 2007). Northern field studies have determined that snow accumulation is influenced by the snow season climate (*Sturm et al.*, 1995). Snow accumulation is also known to be altered by vegetation species compositions. Patches of shrubs reduce wind speeds, leading to the deposition of wind-blown snow particles and an increase in snow accumulation immediately downwind (*Sturm et al.*, 2001a). Regions with greater quantities of evergreen biomass tend to retain less snow due to interception and sublimation (*Pomeroy et al.*, 2002). Changes in snow accumulation have also been found to alter vegetation species composition at an Arctic tundra site (*Wahren et al.*, 2005), and have been found to result in anomalous soil moisture values over the following growing season in a semiarid area of Eurasia (*Shinoda*, 2001). However, due to the heterogeneity displayed by northern regions as well as the scale dependence of many environmental processes, feedbacks and interactions, the pan-Arctic linkages between snow and growing season land surface properties have not previously been well understood.

A systematic pan-Arctic analysis of these associations over annual and seasonal timescales, and how they vary across vegetation classes, can therefore provide important insights into feedbacks and spatial linkages between snow season and growing season land surface characteristics. Due to the lack of exhaustive coverage by ground-based sampling, understanding the complex response of pan-Arctic environments to climate change relies on the ability to characterize land surface properties using remote sensing observations, and to analyze shifts in the associations between snow and growing properties at the regional to circumpolar resolution. The passive microwave data products analyzed in this study were created by a consortium of researchers led by the Finnish Meteorological Institute (FMI) (e.g. *Luojus et al.* (2009)) and the University of Montana's Numerical Terradynamic Simulation Group (NTSG) (e.g. *Jones and Kimball* (2012)) from Advanced Microwave Scanning Radiometer for the Earth Observing System (AMSR-E) observations. The FMI-based research group produced GlobSnow SWE, and the NTSG group produced AMSR-E Land Parameter growing season estimates of air temperature, soil moisture, vegetation transmissivity and fractional water content. a comprehensive summary of these datasets can be found in Appendix A.2.

The objective of this study was to analyze linkages between GlobSnow SWE and NTSG growing season air temperature, soil moisture and vegetation transmissivity for the entire terrestrial region north of 60°N. The aims were to examine:

- similarities in general tendencies of the land surface between seasons (e.g. do regions that have greater quantities of vegetation also tend to have more SWE?);
- whether regions that experience certain conditions at the end of the growing season tend to receive altered quantities of SWE (e.g. do areas that tend to be warmer at the end of the growing season tend to accumulate less snow in the early portion of the snow season?); and
- associations between snow accumulation at the end of the snow season and land surface variables at the start of the growing season (e.g. do sites with slower snowmelt at the end of the snow season tend to have drier soil moisture at the start of the growing season?).

The modern nonparametric approach of Alternating Conditional Expectations (ACE) was applied to analyze the relationships between each pair of snow and growing season variables from passive microwave observations. As the ACE technique has not yet been widely used in the biogeosciences, a thorough explanation of the theory behind ACE and the strategies used to assess ACE output are provided below.

4.2 Alternating conditional expectations (ACE)

The ACE approach can be used to describe the underlying, non-linear relationships that exist between predictor and response variables (*Breiman and Friedman*, 1985; *Frank and Lanteri*, 1988). Previous work has indicated that the ACE technique can be used to reveal complex relationships that exist in large datasets (e.g. *Gel* (2007)).

A standard linear regression approach provides a least squares estimate of the linear relationship between a response variable (y) and one or more predictor variables (x_j) according to regression coefficients (a_j) and an intercept (a_0):

$$y = a_0 + \sum_{j=1}^{p} a_j x_j \tag{4.1}$$

Techniques such as linear regression and principal component analysis (PCA) are based on the assumption that linear associations exist between response and predictor variables. However, in cases where this assumption is unfounded, applying a linear regression or PCA approach can lead to erroneous or misleading results (*Wang and Murphy*, 2004).

A non-linear approach should therefore be applied whenever it is recognized that only a small portion of the variance in the response variable can be explained using a linear model. One common approach is to apply non-linear transformations (e.g. polynomial, logarithmic, square root) to the response or predictor variables in order to linearize their association, and to then use the transformed output in a linear model. However, selecting the best possible transformation for a given dataset can be challenging, especially over large or noisy datasets, and can be complicated by the fact that the optimal transformation may not be monotonic or of a standard analytic form.

The ACE technique uses an iterative method to find the least squares optimal smoothing functions g and f_j that linearize the association between $g(y)$ and $f_j(x_j)$:

$$g(y) = \sum_{j=1}^{p} f_j(x_j) \tag{4.2}$$

where the g and f_j functions need not be monotonic or of a standard analytic form. By analyzing the shape of the point pairs $[x_j, f_j(x_j)]$ and $[y, g(y)]$, insights can be gained into the underlying non-linear relationships between y and x_j (*Wang and Murphy*, 2004; *Breiman and Friedman*, 1985; *Frank and Lanteri*, 1988).

The optimal smoothing functions g and f_j are identified by minimizing the error function

$$\epsilon^2(g, f_1, \ldots f_p) = E\left[g(y) - \sum_{j}^{p} f_j(x_j)\right]^2 \tag{4.3}$$

through an iterative two-loop process for p predictors. The ACE algorithm uses initial guesses $g^0(y) = \frac{y}{\sqrt{[E(y)^2]}}$ and $f_j^0(x_j) = b_j x_j, j = 1, p$, where b_j are coefficients estimated through ordinary least squares regression. A loop is then used to optimize the predictor transformation function f_j^k where k refers to the iteration:

$$f_j^{k+1}(x_j) = E\left[g^k(y) - \sum_{i \neq j} f_i^k(x_i) | x_j\right] \tag{4.4}$$

Once ϵ^2 fails to decrease, the values of $f_j(x_j)$ have been selected. The response transformation function $g(y)$ is then optimized in an outer loop using the final values of $f_j^k(x_j)$

$$g^{k+1}(y) = \frac{E\left[\sum_j f_j^k(x_j) | y\right]}{\sqrt{E\left[E\left[\sum_j f_j^k(x_j) | y\right]\right]^2}} \tag{4.5}$$

until ϵ^2 again fails to decrease (*Breiman and Friedman*, 1985; *Frank and Lanteri*, 1988). Through this algorithm, the optimal transformations $f_j(x_j)$ and $g(y)$ are identified.

Proof exists that the ACE algorithm results in convergence of f_j and g to their optimal transformations, which need not be either of a specific analytic form or monotonic (*Breiman and Friedman*, 1985; *Frank and Lanteri*, 1988). The resulting output is therefore expressed according to the point pairs $[x_j, f_j(x_j)]$ and $[y, g(y)]$, rather than by a specific mathematical form. Visual analysis consists of examining scatter plots of these point pairs, where each plot indicates the original data values (e.g. y and x_1) relative to their transformed values (e.g. $g(y)$ and $f_1(x_1)$) (*Frank and Lanteri*, 1988). Since the ACE technique finds the least squares optimal values of g and f_j such that the linear association between $g(y)$ and $\sum_{j=1}^{p} f_j(x_j)$ is maximized, it is crucial that the plots of point pairs $[x_j, f_j(x_j)]$ and $[y, g(y)]$ be interpreted relative to one another.

4.2.1 ACE examples

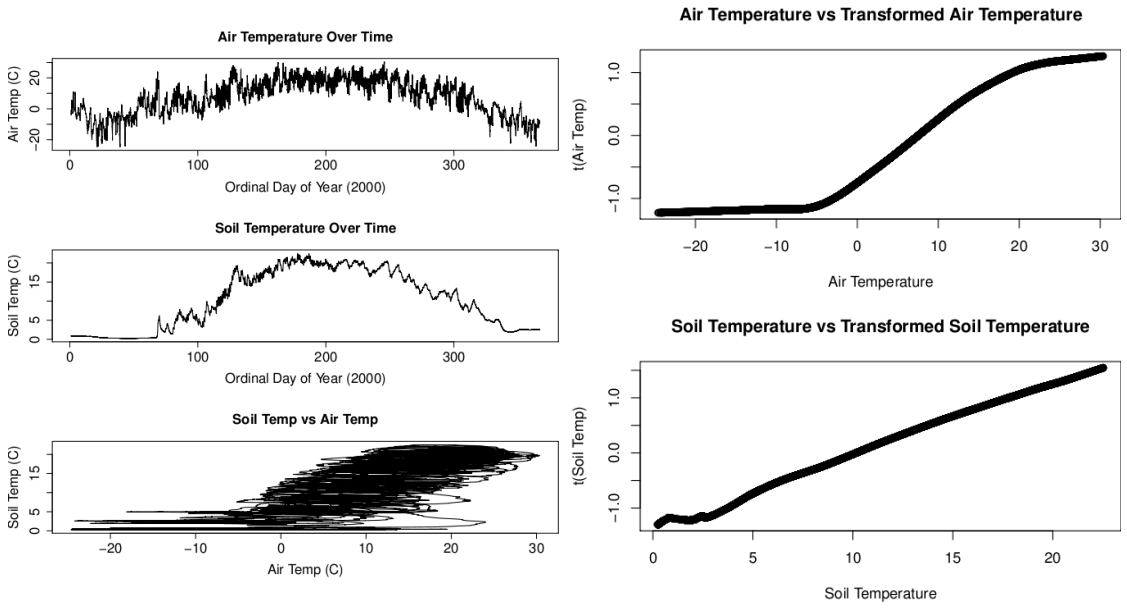

Figure 4.1: First example illustrating the application of the ACE algorithm to input data (**left** – x over time, y over time, x vs. y), and the resulting point pair output (**right** – top:$[x, f(x)]$; bottom:$[y, g(y)]$).

In order to demonstrate how the output from ACE is analyzed, two very simple examples are provided in Figures 4.1&4.2. In both examples, temporal associations are assessed

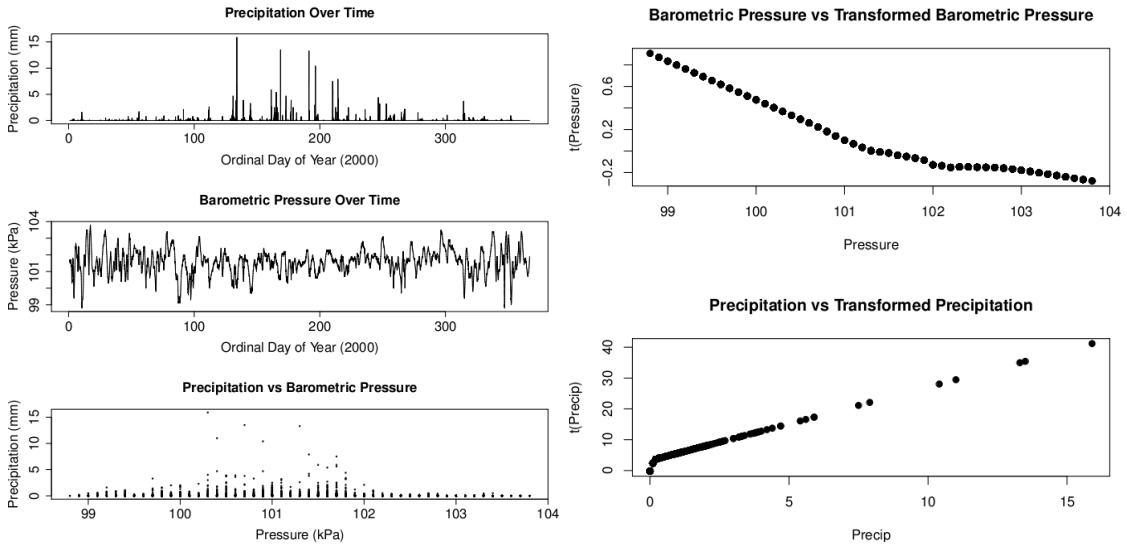

Figure 4.2: Second example illustrating the application of the ACE algorithm to input data (**left** – x over time, y over time, x vs. y), and the resulting point pair output (**right** – top:$[x, f(x)]$; bottom:$[y, g(y)]$).

between two meteorological variables measured at the University of Waterloo Weather Station in 2000. Example 1 focuses on the associations between soil temperature and air temperature, and example 2 describes the associations between barometric pressure and precipitation. The relationships between x and y can be easily detected without the ACE technique in Figure 4.1 but not Figure 4.2.

When both air temperature (x) and soil temperature at 20 cm depth (y) are plotted over time [Figure 4.1 left], examination of these plots indicates that soil and air temperatures are greatest in summer, and that air temperature shows greater diurnal variation than soil temperature in winter. Plotting soil temperature against air temperature (x vs. y) indicates that an approximately linear association appears to exist between these variables at warm air temperatures (≈>-5 °C). Similarly, point pair output from the ACE algorithm [Figure 4.1 right] indicates an approximately positive linear association between soil temperature and transformed soil temperature [y,$g(y)$], and an approximately logarithmic association between air temperature and transformed air temperature [x,$f(x)$] when air temperature is > -5°C.

When analyzed together, these plots of ACE point pair output indicate that a positive association exists between soil and air temperatures. The steepness of the slope in the plot of [x,$f(x)$] appears to diminish at air temperatures above ≈20°C, and below -5 °C.

At subzero air temperatures, an overlying snowpack decouples soil and air temperatures (*Bonan*, 2002), as can be observed in the plots of x and y over time. Similarly, due to the greater diurnal variability of air temperature relative to soil temperature seen in Figure 4.1 left, observations of peak daily air temperature likely do not correspond with as substantial of a peak in daily soil temperature. When considered over all values of x, the slope of $f(x)$ changes shape at air temperatures of x =-5 °C and x =20 °C, and is most strongly positive over intermediate values of x. In other words, if the dataset were to be separated into three bins according to these x values, we could expect that the coefficients from the linear regressions would be largest and most positive at intermediate values of air temperature, and smallest over the coldest values of air temperature.

Likewise, the ACE technique can be applied to find associations within datasets that are not immediately apparent in exploratory plots. When precipitation from a tipping bucket (x) and barometric pressure (y) are plotted over time [Figure 4.2**l**eft], precipitation shows spikes with distinct events whereas barometric pressure varies with greater frequency. As a result, no clear similarity is shown in these plots over time, or when precipitation is plotted against barometric pressure. Point pair output from the ACE approach [Fig 4.2 right] indicates a negative approximately linear association between barometric pressure and its transformed values [x,$f(x)$], and a positive approximately linear association between precipitation and its transformed values [y,$g(y)$]. ACE output therefore shows the tendency for greater quantities of precipitation to be received at lower barometric pressures.

These simple examples were specially selected such that the associations between x and y could be easily identified with and without ACE [Figure 4.1], and such that the associations between [x,$f(x)$] and between [y,$g(y)$] could be described as linear [Figure 4.2]. Conversely, when the ACE approach is applied to assess associations in the GlobSnow SWE and NTSG AMSR-E Land Parameter datasets, the relationships are complex, and non-linear. Likewise, the shape and strength of associations shown in plots of [x, $f(x)$] and [y, $g(y)$] cannot be visually interpreted from plots of [x, y]. The ACE technique therefore provides insights into associations between x and y that could not be gained through the application of techniques that rely on assumptions about the underlying shape of associations.

4.3 Methodology

GlobSnow SWE and NTSG growing season land surface variables were first prepared for analysis and partitioned into vegetation classes. An exploratory analysis was conducted to examine the linear spatial relationships between datasets. The modern nonparametric

method of Alternating Conditional Expectations (ACE) was then applied to examine the potentially non-linear pan-Arctic linkages between SWE and growing season air temperature, soil moisture and vegetation transmissivity.

4.3.1 Data preparation

Preliminary data processing consisted of identifying the start and end dates of the snow season and growing season independently for each 25 km pixel, and each year (2003–2008) as defined by the NTSG and GlobSnow products. Observations from the NTSG product were only used during the period of time when the ground was unfrozen and snow-free according to both the NTSG and GlobSnow products. Conversely, the GlobSnow observations of SWE were only used for the period of time when the ground was frozen and dry snow was present, ranging from the date in autumn when SWE >0 mm was first observed up until the date in spring when the last observation of SWE >0 mm was recorded. The mean annual (2003–2008) values could therefore be calculated, along with mean values for the first thirty days and last thirty days of the snow and growing seasons for each year. As the GlobSnow version 0.9.1 product sets SWE to 0 mm on days where wet snow is observed, smaller values of SWE at the start or end of the snow season are indicative of less snow accumulation or more gradual snow onset/melt. Terrestrial regions with $>50\%$ fractional cover of open water according to the NTSG growing season dataset were masked out of analysis.

4.3.2 Vegetation classes

As vegetation classes are often used to describe snow and growing season characteristics of the land surface, associations between snow and growing season variables were analyzed within seven Arctic vegetation classes defined using two well established categorizations: the SYNMAP (*Jung et al.*, 2006) and the Circumpolar Arctic Vegetation Map (CAVM) (*Walker et al.*, 2005). As CAVM is only available north of the treeline, SYNMAP was first used to classify the entire pan-Arctic, but was substituted with CAVM categorizations where available. The resulting 67 classes were then reorganized into seven vegetation classes shown in Table 4.1. Each 25 km pixel in the NTSG and GlobSnow datasets was then classified according to its fractional vegetation class from the upsampled CAVM-SYNMAP classification.

In order for the analysis to proceed, it was important to first ensure that the aforementioned vegetation classes represent distinct populations of SWE, soil moisture, air

Table 4.1: Aggregation of forest SYNMAP and CAVM vegetation classes into a categorization that divides the pan-Arctic into seven broad vegetation classes: evergreen forest (EVGRN), deciduous forest (DECDS), mixed forest containing shrubs or grasses (MFRST), shrub dominated region (SHRUB), graminoid tundra (GRMTD), shrub tundra (SRBTD), barren vegetated region (BARRN). Regions of water or permanent snow and ice (MASKD) are excluded from the analysis.

Veg class	Source	Description
EVGRN	SYNMAP	Trees needle evergreen; trees broad evergreen; trees mixed evergreen
DECDS	SYNMAP	Trees needle deciduous; trees needle mixed; trees broad deciduous; Trees broad mixed; trees mixed deciduous; trees mixed mixed
MFRST	SYNMAP	Trees and shrubs; trees and grasses; trees and crops; crops
SHRUBS	SYNMAP	Shrubs; shrubs and crops
SRBTD	SYNMAP	Shrubs and barren
SRBTD	CAVM	Prostrate dwarf-shrub, herb tundra; erect dwarf-shrub tundra; Low-shrub tundra
GRMTD	SYNMAP	Grasses; grasses and crops
GRMTD	CAVM	Rush/grass, forb, cryptogam tundra; graminoid, prostrate dwarf-shrub, forb tundra; Prostrate/hemiprostrate dwarf-shrub tundra; nontussock sedge, dwarf-shrub, moss tundra; tussock-sedge, dwarf-shrub, moss tundra
BARRN	SYNMAP	Grasses and barren; barren
BARRN	CAVM	Cryptogam, herb barren; cryptogam barren complex (bedrock); Sedge/grass, moss wetland; sedge, moss, dwarf-shrub wetland; Sedge, moss, low-shrub wetland; noncarbonate mountain complex; Carbonate mountain complex
MASKD	SYNMAP	Urban; Snow and ice
MASKD	CAVM	Nunatak complex; glaciers; water; lagoon

temperature and vegetation transmissivity, and that the interannual variability of each land surface characteristic was small enough that mean 2003–2008 values could be analyzed. Furthermore, it was important to assess whether the vegetation classes represented distinct populations of vegetation net primary productivity.

Analysis of the heterogeneity of distributions of AMSR-E derived variables were assessed between years and between vegetation classes using Levene's test (*Levene*, 1960). Briefly, Levene's test examines the validity of the null hypothesis that two or more groups have equal variance (homoscedasticity). Rejection of the null hypothesis is indicative of heterogeneity of distributions (heteroscedasticity). Levene's test was selected because it provides an assessment of the deviation of an observation from a group mean, is robust

to non-normality, and has been used for a variety of scientific applications, including environmental sciences (*Gatswirth et al.*, 2009). Findings indicated that heterogeneity of variances existed across vegetation classes (p-value $< 10^{-5}$) [Table 4.2], and that homogeneity of variances existed between years ($0.5 \leq p$-value ≤ 0.99). Analysis could therefore proceed by aggregating mean 2003–2008 values, and by assessing linkages separately for each vegetation class.

Table 4.2: Results from Levene's test examining homogeneity of variances of all variables within seven vegetation classes (Table 4.1), and a class containing permanent snow and ice which is masked from analysis (MASKD). These variables are air temperature (TA), volumetric soil moisture (MV), vegetation transmissivity at 10.7 GHz (TC10), and snow water equivalent (SWE). All p-values are $< 10^{-5}$.

	TA	MV	TC10	SWE
EVGRN	2.52	1.06×10^{-3}	4.26×10^{-3}	898
DECDS	1.92	9.25×10^{-4}	3.76×10^{-3}	556
MFRST	1.77	8.35×10^{-4}	3.23×10^{-3}	620
SHRUB	2.46	8.27×10^{-4}	4.76×10^{-3}	675
GRMTD	5.77	6.71×10^{-4}	1.13×10^{-2}	790
SRBTD	4.73	4.90×10^{-4}	1.03×10^{-2}	437
BARRN	6.21	6.67×10^{-4}	1.20×10^{-2}	327
MASKD	6.52	5.56×10^{-4}	8.71×10^{-3}	279
Test statistic	48.4	24.5	67.1	22.3

4.3.3 Exploratory analysis

A brief exploratory analysis of mean values for each variable over the 2003–2008 time period [Figure 4.3a–f] indicated that growing season air temperature and vegetation opacity display a latitudinal gradient, with cooler temperatures and less vegetation at high latitudes, likely due to the temperature dependence of Arctic vegetation (*Hare*, 1968; *Ritchie and Hare*, 1971). Soil moisture and snow water equivalent show greater spatial variability due to topographic, meteorological, atmospheric, and land surface influences (*Callaghan et al.*, 2011; *Serreze and Barry*, 2005).

Greater values of SWE occur in regions where more snowfall occurs, where windblown snow is accumulated, or where snowmelt during the snow season is less frequent or less substantial. Ideally, these contributions to SWE could be partitioned so that the linkages between growing season variables with snowfall, snowmelt and windblown snow deposition

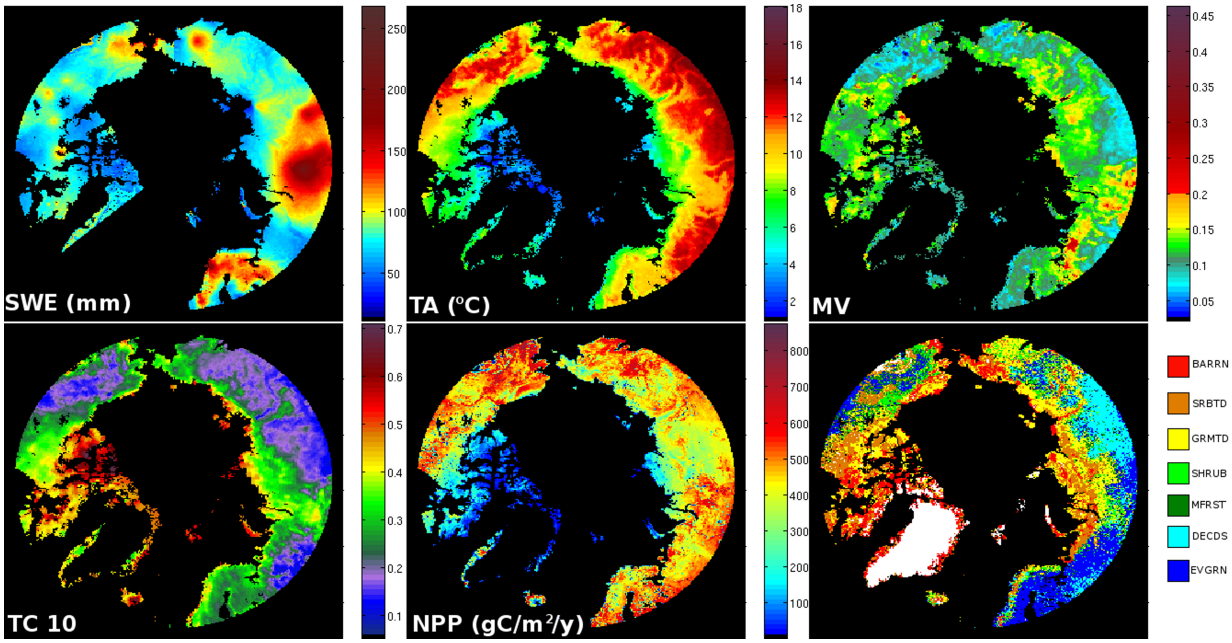

Figure 4.3: Pan-Arctic (north of 60°): a) mean 2003-2008 snow season GlobSnow snow water equivalent (SWE); b-d) mean 2003-2008 NTSG growing season air temperature (TA), volumetric soil moisture at 2cm (MV), and vegetation transmissivity at 10.7 GHz (TC10); e) 1982-2000 mean GloPEM net primary productivity (NPP); and f) vegetation classes used in this study, as described in Table 4.1.

could be analyzed; however, current estimates of precipitation are presently unreliable at high latitudes, especially during the snow season, and the amount of snow must therefore be examined in terms of SWE alone. It is important to note that mean values of SWE at the start and end of the snow season are thus indicative of both accumulation as well as the speed of snow onset/melt. At the start and end of the snow season, mean values of SWE are greater at sites where snowmelt and snow accumulation occur more rapidly, as these have fewer days with low reported values of SWE. Similarly, low values of SWE at the start or end of the snow season are indicative of less snow accumulation, or slower snow onset or melt.

4.3.4 Preliminary regression analysis

Preliminary regression analysis consisted of applying linear regression and principal component analysis (PCA) to assess the possibility of linear relationships between snow and growing season values. However, it is likely that the assumption of linearity cannot be fulfilled, and in addition, application of the Shapiro-Wilk test (*D'Agostino and Stephens*, 1986) indicated that the soil moisture and air temperature datasets had non-normal distributions at high latitudes (p-values < 0.01). Linear regression and PCA therefore do not represent suitable techniques for examining associations between the GlobSnow SWE and NTSG land surface variable datasets, but the findings from these approaches are of interest because PCA and linear regression are widely used to examine environmental linkages. The derived R^2 from classical single and multiple linear regressions [Table 4.3] along with the multiple linear regression of SWE vs factor scores obtained from the principal component analysis (PCA) of air temperature (TA), volumetric soil moisture (MV), and vegetation canopy transmissivity (TC) [Table 4.4] indicated that the linear associations between SWE and growing season variables were very weak or non-existent.

Conversely, a multivariate ACE analysis of these associations yielded much greater R^2 values for every vegetation class and time period relative to the linear regression [Table 4.5], while a univariate ACE analysis indicated highly significant (p-value $< 10^{-5}$) pairwise associations for all vegetation classes, variables and time periods. Moreover, the p-values of all coefficients in multivariate ACE analysis were also highly statistically significant. As a result, we can conclude that there exists no collinearities in the non-parametrically transformed growing season variables when these are transformed to linearize their associations with transformed values of SWE. The findings from this stage of preliminary regression analysis strongly support the employment of the non-parametric ACE technique to explore the non-linear associations within this dataset.

4.3.5 ACE

The ACE approach was applied to determine the strength and directionality of the associations between SWE and growing season values for each vegetation class and time period separately. Associations between these datasets could therefore be examined despite their lack of temporal overlap by comparing: (1) mean growing season with snow season values; (2) mean values of SWE over the last thirty preceding the onset of snowmelt with mean land surface values over the first thirty days with a snow-free and unfrozen land surface following snowmelt; and (3) mean land surface variables over the last thirty days of the

Table 4.3: R^2 values from the linear regressions of SWE and air temperature (TA), SWE and volumetric soil moisture (MV), and of SWE and vegetation transmissivity at 10.7 GHz (TC). Comparisons of SWE and growing season observations were conducted by comparing mean annual 2003–2008 values (mean), and by examining associations between SWE at the end of the snow season with growing season variables at the start of the growing season (spring), and between growing season variables at the end of the growing season with SWE at the start of the snow season (autumn). R^2 values in single linear regression that correspond to a p-value >0.01 are marked with an asterisk.

Var	Time	EVGRN	DECDS	MFRST	SHRUB	GRMTD	SRBTD	BARRN
TA	Annual	0.00	0.01	0.00*	0.02	0.11	0.04	0.20
TA	Spring	0.06	0.01	0.13	0.14	0.16	0.14	0.10
TA	Autumn	0.13	0.12	0.22	0.13	0.06	0.10	0.06
MV	Annual	0.02	0.01	0.01	0.02	0.010	0.02	0.00*
MV	Spring	0.01	0.00*	0.00	0.00*	0.00*	0.00*	0.00
MV	Autumn	0.05	0.06	0.01	0.01	0.00	0.00	0.00
TC	Annual	0.05	0.02	0.02	0.17	0.06	0.05	0.15
TC	Spring	0.20	0.11	0.23	0.28	0.20	0.19	0.18
TC	Autumn	0.16	0.28	0.22	0.16	0.02	0.06	0.03
(TA,	Annual	0.09	0.07	0.07	0.23	0.15	0.07	0.26
MV,	Spring	0.01	0.01	0.00	0.01	0.08	0.06	0.14
TC)	Autumn	0.13	0.11	0.08	0.12	0.04	0.02	0.08

Table 4.4: R^2 values from the multiple linear regression of SWE vs factor scores obtained from the principal component analysis (PCA) of TA, MV, and TC. The retained principal components (PC) are determined based on the proportion of explained variance, i.e. only PC accounting for $> 10\,\%$ of the total variance are included.

Time	EVGRN	DECDS	MFRST	SHRUB	GRMTD	SRBTD	BARRN
Annual	0.03	0.05	0.07	0.10	0.11	0.07	0.24
Spring	0.01	0.01	0.00	0.01	0.08	0.06	0.14
Autumn	0.13	0.11	0.08	0.12	0.04	0.02	0.08

growing season before snow onset with mean values of SWE occurring after the first observation of dry snow on frozen ground after the end of the growing season. These time periods are referred to as "mean", "spring" and "autumn", respectively, throughout the paper.

Table 4.5: R^2 values of ACE transformed SWE and ACE transformed air temperature (TA), volumetric soil moisture (MV) and vegetation canopy transmissivity (TC). Linkages are indicated using observations collected over three non-overlapping time periods of the snow and growing seasons. Associations are therefore indicated between mean annual values of SWE and growing season values, and between mean SWE 30 days prior to snowmelt and growing season values 30 days following full snowmelt (Spring), and vice versa (Autumn). In the multivariate case, the p-values of all coefficients are statistically significant. All p-values corresponding to the pair-wise ACE transformations are $< 10^{-5}$.

Var	Time	EVGRN	DECDS	MFRST	SHRUB	GRMTD	SRBTD	BARRN
TA	Annual	0.08	0.04	0.06	0.04	0.33	0.20	0.38
TA	Spring	0.09	0.04	0.15	0.16	0.17	0.15	0.12
TA	Autumn	0.16	0.14	0.25	0.17	0.07	0.10	0.06
MV	Annual	0.05	0.07	0.05	0.05	0.03	0.02	0.09
MV	Spring	0.04	0.02	0.03	0.17	0.08	0.06	0.05
MV	Autumn	0.06	0.12	0.10	0.08	0.09	0.06	0.07
TC	Annual	0.10	0.03	0.12	0.26	0.25	0.19	0.29
TC	Spring	0.22	0.19	0.24	0.31	0.21	0.22	0.19
TC	Autumn	0.17	0.30	0.27	0.19	0.04	0.09	0.06
(TA,	Annual	0.20	0.33	0.13	0.34	0.37	0.29	0.47
MV,	Spring	0.07	0.14	0.02	0.06	0.17	0.11	0.19
TC)	Autumn	0.16	0.13	0.11	0.17	0.10	0.07	0.12

4.3.6 Limitations

The AMSR-E derived products analyzed in this study are all established products that have been individually validated, as summarized in Appendix A.2. However, the retrieval of accurate estimates of land surface properties from satellite passive microwave observations remains an area of ongoing scientific progress, and uncertainties therefore exist in these estimates. Presently, GlobSnow passive microwave retrievals of SWE are considered reliable over the 15-150 mm range in forested regions, and from 15 to 130 mm in tundra regions. SWE tends to be underestimated over thicker snowpacks. Analysis of the shape of the associations between SWE and growing season variables therefore focuses primarily on values of SWE within these ranges. Furthermore, although the growing season datasets have been found to perform reasonably well, there inevitably exist uncertainties in these datasets. The approach employed in this study takes into account the fact that these uncertainties exist, and therefore only compares relative values which are averaged over given time periods. For example, it is not assumed that estimates of SWE are highly

accurate over very thick snowpacks, but that areas with greater mean reported values of SWE will, in fact, tend to have more snow accumulation than regions with smaller mean reported values of SWE.

The strength of conclusions drawn from the ACE approach is limited due to uncertainties in passive microwave estimates of land surface properties, and due to the inherently weak associations existing between snow and growing season land surface properties as a result of numerous confounding factors (e.g. soil type, vegetation species composition, rainfall, permafrost). Furthermore, although field studies can reveal insight into the exact processes determining land surface properties, an assessment of similarities in coarse resolution (25 km) passive microwave derived estimates of the land surface cannot reveal specific processes. All results presented are therefore discussed in relation to existing literature on *in situ* processes to suggest. Similarities are often found between the associations derived from ACE and observed *in situ*; in these cases, it is likely that the same mechanisms and processes observed at the field scale are dominating regional scale land surface conditions. However, it is beyond the scope of this approach to provide definitive conclusions on regional scale processes.

Finally, the relationships observed through the ACE analysis could be applied to generate estimates within the 2003-2008 time period. However, since these ecological linkages may be altered under changing climate regimes, the ACE derived empirical relationships cannot be used to predict future behaviour. Numerous studies have applied process-based models to predict the response of high-latitude regions to climate change, and this remains an important area of research. The ACE technique could, however, be applied to monitor the strength and directionality of ecological linkages in order to shed light on the response of northern environments to ongoing changes in snow and growing season conditions. The role fulfilled by the analysis presented in this paper therefore fills a gap in literature, but is in no way a replacement for ongoing improvements in passive microwave derived estimates of land surface properties, *in situ* investigations of processes, or predictions of how climate change may affect Arctic regions.

4.4 Results

Findings from the ACE analysis of associations between SWE, air temperature, soil moisture and vegetation transmissivity are presented and discussed below in relation to in situ observations. The results have been divided into separate sections according to the growing season values associated with SWE, with subsections corresponding to different time periods. Each section contains tables showing the strength of associations (R^2 value) of

ACE transformed SWE and growing season values [Table 4.5], and plots indicating the optimal transformations of SWE and growing season values according to the seven vegetation classes [Figures 4.4–4.6].

4.4.1 Air temperature and SWE

At tundra sites, a positive, non-linear association exists between mean annual SWE and mean growing season temperatures such that sites which tend to be slightly warmer tend to accumulate more snow than cooler sites. Yet, sites that tend to be warmer at the start and end of the growing season tend to contain less snow during initial snow onset and final snow melt each year.

North of the treeline, greater mean annual SWE with warmer growing seasons

The associations between mean 2003–2008 SWE and growing season air temperature at tundra sites are non-linear. As a result, findings from the linear regression approach indicate weaker associations at tundra sites (R^2 = 0.04–0.20) [Table 4.3] than detected by the ACE transformations (R^2 = 0.20–0.38) [Table 4.5]. The associations between growing season air temperature and SWE are weaker over forested regions, likely due to seasonal discrepancies in the mean growing season and mean snow season air temperatures (*Overland et al.*, 1997; *Rigor et al.*, 2000; *Adams et al.*, 2000; *Serreze and Barry*, 2005). The following analysis therefore focuses mainly on the associations observed north of the treeline, although all plots can be found in Figure 4.4.

Examinations of Figure 4.4e–g indicate sharp, positive transformations applied to low values of SWE (<75 mm). Likewise, these plots show that the positive association between air temperature and SWE at these locations exists for sites with a mean annual growing season temperature of <10 °C. Analysis of the ACE transformations provides an important source of information for understanding these linkages. Arctic tundra regions are characterized by very cold temperatures during the snow season that limit the availability of water vapor and the rate of precipitation (*Bonan*, 2002; *Serreze and Barry*, 2005), thereby resulting in diminished accumulation of snow, and it is likely that the influence of diminished water vapor explains the association between SWE and growing season air temperature. Analysis of the ACE transformations therefore indicates that in tundra regions with <75 mm of SWE and mean growing season temperatures of 0–10 °C, sites that tend to have slightly warmer air temperatures will likely tend to accumulate greater quantities of SWE.

Warmer spring/autumn temperatures and less SWE

ACE analysis indicated that weak, approximately linear associations exist between warmer air temperatures and diminished SWE at the start and end of the snow season [Table 4.5]. Regions that tended to be warmer at the start and end of the snow season therefore tended to have less SWE at the start and end of the snow season, or more gradual snow onset or melt.

The associations between autumn SWE and air temperature were found to be weaker over tundra regions (ACE $R^2 = 0.06$–0.10) than forested regions (ACE $R^2 = 0.14$–0.25). As forest soils have been observed to be warmer and to freeze more gradually than tundra soils at the start of the snow season (*Rouse*, 1984; *Smith et al.*, 1998), it is likely that the influence of antecedent growing season temperatures on the capacity of a dry snowpack to develop at the start of the snow season would be stronger over regions without permafrost.

Whereas the associations between SWE and air temperature are stronger in autumn over forested regions, these associations are weaker over forested regions (ACE $R^2 = 0.04$–0.15) than areas north of the treeline (ACE $R^2 = 0.12$–0.17) [Table 4.5]. High latitude Arctic sites undergo rapid snowmelt due to the low shading of Arctic vegetation (*Pomeroy and Dion*, 1996), and similarity in the timing of the summer equinox and date of snowmelt (*Bonan*, 2002). As these effects are stronger at high latitude sites, it is reasonable that the most rapid snowmelt would be observed in regions north of the treeline.

4.4.2 Soil moisture and SWE

Although the ACE transformed associations between mean annual SWE and mean growing season soil moisture are weak across all vegetation classes (0.02–0.09) [Table 4.5], an examination of the shape of these non-linear associations indicates a positive association between mean annual SWE and soil moisture at sites with very low SWE (< 90 mm) and low soil moisture (< 0.17), with thresholds that correspond with in situ observations. When output from ACE transformations are considered over this range of SWE and soil moisture values, R^2 values of 0.08 can be observed over barren vegetated regions. The seasonal associations between SWE and soil moisture are complex, resulting in deeper freezing and faster runoff on drier soils, such that an inverse association exists between SWE and soil moisture in spring and autumn [Figure 4.5].

Mean annual SWE and soil moisture

The relationships between mean annual SWE and soil moisture are weak, non-linear, and vary according to vegetation class over which they are examined. Seasonal differences in precipitation patterns (*Serreze and Barry*, 2005), as well as confounding factors such as soil freeze patterns, vegetation (*Hardy et al.*, 2001; *Johnsson and Lundin*, 1991), ponds (*French and Binley*, 2004), topography (*Burt and Butcher*, 1985) and soil type (*Janowicz et al.*, 2003; *Williams and Ratsetter*, 1999) are likely to limit the strength of the associations between SWE and soil moisture, and limit the extent to which these associations can be regionally generalized. Nevertheless, the ACE transformations indicate that positive associations exist between mean annual SWE and soil moisture in forested and barren regions that accumulate little snow (SWE < 90 mm) and have low soil moisture (< 0.17). Similarly, a positive association between soil moisture and SWE is observed over shrub dominated regions for all values of SWE and soil moisture, and over mixed forest regions accumulating less than 100 mm of SWE.

The influence of very low SWE (< 100 mm) has been studied in situ at barren (*Ayres et al.*, 2010) and hardwood (*Hardy et al.*, 2001) sites. Findings indicated that snow removal at the hardwood site resulted in greater soil heat loss, and therefore increased the proportion of ice in soil. As a result, snowmelt infiltration and soil moisture were reduced in plots where snow was removed (*Hardy et al.*, 2001). Similarly, experimental manipulation of snow accumulation at a polar desert indicated that sites where greater quantities of snow were accumulated tended to have greater levels of soil moisture during the following growing seasons relative to paired control sites (*Ayres et al.*, 2010). In the previously described experimental plots simulating low snow conditions, the barren site accumulated 10–50 mm of SWE and the hardwood site accumulated 80–100 mm of SWE. As a result, these studies indicated that diminished SWE led to diminished soil moisture in barren and hardwood plots with < 100 mm of SWE. Therefore, although the R^2 values from this study indicate that a weak and non-linear association exists between SWE and soil moisture across all vegetation classes, the ACE approach has elucidated similar thresholds and linkages as those which have been recorded in situ.

The ACE approach also indicated that a greater mean annual SWE is associated with greater soil moisture across all values observed over shrub dominated regions, and at low (< 0.15) levels of soil moisture in evergreen forests and graminoid tundra. Similarly, in a study conducted at the regional scale, anomalies in maximum annual snow depth and soil moisture were found to be associated in a semiarid region of Eurasia north of the Caspian-Aral seas (*Shinoda*, 2001). This region has maximum annual values of < 150 mm of SWE, and is classified as evergreen and deciduous forest in the present study. In

years where snow accumulation tended to be greater, snowmelt onset was found to occur later and larger values of soil moisture were observed during the following growing season. The finding by *Shinoda* (2001) that SWE and soil moisture tend to be associated over semiarid evergreen regions is therefore consistent with findings from this study, which indicate positive associations between mean annual SWE and soil moisture at sites that tend to receive less mean annual SWE and tend to have low soil moisture.

SWE and soil moisture in spring and autumn

The associations between soil moisture and SWE are weak when examined over thirty day time periods in spring (ACE $R^2 = 0.02$–0.17) and autumn (ACE $R^2 = 0.06$–0.12). At mixed forest and deciduous sites, ACE transformations indicates that a positive association exists between spring soil moisture and SWE at sites with low (< 75 mm) snow accumulation. Similarly, results from a snow depth manipulation experiment conducted in a hardwood forest indicated diminished soil moisture following snowmelt in a hardwood forest with very low snow accumulation (*Hardy et al.*, 2001).

The associations between SWE and soil moisture over remaining vegetation classes and time periods are slightly more complex. Although snow accounts for a large portion of annual precipitation, little of the moisture released through snowmelt in the Arctic is retained by soil (*Willis et al.*, 1961) due to rapid snowemlt, runoff and outflow (*Hardy et al.*, 2001; *Johnsson and Lundin*, 1991). For example, in a study at the Imnaviat Creek Arctic headwater, snow accumulation in spring accounted for 28–40 % of annual precipitation, only 10–19 % of the liquid water arising from snowmelt was stored in the active layer (*Kane et al.*, 1991). Regions with greater accumulation of snow tend to contribute a larger percentage of snowmelt to runoff (*Willis et al.*, 1961; *Staple et al.*, 1960). It is therefore less likely that a positive association would be observed between SWE and soil moisture in spring and autumn in areas underlain by permafrost.

An inverse relationship is observed to exist between soil moisture at the end of the growing season, and the accumulation of SWE at the start of the snow season for all vegetation classes [Figure 4.5]. Soil freezing occurs more slowly over wet soils than dry soils due to the influence of moisture on soil heat capacity (*Willis et al.*, 1961; *Hardy et al.*, 2001). As snow can only accumulate over cool soil surfaces, it is reasonable that soils which cool more rapidly at the start of the snow season may undergo greater net snow accumulation after freezing than warmer, wetter soils.

Likewise, in spring, an inverse association between soil moisture and SWE was observed over evergreen, shrub, tundra and barren regions with low (< 0.1) soil moisture. The

portion of snowmelt that infiltrates into the soil surface relies on the rate of snow melt, soil water, soil frost and soil drainage (*Hardy et al.*, 2001; *Johnsson and Lundin*, 1991). An inverse association therefore exists between seasonal infiltration and soil moisture levels during snowmelt (*Zhao and Gray*, 1999). The soil frost and soil drainage patterns at the end of the snow season can also be influenced by the levels of soil moisture observed prior to soil surface freezing at the start of the snow season (*Hardy et al.*, 2001; *Suzuki et al.*, 2006). Soils which are drier at the start of the snow season freeze more deeply than wetter soils and also thaw out more gradually (*Willis et al.*, 1961). Furthermore, soils with frozen upper layers have diminished infiltration due to the influence of ice on reducing soil pore size and permeability (*Zhao and Gray*, 1999). Therefore, since drier soils tend to freeze faster and more deeply than wet soils, more opportunity exists for snow accumulation to occur at the start and end of the snow season over dry soils because melt is less likely to occur. Soils which are more thoroughly frozen throughout the snow season are likely to receive less infiltration of snowmelt, and are therefore likely to be drier at the start of the growing season.

4.4.3 Vegetation transmissivity and SWE

Mean annual SWE and vegetation transmissivity generally have a negative association north of the treeline, indicating greater SWE accumulation in regions with greater surface roughness or aboveground biomass [Figure 4.6]. Conversely, the association between SWE and vegetation transmissivity in forested regions tends to be positive, such that SWE accumulation is limited in areas with greater aboveground biomass. At the start and end of the snow season, vegetation transmissivity is positively associated with SWE, which indicates more rapid melt or less snow accumulation at the start and end of the snow season in regions with more vegetation.

Mean annual SWE and vegetation transmissivity

The association between mean annual SWE and mean vegetation transmissivity (2003–2008) varies according to the predominant land cover, as well as the quantity of SWE received. In Arctic regions north of the treeline with a mean SWE accumulation of < 75 mm, an inverse association exists between vegetation transmissivity and SWE, indicating that locations with slightly more vegetation lost less snow to sublimation than regions with less vegetation. Shrub dominated regions north of the treeline have often been observed to trap snow more readily than regions which are more sparsely vegetated (*Pomeroy et al.*, 1997; *Sturm et al.*, 2001a,b; *Liston and Sturm*, 2002; *Essery and Pomeroy*, 2004). Shrubs

have greater snow-holding capacity then graminoid or barren vegetation since shrubs reduce near-ground wind speeds, thereby allowing greater deposition and less loss due to sublimation (*Essery and Pomeroy*, 2004; *Sturm et al.*, 2001a; *Fitzgibbon and Dunne*, 1979). From the ACE analysis, it appears that this influence is strongest over regions with less SWE. Due to the non-linearity of the association between mean annual SWE and vegetation transmissivity over tundra and barren sites, the ACE transformation is useful since it identifies the shape of this association ($R^2 = 0.19$–0.29) whereas a linear regression approach would only have indicated that a weak linear association exists between variables ($R^2 = 0.06$–0.15).

The association between vegetation cover and SWE may also be due in part to the influence of local precipitation on vegetation species compositions, which has previously been observed over the Brooks Range of Alaska by *Evans et al.* (1989). In northern regions, the health and productivity of vegetation can be compromised by very cold air, low soil temperatures and rain-on-snow events. Snow has been observed to provide vegetation with insulation from cold soil temperatures, and protection from dehydration, frost damage and high winds (*Wardle*, 1968; *Tranquillini*, 1964). Therefore, where snow accumulation is more substantial and remains on the ground for a longer time in spring, higher NDVI values have been observed (*Grippa et al.*, 2005), which indicate greater health or quantity of aboveground biomass (*Jensen*, 2007).

Areas that tend to lose less snow through sublimation, and accumulate more snow through windblown deposition, also tend to accumulate greater quantities of windblown organic materials throughout the snow season (*Walker et al.*, 2001), and undergo greater rates of organic matter decomposition throughout the snow season since they have warmer soil temperatures (*Nowinski et al.*, 2010). Both of the aforementioned influences can lead to nutrient rich conditions in regions receiving greater accumulation of snow, which can create growing season conditions that are conducive to plant growth. It is therefore possible that greater quantities of snow and vegetation tend to be collocated in Arctic regions due to the influence of snow on encouraging plant growth, and the influence of vegetation on encouraging snow accumulation. Spatial variability may therefore also play a role in this association, as high Arctic regions both accumulate small quantities of snow and contain little aboveground biomass.

The ACE analysis indicates that snow accumulation at low SWE (< 115 mm) evergreen forest sites is maximized when less vegetation is present ($R^2 = 0.10$). Likewise, field studies have found that snow accumulation is greater in clearings than coniferous forests (*Golding and Swanson*, 1986; *Gelfan et al.*, 2004), since coniferous trees intercept snowfall, and have been observed to allow 20–50 % of precipitation to evaporate or sublimate *Lundberg and Halldin* (2001). However, although coniferous stands with dense crowns limit snow

accumulation, sparser evergreen forests can encourage snow deposition (*Church*, 1933). Based on the findings from the ACE analysis, it appears that the effects of evergreen forests on limiting snow accumulation are strongest at lower SWE (< 115 mm) sites, whereas at higher SWE (>115 mm) sites, a slightly positive association appears to exist between vegetation biomass and SWE. This could be due to the effect of dense boreal forest cover, which causes SWE to be underestimated from satellite passive microwave observations. However, it is also reasonable that wind redistribution would be a dominant process when availability of fresh snow is great, but that sublimation, interception and melt would be dominant processes when snow accumulation is limited. It is also interesting to note in this context that over deciduous forests, vegetation biomass and SWE are inversely associated over all levels of SWE.

Assessment of these associations over mixed forest and shrub classes indicates that the associations between SWE and vegetation transmissivity are intermediate between those observed over tundra regions, and forested regions. Likewise, as the vegetation classes represent fractional portions of 25 km pixels according to the CAVM-SYNMAP derived classification, both the mixed forest and shrub classes contain a mixture of forest and non-forest vegetation. Over mixed forested regions, vegetation biomass and SWE are positively associated over areas with lower SWE (<75 mm), just as observed as a result of shrub cover over tundra regions. In shrubland areas containing large quantities of biomass and SWE, vegetation biomass and SWE are inversely associated. Conversely, in shrublands with diminished vegetation biomass, regions with greater biomass have greater SWE. Further field investigations would be required to better elucidate these drivers and clarify the dependence of these associations on the stated thresholds.

In spring and autumn, slower snowmelt in areas with more vegetation

Across all vegetation classes, positive associations of moderate strength exist between the mean values of SWE over the last thirty days of the snow season and the mean values of vegetation transmissivity over the first thirty days of the growing season (ACE $R^2 = 0.19$–0.31). The presence of this association indicates that regions with greater quantities of vegetation or greater surface roughness tend to contain a lower mean quantity of snow over the last thirty days of the snow season. This association is approximately linear across all vegetation classes [Figure 4.6].

Field studies have largely indicated that snow depletion occurs more gradually in regions with greater quantities of vegetation. The rates of snowmelt in boreal and taiga forests have been observed to diminish with increasing canopy density (*Pomeroy et al.*, 1997; *Metcalfe and Buttle*, 1998; *Gelfan et al.*, 2004). This effect is due to the influence of the

forest canopy on limiting shortwave radiation received by snow, and its effect on slowing wind speeds, thereby limiting fluxes of latent and sensible heat (*Metcalfe and Buttle*, 1998).

When examining vegetation transmissivity over the last thirty days of the growing season against SWE over the first thirty days of the snow season, a positive, approximately linear association of moderate strength can be identified for all sites south of the treeline (ACE $R^2 = 0.17$–0.30). Forested sites containing greater quantities of aboveground biomass therefore tend to accumulate less snow over the first thirty days following the date of initial snowfall than sites with less biomass. Field studies have indicated that interception and sublimation by dense canopies diminish snow accumulation (*Pomeroy et al.*, 1999, 2002; *Lundberg and Halldin*, 2001). The observed associations between SWE and vegetation biomass over tundra and barren regions appear weak but positive. However, to date, field studies have focused mainly on characterizing the influence of vegetation on mean annual snow accumulation, and on the magnitude and timing of snowmelt. A better understanding of these interactions could therefore be acquired through in situ observations of the effects of vegetation compositions on distributions of snow at the start of the snow season.

4.5 Conclusions

The Alternating Conditional Expectation (ACE) approach revealed non-linear associations between passive microwave derived snow water equivalent, and growing season air temperature, soil moisture and vegetation transmissivity. Although the drivers of snow accumulation vary according to the scale at which they are examined (*Pomeroy et al.*, 2002), and uncertainty exists in passive microwave estimates of the Arctic land surface due to its heterogeneity and high lake fraction (*Duguay et al.*, 2005; *Rees et al.*, 2006; *Green et al.*, 2012), it is interesting to note the similarity existing between the linkages, thresholds and associations found in situ and through ACE analysis of passive microwave observations (at 25 km).

Across all vegetation classes, sites with more aboveground biomass at the start and end of the growing season tend to have lower mean values of SWE over the first and last thirty days of the snow season. Field studies have found that snowmelt occurs more gradually over barren or graminoid tundra regions with more vegetation due to shading and slowed wind speeds (*Metcalfe and Buttle*, 1998), and that snow accumulation is diminished over forested regions with greater canopy density due to interception and sublimation (*Pomeroy et al.*, 2002). The ACE technique also indicated that sites with drier soils at the end of the growing season tended to accumulate more snow at the start of the snow season. Likewise, in situ observations have indicated more rapid and thorough freezing of soils which were dry

at the start of the snow season (*Willis et al.*, 1961), which could allow snow to accumulate more easily over cooler soils.

In forested regions, sites that tend to accumulate less snow also tend to have greater canopy density, as indicated by diminished vegetation transmissivity. Field studies have indicated that snow accumulation in heavily forested areas is limited due to canopy interception and sublimation (*Church*, 1933; *Pomeroy et al.*, 2002). ACE analysis also indicated that within forested regions accumulating < 90 mm of SWE, sites with greater SWE tended to also have greater soil moisture, an observation similar to the in situ findings by *Hardy et al.* (2001).

In Arctic tundra regions with lower (< 75 mm) SWE, more snow is accumulated at sites with warmer growing season temperatures and greater biomass or surface roughness, as indicated by diminished values of vegetation transmissivity. Arctic regions with warmer annual air temperatures have greater moisture availability for snow season precipitation (*Serreze and Barry*, 2005), and snow is preferentially accumulated in regions with greater vegetation or surface roughness (*Walker et al.*, 2001). Over dry (< 0.1 soil moisture) Arctic areas, sites that have more snow at the end of the snow season tend to have wetter soils at the start of the growing season. Arctic regions that have more snow for the last thirty days of the snow season also tend to have have cooler temperatures at the start of the growing season, likely due to the rapid snowmelt undergone by cold, high latitude sites (*Bonan*, 2002).

Recent circumpolar predictions indicate that climate change may diminish the annual duration of snow cover and increase maximum annual SWE (*Callaghan et al.*, 2011), and that high latitude warming and altered snow season length can affect Arctic vegetation phenology and species composition (*Arft et al.*, 1999; *Walker et al.*, 1999). As the ACE technique has uncovered linkages between snow and growing season land surface variables that bear great similarity to associations observed in situ, this also suggests that climate-driven changes in soil moisture, vegetation composition and air temperature may both influence, and be influenced by, shifts in the timing and accumulation of snow. We therefore suggest that continued monitoring of Arctic ecosystems at the field scale be accompanied by applying the ACE technique to monitor linkages between satellite passive microwave observations of snow and growing season variables.

4.6 Acknowledgements

The authors would like to thank John Kimball and Lucas Jones (NTSG), and the GlobSnow FMI-led consortium for providing the AMSR-E Land Surface Parameter and SWE datasets.

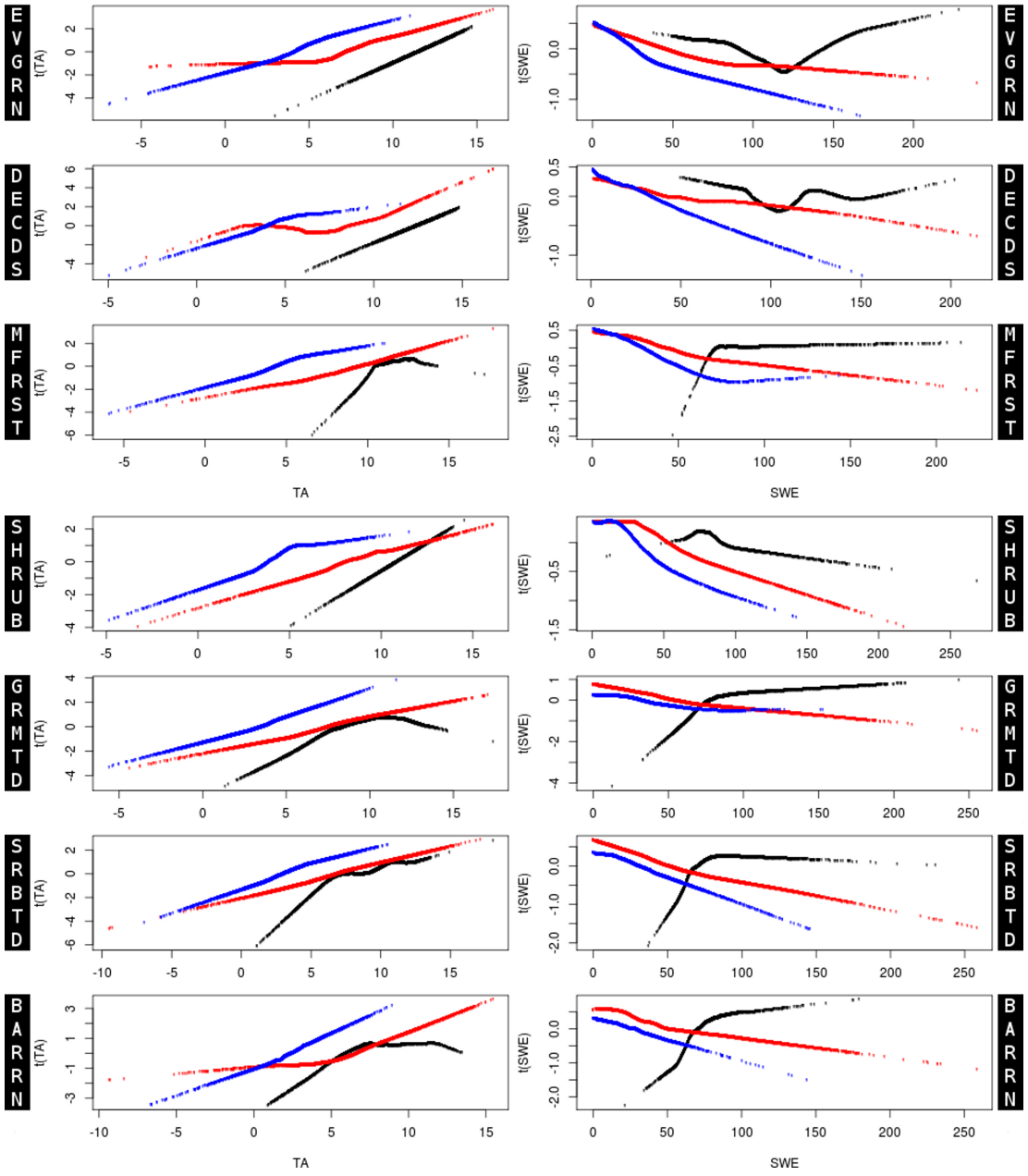

Figure 4.4: Point pair output from the ACE algorithm indicating associations between air temperature (TA) and SWE ([TA,t(TA)] and [SWE,t(SWE)]) over three time periods: mean annual (black), 30 days preceding and 30 days following snowmelt (red), and 30 days preceding and 30 days following snow onset (blue). Results are indicated for all seven vegetation classes separately.

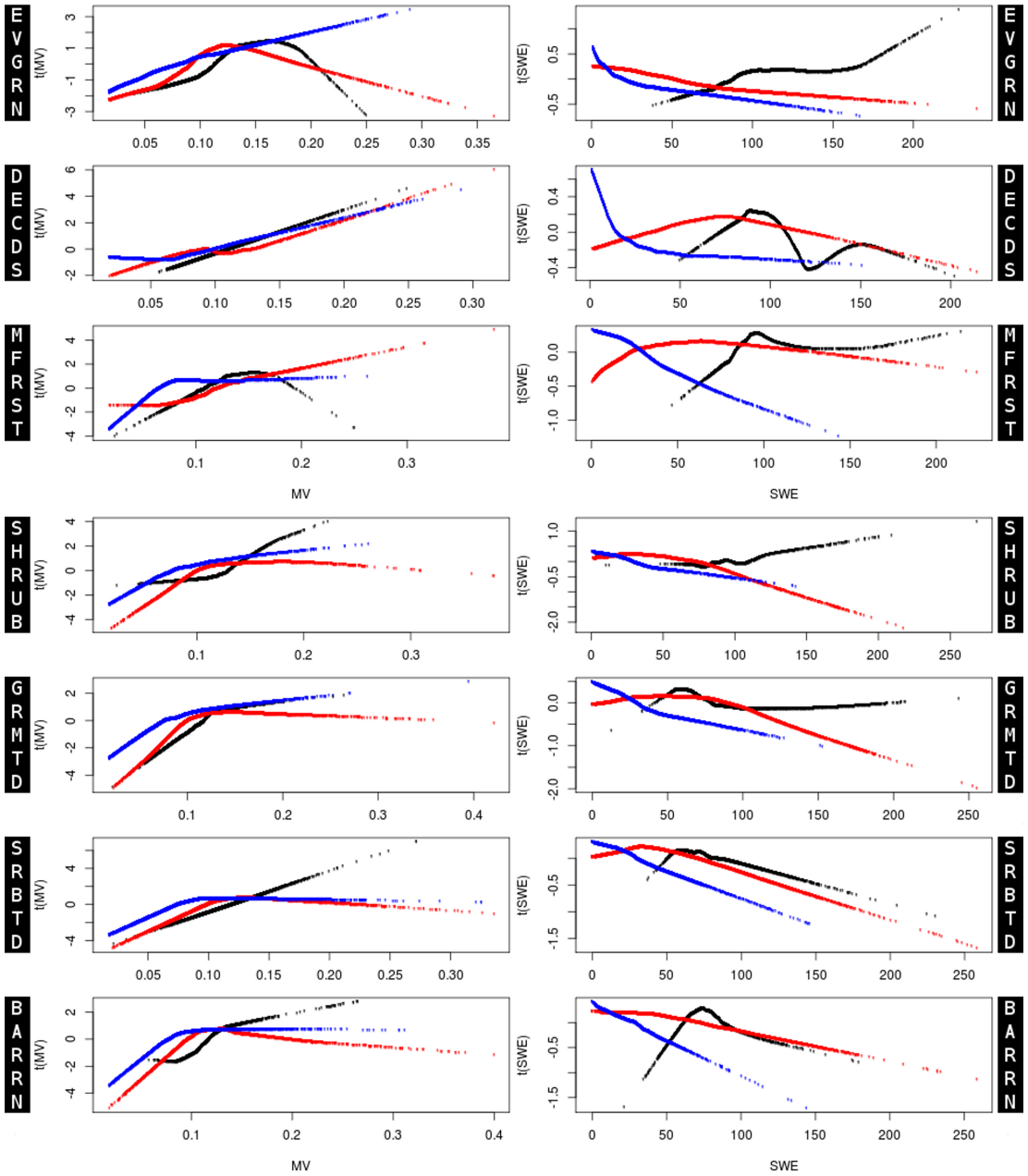

Figure 4.5: Linkages between SWE and volumetric soil moisture (MV), as indicated by the optimal transformations identified using the ACE approach. The point pairs [MV,t(MV)] and [SWE,t(SWE)] were independently calculated for each vegetation class. Associations between mean 2003-2008 values are shown in black, and associations in 'spring' and 'autumn' are shown in red and blue.

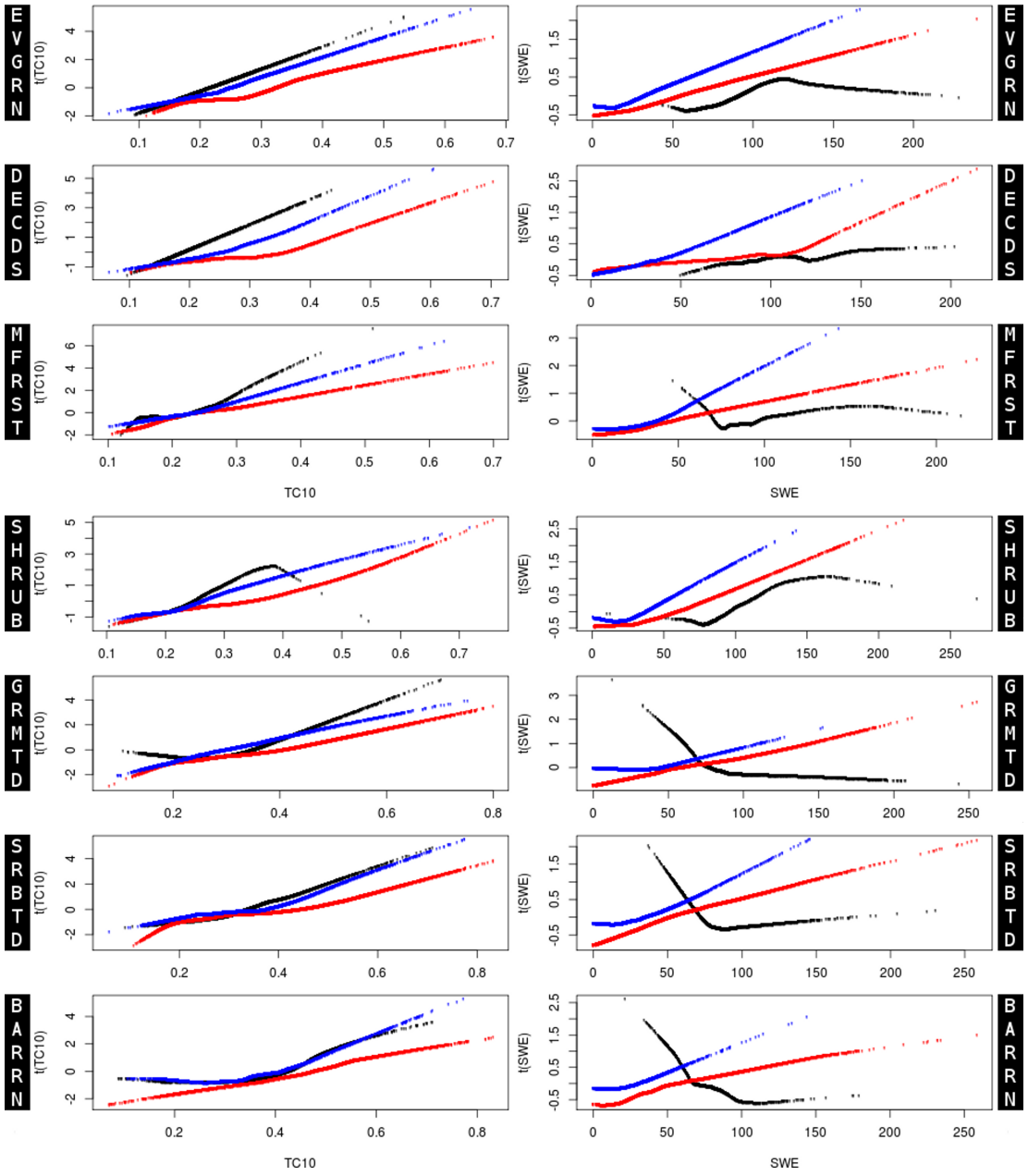

Figure 4.6: Associations between satellite estimates of vegetation transmissivity at 10 GHz (TC10) and SWE over seven vegetation classes, and three time periods: mean 2003-2008 (black), before and after snowmelt (red), and preceding and following snow onset (blue). Each plot indicates the point pairs [TC10,t(TC10)] and [SWE,t(SWE)] identified using the ACE technique.

Chapter 5

PolarVPRM: A remote sensing based model for estimating high-latitude net ecosystem CO_2 exchange

Overview

We introduce here the Polar Vegetation Photosynthesis Respiration Model (PolarVPRM), a remote sensing based approach for generating high resolution ($\geq$1 km, three-hourly) estimates of net ecosystem CO_2 exchange (NEE) north of 55°N. Recent field studies have indicated that the species of Arctic vegetation present at a site and the timing and duration of snow onset/melt influence NEE. We therefore incorporated Arctic-specific vegetation classes and remote sensing estimates of fractional snow cover and its influence on NEE into the existing VPRM in order to create PolarVPRM. We present here a complete description, validation and error analysis of PolarVPRM, followed by a model inter-comparison, and an analysis of inter-annual variability in PolarVPRM estimates of high-latitude North American NEE (2001–2012). PolarVPRM was validated by comparing model estimates of daily average NEE to unfilled eddy covariance observations from nine Arctic sites, of which three were used in model calibration. Model validation indicated that PolarVPRM estimates of snow season NEE in which the influence of snow on NEE was explicitly represented had lower MAEs (0.20 μmol/m^2/s) relative to PolarVPRM estimates of snow season NEE in which the influence of snow was not explicitly represented (MAE=0.24 μmol/m^2/s). Furthermore, more realistic estimates of the annual net carbon exchange were generated at all sites when the influence of snow on NEE was explicitly represented. Model intercomparison indicated that PolarVPRM's estimates of mean daily and monthly NEE fit more closely against eddy covariance observations than estimates of NEE by FLUXNET Multi-Tree Ensemble and CarbonTracker at the same temporal resolutions. Further analysis therefore consisted of examining inter-annual variability in PolarVPRM estimates of North American NEE and PolarVPRM driver data (2001–2012). Over time, a slight increase in high-latitude air temperatures with concurrent rises in EVI and growing season length lead to estimates of increased respiration over time, with increased photosynthesis over tundra regions and diminished photosynthesis over forests. PolarVPRM estimates indicate that high-latitude regions of North America are changing from a carbon sink to a weak carbon source over time (2001–2012).

5.1 Introduction

The high-latitude carbon cycle contains 1400 to 1850 Gt of soil organic carbon (*McGuire et al.*, 2010), a portion of which is likely to be released due to a warming climate (*Schaefer et al.*, 2011). The magnitude of future climate change will therefore be influenced by the response of the high-latitude carbon cycle to climate change. Accurate estimates of the high-latitude net ecosystem CO_2 exchange (NEE) are therefore crucial. However, substantial uncertainties presently exist in model estimate of North American NEE, leading models to estimate a wide range of possible carbon budgets (*Huntzinger et al.*, 2012). For example, a recent inter-comparison of 27 land surface models found substantial uncertainties in their estimates of Alaskan Arctic NEE (*Fisher et al.*, In Preparation). Models disagreed on whether the Alaskan Arctic was a strong carbon source, a strong carbon sink, or carbon neutral. Uncertainty regarding the magnitude of the Arctic carbon cycle and its responses to climate change are crucial scientific questions (*Lafleur and Humphreys*, 2008). It is therefore important that model estimates of high-latitude NEE be generated by a model specifically designed to simulate high-latitude influences on NEE, and that the sources and magnitude of uncertainty in this model be well understood.

To address these needs, we introduce the PolarVPRM model of high-latitude net ecosystem CO_2 exchange. PolarVPRM is a diagnostic, remote sensing based model well suited for representing the high-latitude land surface drivers of NEE using a simple mathematical structure with few parameters. Following a description of PolarVPRM formulation, a thorough validation and error assessment are provided by comparing model output to eddy covariance measurements from calibration and validation sites. Output from PolarVPRM across North America (north of 55°N) is then compared against monthly NEE from Carbon Tracker and the FLUXNET Multi-Tree Ensemble (MTE), and all model outputs are compared against eddy covariance observations. Comparisons of output from all three models against eddy covariance observations indicated that PolarVPRM had the lowest error values. Therefore, changes over time (2001–2012) in PolarVPRM estimates of the high-latitude carbon cycle are examined in context of changes over time in driver data. Findings indicate that high-latitude regions may be slowly shifting from being a carbon sink, to a very weak carbon source in response to warming air temperatures and changing land surface conditions.

5.2 PolarVPRM

PolarVPRM estimates net ecosystem CO_2 exchange (NEE) at high resolution (3-hourly, $\frac{1}{4} \times \frac{1}{2}^{\circ}$) over regions north of 55°N. The original Vegetation Photosynthesis Respiration Model (VPRM) was developed by *Mahadevan et al.* (2008). VPRM has been validated and found to generate realistic estimates of NEE across the USA and southern Canada (30–56° N) (*Mahadevan et al.*, 2008). VPRM is a diagnostic remote sensing based model through which spatial estimates of biospheric respiration and photosynthesis are generated. Respiration is simulated as a piecewise linear function. When air temperature (T_{air}) exceeds a threshold specific to each vegetation class (T_{low}, $1<T_{low}< 5$), respiration is calculated as a linear function of air temperature; in colder conditions ($T_{air}<T_{low}$), respiration is set to a low constant. Photosynthesis is calculated according to air temperature, the amount of incoming shortwave radiation, and MODIS derived indices estimating the health or amount of vegetation (enhanced vegetation index, EVI) and water availability (land surface water index, LSWI). Each vegetation class contains four parameters which are set according to meteorological and eddy covariance tower observations:

- α and β, regression coefficients describing the linear association between respiration and air temperature ($R = \alpha T_{air} + \beta$)
- PAR_0, which represents the sensitivity of photosynthetic uptake to the quantity of incoming shortwave radiation
- λ, which represents light use efficiency, or quantum yield, of vegetation

In this study, we develop an Arctic version of VPRM in order to reduce uncertainty in model estimates of high-latitude NEE. PolarVPRM uses remote sensing observations to represent Arctic-specific drivers of NEE, as observed in recent *in situ* studies. Arctic field studies have shown that >50% of annual carbon efflux can occur during the snow season (*Aurela et al.*, 2004; *Sullivan et al.*, 2008; *Elberling and Brandt*, 2003), and that the timing and magnitude of NEE are influenced by snowpack dynamics (*Larsen et al.*, 2007a; *Walker et al.*, 1999; *Morgner et al.*, 2010). Specifically, the low thermal conductivity of Arctic snowpacks decouples soil and air temperatures, thereby allowing respiration to persist throughout mid-winter and preventing large effluxes of CO_2 during snowmelt, when air temperatures exceed soil temperatures. Investigations at a low Arctic site showed good agreement between MODIS and local observations of snow cover area, and found that representing the aforementioned influence of snow on respiration reduced model error over two low Arctic sites (*Luus et al.*, Submitted). As a result, MODIS observations of snow

cover area (SCA) were incorporated into PolarVPRM. During the growing season (when SCA$<$ 50%), respiration is estimated as a function of T_{air}; during the snow season (when SCA$\geq$50%), respiration is estimated as a function of soil temperature (T_{soil}). The resulting variability in respiration throughout the snow season can therefore be more realistically simulated.

Arctic vegetation is highly heterogeneous, and different types of vegetation within a single site can show important differences in NEE (*Humphreys and Lafleur*, 2011; *Elberling*, 2007). The seven vegetation classes in PolarVPRM are therefore Arctic specific, and set according to a combination of the Synergistic Land Cover Product (SYNMAP) (*Jung et al.*, 2006) and the Circumpolar Arctic Vegetation Map (CAVM) (*Walker et al.*, 2005). The PolarVPRM vegetation classes divide the pan-Arctic region north of 55°N into seven zones. Statistical analysis has previously indicated that these seven vegetation classes capture spatial variability in snow and growing season influences on NEE (*Luus et al.*, 2013). The resulting classification is therefore likely to capture the varying responses of the Arctic carbon cycle to meteorological and site conditions. The influence of water stress on diminishing photosynthesis is represented only over forested regions as *in situ* studies have indicated that water stress does not play a critical role in determining the productivity of Arctic vegetation (*Oberbauer and Miller*, 1979; *Chapin III and Shaver*, 1985; *Shaver et al.*, 1986; *Johnson and Caldwell*, 1975).

Several changes were made in the remote sensing derived input data used by PolarVPRM, relative to VPRM. Firstly, MODIS MOD10A1 observations of fractional snow cover were included to differentiate the snow and growing seasons. False positives and negatives in MODIS estimates of fractional snow cover were eliminated through the selection of MODIS observations only over time periods when the surface reflectance observations were flagged as 'excellent', and through the implementation of a mask from NARR T_{soil} (at 0–10 cm) to eliminate mid-summer false positives and mid-winter false negatives. Furthermore, since snowmelt and snow onset occur rapidly in Arctic regions, a smoothing algorithm was applied to reduce noise in estimates of fractional snow cover during these periods of time. When MODIS MOD10A1 observations were corrected using this approach, good agreement was then found between remotely sensed and locally observed fractional snow cover (*Luus et al.*, Submitted).

The original VPRM calculated LSWI and EVI from MOD09 surface reflectance. However, initial time series analyses of MOD09 derived observations of EVI at high-latitudes showed substantial noise exists in the EVI. Conversely, MODIS MOD13A1 estimates of EVI have been corrected to eliminate a variety of land surface, atmospheric and topographic errors (*Solano et al.*, 2010). As a result, MOD13A1 estimates of EVI were used at high-latitudes.

Furthermore, whereas VPRM typically used meteorological observations from the North American Land Data Assimilation System (NLDAS), meteorological observations from the North American Regional Reanalysis (NARR) were used to drive PolarVPRM. Arctic meteorological estimates tend to be biased towards overestimating shortwave radiation (*Walsh et al.*, 2009). Preliminary assessments over Daring Lake, NWT, indicated that the overestimate in air temperature at 2m above ground (T_{air}) and downward shortwave radiation from NARR was smaller than that from NLDAS. NARR estimates of downward shortwave radiation, T_{air} at 2m and soil temperature at 0–10cm (T_{soil}) were therefore incorporated into PolarVPRM.

5.3 Methodology

Parameters for PolarVPRM's three Arctic vegetation classes were set using observations from eddy covariance and meteorological towers collected at three sites in 2005: Daring Lake, NWT (shrub tundra, *Lafleur and Humphreys* (2008); *Humphreys and Lafleur* (2011)); Ivotuk, AK (graminoid tundra, *Laskowski* (2010)); and Atqasuk, AK (wetland, *Laskowski* (2010)). Parameters for vegetation classes south of the treeline were set according to the parameterizations presented *Mahadevan et al.* (2008) for evergreen forest (NSA old black spruce forest site), deciduous forest (Harvard forest main site), mixed forest (Howland forest main site) and shrubs (Walnut-Gulch Lucky Hills shrubland site). Further information about these sites can be found in *Mahadevan et al.* (2008).

PolarVPRM estimates of NEE were then generated across North America (north of 55°N) at a $\frac{1}{6} \times \frac{1}{4}^{\circ}$ and three-hourly resolution for years 2001–2012. PolarVPRM estimates of NEE were then validated against eddy covariance observations of daily NEE, and compared against CarbonTracker and FLUXNET MTE estimates of mean monthly and daily NEE. As PolarVPRM's estimates of NEE were found to be in better agreement with eddy covariance observations than CarbonTracker and FLUXNET MTE, analysis then proceeded by assessing the implications of PolarVPRM output. Changes over time (2001–2012) were therefore assessed in PolarVPRM estimates of the carbon cycle and in driver data over both the snow and growing seasons.

5.3.1 Error analysis

Due to the simple mathematical formulation of VPRM and PolarVPRM, uncertainties in estimates of NEE can be easily partitioned into systematic versus random errors (*Lin*

et al., 2011), where systematic errors or biases are due to specific inputs or parameters, and random errors are not. In order to better understand the deviation between PolarVPRM estimates of NEE and eddy covariance measurements, a comprehensive error analysis was completed according to the framework developed by (*Lin et al.*, 2011). Within this framework, errors are quantified, and classified as either systematic or random. Systematic errors are then attributed to input variables and parameters, and their total contributions to uncertainty in estimates of NEE are examined. Plotting the contribution of each component to model error allows their relative contributions to be assessed.

5.3.2 Validation

Arctic eddy covariance sites [Figure 5.1] were initially paired in order to allow validation to be conducted over sites similar to those over which calibration occurred. Ivotuk was paired with Imnavait, AK (graminoid tundra, *Euskirchen et al.* (2012)). Atqasuk, AK was paired with Barrow (wetland, *Zona et al.* (2010, 2011)). Sites were then designated as either calibration or validation sites on the basis of having data available for a common year. As Daring Lake, Atqasuk and Ivotuk all had data collected in 2005, model calibration was conducted over these sites using 2005 observations. Both validation and calibration were conducted with unfilled observations of NEE, which were only filtered to remove periods of time with low frictional velocity (u$*$ <0.2) (*Goulden et al.*, 1996).

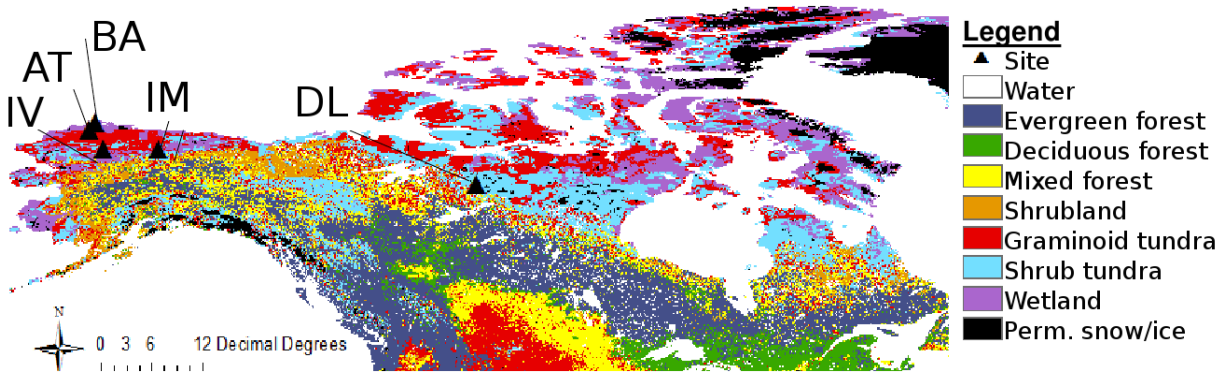

Figure 5.1: PolarVPRM calibration and validation eddy covariance sites: Ivotuk (IV), Atqasuk (AT), Barrow (BA), Imnavait (IM) and Daring Lake (DL) plotted over a map of PolarVPRM's seven vegetation classes.

Model evaluation consisted of examining the Mean Absolute Error (MAE) and Root Mean Squared Error (RMSE) between PolarVPRM estimates of NEE (pred_i), and eddy

covariance observations of NEE (obs_i) (*Willmott and Matsuura*, 2005):

$$MAE = n^{-1} \sum_{i=1}^{n} |pred_i - obs_i| \tag{5.1}$$

$$RMSE = \left[n^{-1} \sum_{i=1}^{n} |pred_i - obs_i|^2 \right]^{\frac{1}{2}} \tag{5.2}$$

Validation was conducted against 2005 eddy covariance observations at the three calibration sites, and against observations from 2008 and 2001 at Imnavait and Barrow. 2008 and 2001 were selected as these were the closest years to 2005 for which year-round observations existed. Validation was also conducted using observations of NEE collected in July 2008 by *Lafleur et al.* (2012) from four Canadian Arctic sites: Cape Bounty, Iqualuit, Lake Hazen and Pond Inlet. Validation therefore described the fit between model output, and *in situ* observations of NEE.

5.3.3 Model inter-comparison

PolarVPRM estimates of NEE were then compared against those generated by existing models with different formulations, and all models were compared against eddy covariance observations of NEE. The models selected for inter-comparison were CarbonTracker and FLUXNET Model-Tree Ensemble (MTE). CarbonTracker (*Peters et al.*, 2007) and FLUXNET MTE (*Jung et al.*, 2009) were selected on the basis that they are established models which estimate NEE over northern regions using a very different approach than PolarVPRM.

CarbonTracker derives estimates of CO_2 surface fluxes by analyzing atmospheric CO_2 observations using a transport model (Transport Model 5, TM5) in combination with a land surface biospheric flux model (Carnegie-Ames-Stanford Approach, CASA), and fossil fuel inventories. One identified source of small uncertainties in CarbonTracker estimates is from measurement errors or biases in CO_2 dry mole fractions (*Masarie et al.*, 2011). FLUXNET MTE generates regional estimates of mean monthly NEE by first training an ensemble of model trees using eddy covariance observations from FLUXNET sites and inputs from the Lund-Potsdam-Jena managed Land (LPJmL) model, and then upscaling these measurements accordingly. Uncertainty in FLUXNET MTE estimates of NEE has previously been assessed through comparison of GPP against GPP generated by the LPJmL (*Jung et al.*, 2009).

PolarVPRM, CarbonTracker and FLUXNET MTE estimates of mean daily and monthly NEE were compared against mean daily and monthly observations of unfilled NEE available at the PolarVPRM calibration and validation sites for which annual observations were available: Atqasuk, Barrow, Daring Lake, Imnavait and Ivotuk. Median values were calculated from eddy covariance observations in order to reduce the impacts of large outliers on monthly estimates of NEE.

5.3.4 Inter-annual variability

Inter-annual variability in PolarVPRM estimates of the carbon cycle (NEE, GEE & respiration) was first assessed in a qualitative manner. Plots were created of mean monthly values for each variable, and of the cumulative carbon balance for each vegetation class. Results found an increase in net carbon efflux across high-latitude regions, occurring primarily during the growing season over forested regions.

To determine the trends in annual net carbon uptake, NEE, GEE and respiration between 2001–2012, a non parametric method (Theil-Sen estimator; aka Sen's slope) was applied. To further understand the specific influences driving these shifts, changes over time in carbon cycle variables and driver data were separately analyzed over the snow season (SS) and growing season (GS). These time periods were differentiated using MODIS MOD10A1 snow cover area (SCA), such that the time period with SCA$\geq$50% was considered the snow season, and the time period with SCA$<$50% was considered the growing season. The variables studied were GS GEE, GS respiration, GS air temperature, GS EVI, GS LSWI, SS respiration, SS air temperature and SS length. The mean values of these variables were first calculated for each annual growing season and snow season using only non-zero values. The Sen's slope estimates of median changes in carbon cycle and land surface variables over time (2001–2012) were then reported for each pixel in the model domain corresponding to significant (p-value$<$0.05) change.

5.4 Results and Discussion

5.4.1 Error analysis

Errors in PolarVPRM were assessed over two non-calibration sites, Barrow and Imnavait, using observations collected in 2001 and 2008. Findings from the error analysis indicated that the main sources of error in PolarVPRM estimates of NEE arose from biases in how

the associations between PAR and GEE, and between LUE and GEE, were parameterized [Figure 5.2]. Despite this large source of uncertainty, the total observed bias in NEE was very small at both sites, potentially due to correlated errors. Mid-growing season NEE was overestimated at Barrow, but underestimated at Imnavait. Analysis also indicated good agreement between most of the the parameter values calibrated at the corresponding calibration sites (Atqasuk and Ivotuk), and the parameter values which were calculated according to validation site measurements during the error analysis. The main exception is in light use efficiency (λ), represented in light blue [Figure 5.2].

It is interesting to note that the vegetation at Atqasuk and Ivotuk showed a diminished photosynthetic response to incoming photosynthetically active radiation relative to the vegetation at Barrow and Imnavait. The main bias which appeared in analysis was that PolarVPRM estimated Barrow to have less GEE than Atqasuk primarily due to its cooler temperatures, but Barrow in fact uptakes more CO_2 than Atqasuk due to differences in respiration and photosynthesis at the two sites (*Oechel et al.*, 2005). However, the exact drivers of these opposite patterns in NEE have not yet been well described in literature.

Differences in the carbon balance of Barrow and Atqasuk remain a key question to be addressed, especially since Barrow is more frequently used as a calibration site than Atqasuk. Since PolarVPRM is calibrated according to eddy covariance and meteorological observations collected at Atqasuk, it may therefore estimate that low Arctic wetlands have a greater net annual efflux of carbon than other models. NASA's ongoing Carbon in Arctic Reservoirs Vulnerability Experiment (CARVE) (*Miller and Dinardo*, 2012) is presently providing new insights into the Arctic carbon balance and its land surface drivers. As a small portion of CARVE observations are being collected over regions near Barrow and Atqasuk, it is hoped that this experiment may also help elucidate the varying drivers of NEE between these two sites.

Although substantial differences exist in the parameters describing light use efficiency at Barrow and Atqasuk, the overall influence of this discrepancy appears to have little influence on the ability of PolarVPRM to simulate NEE at these sites. The total bias at Barrow is most substantial during the growing season, but is still always < 0.5 tC/ha. Similarly, at Imnavait, the parameter describing the association between light use efficiency and GEE is too small, but results in minimal errors in GEE (< 0.1 tC/ha). Characterizing errors in GEE and respiration according to their drivers is complicated by difficulties in partitioning GEE and respiration, especially during mid-summer in polar regions. The fact that PolarVPRM underestimates GEE but can still simulate NEE well is therefore indicative of error correlation. Conducting a thorough error validation over a larger number of sites would assist in better understanding the biases in PolarVPRM, and their influences on estimates of NEE.

5.4.2 Validation

Uncertainty in PolarVPRM estimates of NEE was generally reduced when the influence of snow on respiration was explicitly represented [Table 5.1]. Specifically, incorporating remote sensing observations of snow cover to differentiate the snow and growing seasons, then calculating snow season respiration as a function of T_{soil}, and growing season respiration as a function of T_{air}, prevented respiration from being overestimated during the snow season and underestimated during the growing season. Reductions in uncertainty were most substantial over the time period when the land surface is snow-covered, but as observations are primarily collected during the growing season, the true reductions in model error are likely underestimated. Although the reductions in model error are small at daily time scales, these modification have an important influence on estimates of the annual carbon budget for each site [Figure 5.3].

Model	Error	AT	BA	DL	IM	IV	Mean
PolarVPRM without snow	MAE	0.02	0.36	0.16	0.54	0.11	0.24
PolarVPRM with snow	MAE	0.03	0.34	0.19	0.36	0.10	0.20

Table 5.1: MAE values (in μmol/m^2/s) comparing median daily average NEE from PolarVPRM with snow and without snow to observations of NEE from five eddy covariance sites: Atqasuk (AT), Barrow (BA), Daring Lake (DL), Imnavait (IM) and Ivotuk (IV).

Model estimates of NEE in July 2008 were also compared against unfilled observations acquired at four Canadian Arctic sites in July 2008 (*Lafleur et al.*, 2012). None of these sites were used for calibration purposes, and all are located far away from the validation sites. Despite the long distances from corresponding validation sites, PolarVPRM was able to estimate NEE relatively well across all sites [Table 5.2]. The mean RMSE across all sites was 0.68 μmol/m^2/s, and the mean MAE was 0.21 μmol/m^2/s. This indicates that PolarVPRM's representation of vegetation is likely to be suitable for high-latitude regions of North America, even though the calibration sites are found mainly in Alaska.

	CB	IQ	LH	PI
MAE	0.12	0.13	0.26	0.32
RMSE	0.55	0.92	0.44	0.82

Table 5.2: MAE and RMSE values (in μmol/m^2/s) comparing three-hourly PolarVPRM NEE to eddy covariance observations of NEE in July 2008 at four Canadian Arctic validation sites: Cape Bounty (CB), Iqaluit (IQ), Lake Hazen (LH) and Pond Inlet (PI).

However, although these estimates of NEE have low errors, it is important to note that the tendency for GEE to be underestimated in the peak of the growing season is observed when analysis is run over the four Canadian Arctic sites. It is likely that this bias arises from the tendency for the response of GEE to the amount of incoming photosynthetically active radiation to be underestimated, as identified previously in the error analysis. A slight bias is therefore identified in PolarVPRM estimates [Figure 5.2]. However, this bias appears to have a limited effect on the ability of PolarVPRM to estimate NEE. Before analyzing inter-annual variability in PolarVPRM, it is therefore important that PolarVPRM is inter-compared with two existing models.

5.4.3 Model inter-comparison

Both CarbonTracker and PolarVPRM estimated very low rates of mid-winter respiration, whereas the FLUXNET Model-Tree Ensemble (MTE) assessed greater rates of mid-winter respiration. All three models show reasonably good agreement in growing season estimates of mean monthly NEE [Figure 5.4]. The root mean squared deviation (RMSD) and mean absolute deviation (MAD) RMSD and MAD between MTE and PolarVPRM are greatest between September to April, with mean values of 0.87 μmol/m^2/s. The RMSD and MAD values are very similar in mid-winter because PolarVPRM estimates of mid-winter respiration are very low in comparison to MTE estimates of mid-winter respiration. Conversely, as both CarbonTracker and PolarVPRM estimate very low rates of winter respiration, good agreement is found, with mean September–April RMSD and MAD of 0.09 and 0.05 μmol/m^2/s, respectively.

When comparing mean monthly NEE estimated by PolarVPRM and CarbonTracker across eight three-hourly time periods, it is interesting to note that PolarVPRM consistently estimates lower rates of GEE than CarbonTracker, but estimates that respiration continues for a much longer duration of the day. These differences are especially noticeable when examining plots of NEE at 3:00 and 12:00 UTC. PolarVPRM shows a distinct uptake that is especially noticeable at dates closest to the summer solstice. These differences may either be due to underestimates of the amount of daylight available near solstice by CarbonTracker, or underestimates in peak midday GEE by PolarVPRM due to a bias in the parameter describing the response of GEE to photosynthetically active radiation, as described in section 5.4.1. Despite this diurnal difference between these models, they generate very similar mean monthly rates of NEE across all time periods. Comparisons across the peak of the Arctic growing season indicated that PolarVPRM appears to slightly underestimate GEE in some years relative to FLUXNET MTE, and appears to slightly overestimate GEE relative to CarbonTracker. Overall, PolarVPRM shows more

similarity with CarbonTracker (RMSD= 0.27 μmol/m^2/s, MAD= 0.04 μmol/m^2/s), and is more distinct from FLUXNET MTE (RMSD=0. 78 μmol/m^2/s, MAD=0.71 μmol/m^2/s) ,especially during the snow season [Table 5.3].

	Jan	Feb	Mar	Apr	May	Jun	Jul	Aug	Sep	Oct	Nov	Dec
CT-RMSD	0.03	0.03	0.04	0.08	0.17	0.37	0.66	0.42	0.21	0.19	0.14	0.06
MTE-RMSD	0.85	0.85	0.62	0.64	0.25	0.50	0.71	0.41	0.80	1.13	1.13	0.98
CT-MAD	0.02	0.02	0.04	0.07	0.12	0.28	0.54	0.36	0.14	0.14	0.13	0.05
MTE-MAD	0.85	0.85	0.62	0.64	0.19	0.47	0.64	0.31	0.76	1.12	1.13	0.97

Table 5.3: Root mean squared deviation (RMSD) and mean absolute deviation (MAD) of mean monthly PolarVPRM relative to CarbonTracker (CT) and FLUXNET Model-Tree Ensemble (MTE) from 2001–2009 over the North American region north of 55°N.

Estimates of NEE generated by the three models were then compared against eddy covariance observations at the PolarVPRM calibration and validation sites [Table 5.4]. Results indicated that PolarVPRM's estimates of mean monthly NEE (RMSE= 0.72 μmol/m^2/s, MAE= 0.41 μmol/m^2/s) and daily mean NEE (RMSE= 1.76 μmol/m^2/s, MAE= 0.50 μmol/m^2/s) were in better agreement with eddy covariance observations at the three sites than monthly estimates of NEE by MTE (RMSE= 0.95 μmol/m^2/s, MAE= 1.38 μmol/m^2/s) or daily mean estimates by CarbonTracker (RMSE= 2.09 μmol/m^2/s, MAE= 0.62 μmol/m^2/s). Based on this analysis, it appears that PolarVPRM is better able to capture diurnal patterns of NEE than CarbonTracker. Comparisons of monthly estimates of NEE by CarbonTracker and PolarVPRM indicated that CarbonTracker had slightly lower MAE values (0.39 vs 0.41 μmol/m^2/s) but greater RMSE values than PolarVPRM (0.72 vs 0.83 μmol/m^2/s). Overall, PolarVPRM's estimates of high-resolution NEE fit more closely against year-round eddy covariance measurements of NEE at Arctic sites than daily mean estimates by CarbonTracker, or monthly mean estimates by MTE.

5.4.4 Inter-annual variability

PolarVPRM output indicates that on average, North American regions appear to have lost strength as a carbon sink from 2005–2010 [Figure 5.5]. Since PolarVPRM estimates of NEE are generated using the same parameter set and input data sources across all years (2001–2012), analyzing inter-annual variability in PolarVPRM estimates of the northern carbon cycle, and in PolarVPRM input data, can provide insights into the potential responses of the Arctic carbon cycle to recent changes in environmental conditions.

Resolution	Error	Model	AT	BA	DL	IM	IV	Mean
Monthly	RMSE	PolarVPRM	0.34	0.81	0.38	1.65	0.40	0.72
Monthly	RMSE	CarbonTracker	0.52	0.47	0.95	1.58	0.64	0.83
Monthly	RMSE	FLUXNET MTE	0.61	0.71	1.32	1.53	0.60	0.95
Daily	RMSE	PolarVPRM	1.29	1.52	0.75	3.27	1.97	1.76
Daily	RMSE	CarbonTracker	1.51	1.23	1.97	3.38	2.36	2.09
Monthly	MAE	PolarVPRM	0.11	0.47	0.03	1.20	0.22	0.41
Monthly	MAE	CarbonTracker	0.06	0.16	0.67	0.99	0.07	0.39
Monthly	MAE	FLUXNET MTE	1.05	1.06	1.55	2.13	1.13	1.38
Daily	MAE	PolarVPRM	0.03	0.65	0.23	1.43	0.12	0.50
Daily	MAE	CarbonTracker	0.19	0.38	0.63	1.69	0.22	0.62

Table 5.4: Error statistics (RMSE and MAE, in μmol/m^2/s) found through the comparison of monthly mean and daily mean estimates of NEE from PolarVPRM, CarbonTracker and FLUXNET Model-Tree Ensemble relative to observations of daily and median monthly NEE from Atqasuk (AT), Barrow (BA), Daring Lake (DL), Imnavait (IM) and Ivotuk (IV) at a matching temporal resolution.

Further analysis then consisted of examining spatial patterns of changes over time in carbon cycle variables using the Theil-Sen estimator (Sen's slope). Initial analyses were conducted according to mean annual values of net carbon uptake, NEE, respiration, and GEE [Figure 5.6]. Findings indicated that substantial rises were observed over time in net carbon efflux, especially from forests. The observed increase over time in net carbon efflux from forested regions was due to the tendency of these regions to uptake less photosynthesis, shown as an increase in the values of GEE. Although northern Alaskan regions and portions of the Yukon showed increased uptake over time, the trend was much weaker. Smaller increases were observed over time in high Arctic respiration, leading to increased rates of net carbon efflux.

Changes over time in carbon cycle variables and driver data were then analyzed separately over the growing seasons and snow seasons using the Theil-Sen estimator [Figure 5.7]. A qualitative assessment of Sen's slope output shows an increase in photosynthetic uptake by low and high Arctic vegetation, with concurrent rises in respiration over Arctic regions. The number of days per year for which the land surface was >50% snow covered (snow season, SS) appeared to decrease by several days per year across northern North America. In these plots, the growing season (GS) refers to the mean annual values over the portion of the year when the ground is <50% snow covered and GEE>0.

It is interesting to note that the mean annual values of GEE showed less photosynthetic

uptake by vegetation over time, but when these same calculations were over the growing season ($GEE > 0$), growing season GEE showed increased uptake over time. The decline in photosynthetic uptake over forested regions is due to warming temperatures. When temperatures reach higher values in summer, rates of photosynthetic uptake are hindered, especially in plants adapted to cool temperatures. PolarVPRM contains parameterizations of these physiological maximums and optimal temperatures for photosynthesis according to values set in literature. For example, portions of northern forests contain vegetation classified as shrub and graminoid tundra, both of which perform photosynthesis optimally under temperatures of 15°C (*Chapin*, 1983). If growing seasons are substantially warmer, rates of photosynthesis can be suppressed.

GS air temperature rose over time, especially over northern boreal and tundra regions, which increased subsequent rates of GS respiration and GS GEE at high latitudes. Conversely, SS T_{air} declined over time over boreal regions, and increased over time at higher latitudes. Boreal sites have greater nutrient levels and temperature-driven responses of respiration to warming air temperatures than Arctic sites. The net effect of declines in SS T_{air} were therefore declines in SS respiration over boreal regions. However, the concurrent rises in GS T_{air} meant that over boreal regions, declines in SS respiration were counterbalanced by increases in GS respiration. As a result, only a slight increase in net annual respiration is observed over Arctic regions, which is influenced by rising T_{air} throughout the SS and GS.

Previous studies have described the influence of warming air temperatures on inducing increased rates of net carbon uptake by vegetation near the shrub and tree lines (*Hinzman et al.*, 2005; *Tape et al.*, 2006), and on increasing rates of CO_2 efflux (*Schuur et al.*, 2009; *Tarnocai*, 2006). Remote sensing studies have found trends towards increased growing season length (*Zeng et al.*, 2011), increased NDVI over tundra regions due to warming (*Stow et al.*, 2004), and diminished NDVI over boreal regions due to reduced rates of photosynthesis (*Bi et al.*, 2013; *Verbyla*, 2008) [Figure 1.1]. Arctic greening and boreal browning are likewise observed in the trend of GEE [Figure 5.6]; however, when mean values of EVI were considered only for the portion of the year when vegetation was productive ($GEE > 0$), EVI appeared to show an increase over time across North America. The simultaneous influences of air temperature on allowing greater quantities of biomass to grow with more limited photosynthetic capacity is thus elucidated.

Since PolarVPRM is driven by remote sensing observations, the influence of these changes over time in input remote sensing observations can be understood in terms of its net contribution to the carbon cycle. Using this approach, insights were provided into the net influence of changes in land surface properties and conditions on the snow and growing season net ecosystem exchange of CO_2.

5.5 Conclusions

PolarVPRM represents a remote-sensing based approach for generating high resolution estimates of NEE north of 55°N that are in agreement with eddy covariance observations collected year-round at Arctic sites (MAE=0.20 μmol/m^2/s). Although substantial differences existed in the optimal values of the parameters describing the response of GEE to photosynthetically active radiation between calibration and validation sites, error correlations meant that only small biases were observed in NEE at both validation sites.

this source of error appears to have had little net influence on error in NEE. PolarVPRM generated estimates of mean daily and monthly NEE that were in better agreement with eddy covariance measurements of NEE than mean daily and monthly estimates of NEE generated by CarbonTracker and FLUXNET Multi-Tree Ensemble, respectively.

Incorporating remote sensing observations of snow into PolarVPRM not only reduced uncertainty in high-latitude estimates of NEE relative to eddy covariance observations, but also allowed insights to be gained into the responses of the high-latitude carbon cycle to shifting snow and growing season conditions. PolarVPRM estimates of high-latitude (55–83°N) North American NEE showed an increase over time (2001–2012) in net carbon efflux by high-latitude ecosystems. Arctic sites are likely to undergo increased rates of respiration due to warming soil and air conditions. Rates of Arctic photosynthesis are increasing due to greater availability of light, moisture, along with warmer temperatures. However, these increases in net carbon uptake are outweighed by diminished rates of photosynthesis in forests when air temperatures exceed the physiologically optimal temperatures for photosynthesis. Changes over time in meteorological conditions and land surface properties are therefore likely to diminish growing season GEE, and increase annual rates of respiration. High-latitude ecosystems appear to be losing strength as a carbon sink in response to changing conditions, and becoming a small net source of CO_2.

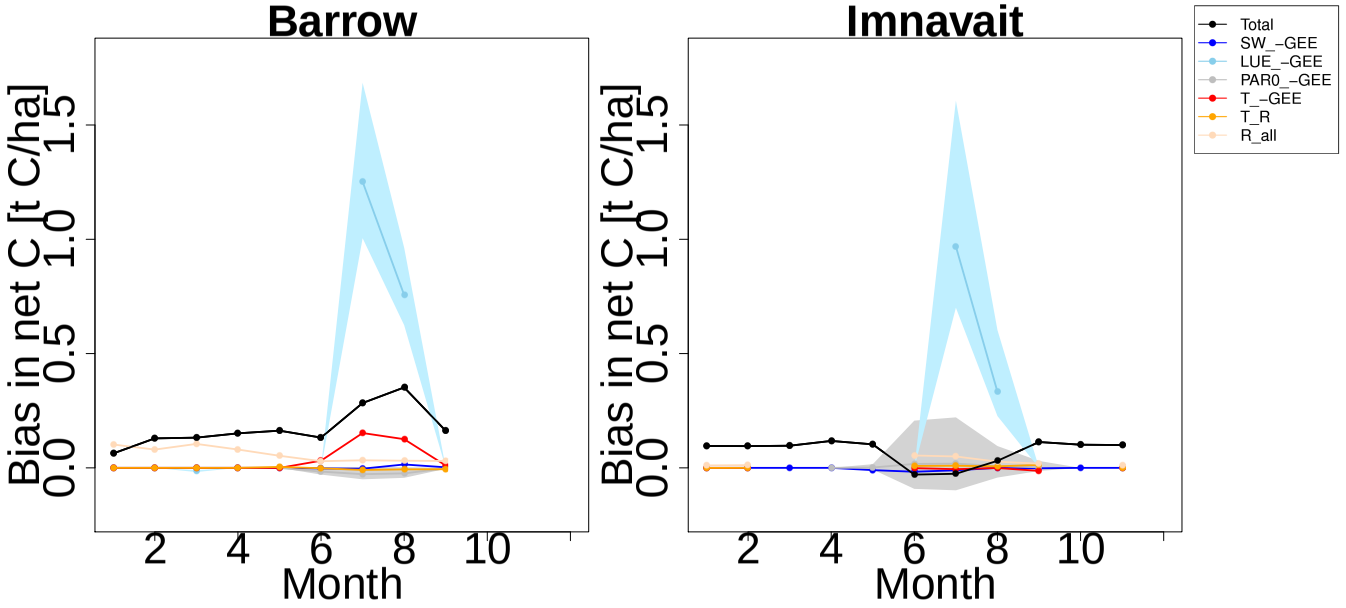

Figure 5.2: Monthly bias, in PolarVPRM estimates of net C exchange at Barrow (left) and Imnavait (right), relative to eddy covariance observations at these sites. Errors in GEE are designated as being due to the associations between GEE and downward shortwave radiation (SW_GEE), GEE and light use efficiency (LUE_GEE), and of the parameter describing the association between GEE and PAR0 (PAR0_GEE). Shaded areas surrounding (PAR0_GEE) and (LUE_GEE) represent the range of biases possible from the determination of PAR0 and LUE from eddy covariance observations. Total biases in temperature and GEE (T_GEE), and between temperature and respiration (T_R) are also described, along with the total biases in respiration (R_all) and NEE. Comparisons are shown for the range of months for which eddy covariance observations were acquired at Barrow in 2001, and at Imnavait in 2008.

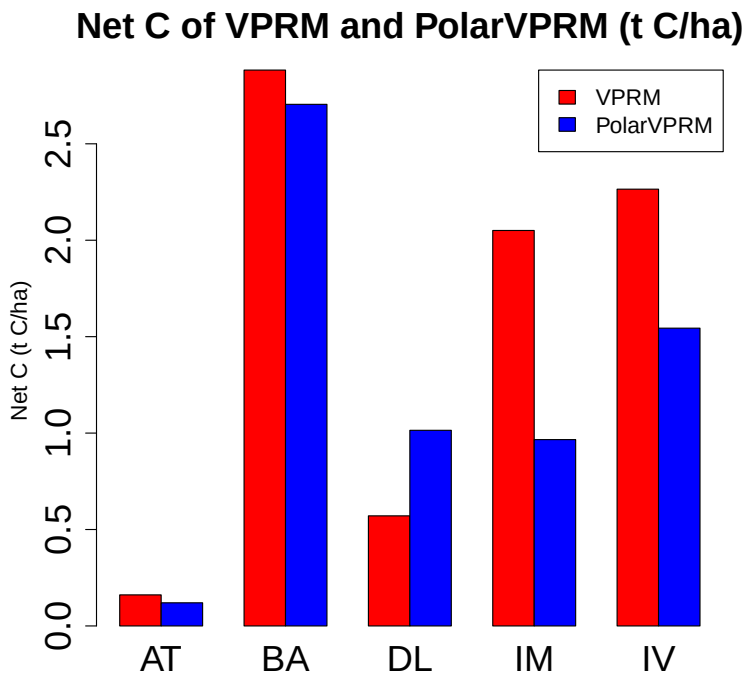

Figure 5.3: Net carbon balance of all calibration and validation sites according to PolarVPRM formulations with (red) and without (blue) snow.

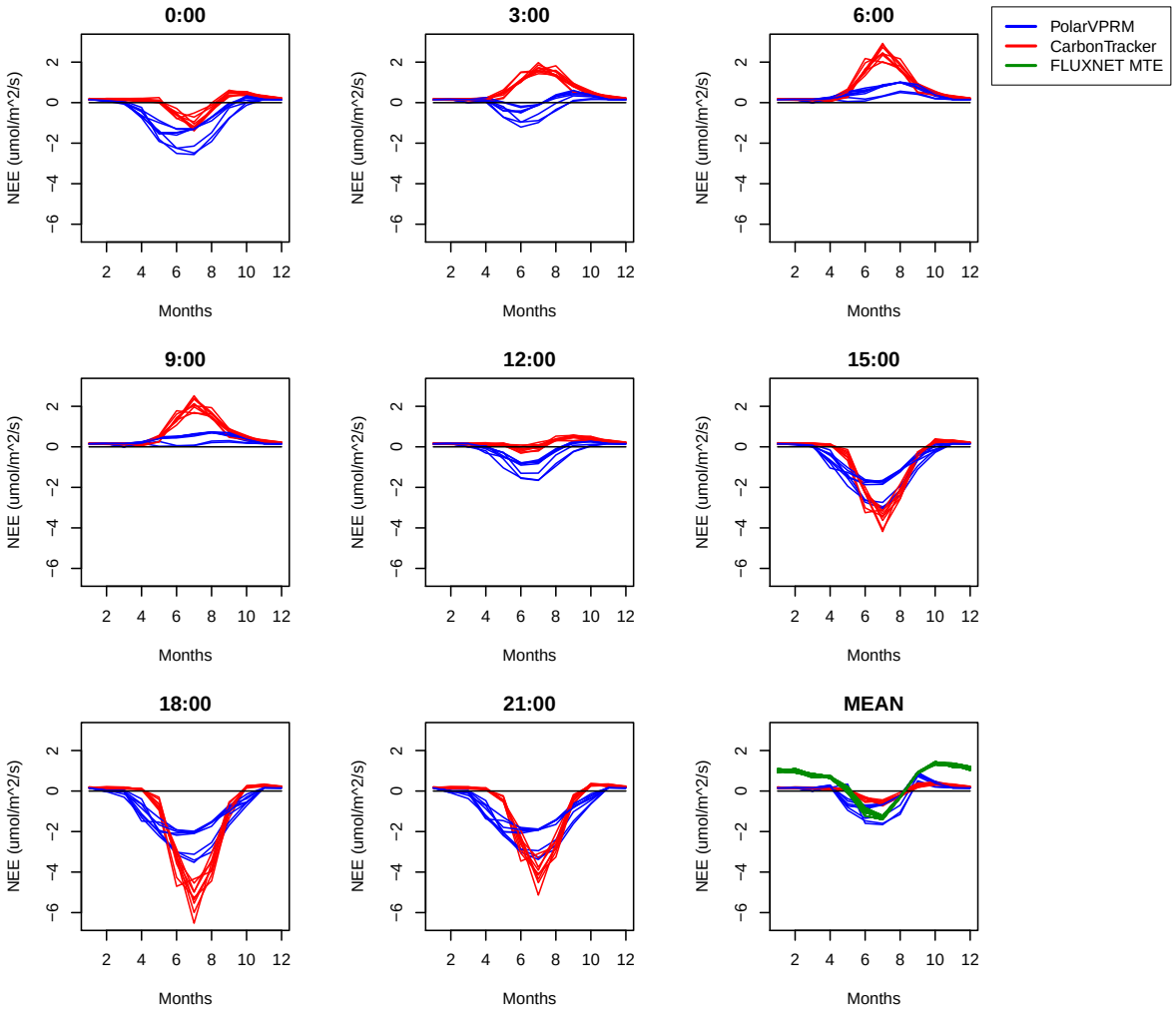

Figure 5.4: Monthly average NEE from PolarVPRM (blue) and CarbonTracker (red) is shown across each 3 hour time period (in UTC), with years 2001–2009 indicated with separate lines on each plot. Mean monthly NEE for all time periods is shown in the final plot for PolarVPRM, CarbonTracker and FLUXNET MTE (green). FLUXNET MTE is only available at a monthly resolution, so is only indicated in the last plot.

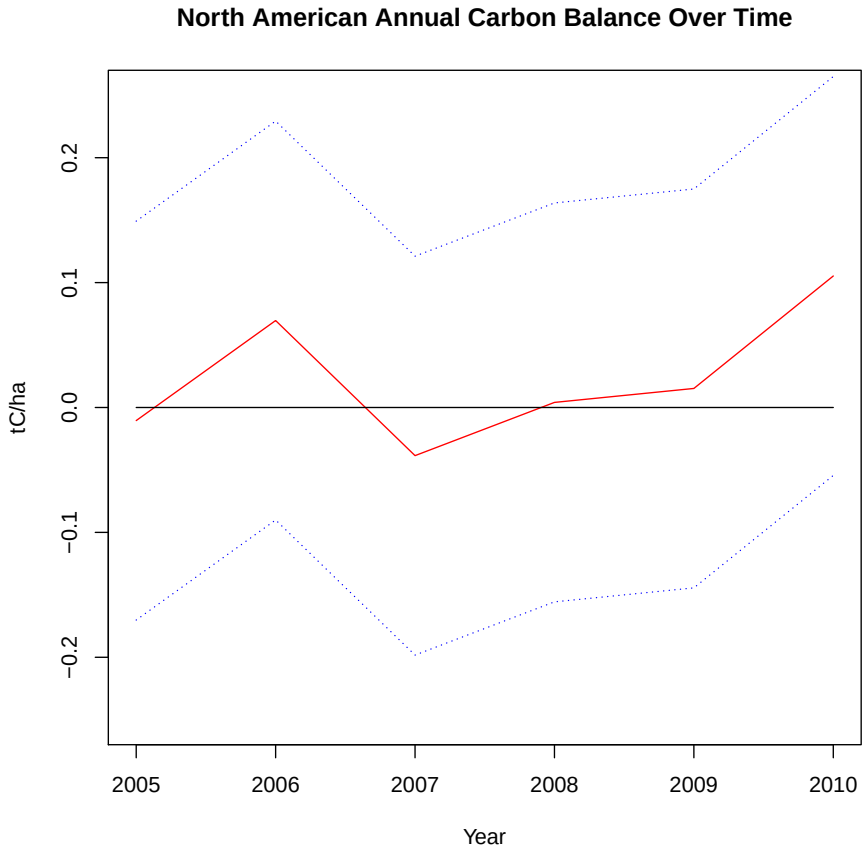

Figure 5.5: Net carbon balance of North America (north of 55° N, 2005–2010) according to PolarVPRM (in tC/ha). The dotted lines indicate error bars, with values set according to the mean error in net C at the validation sites [Figure 5.2].

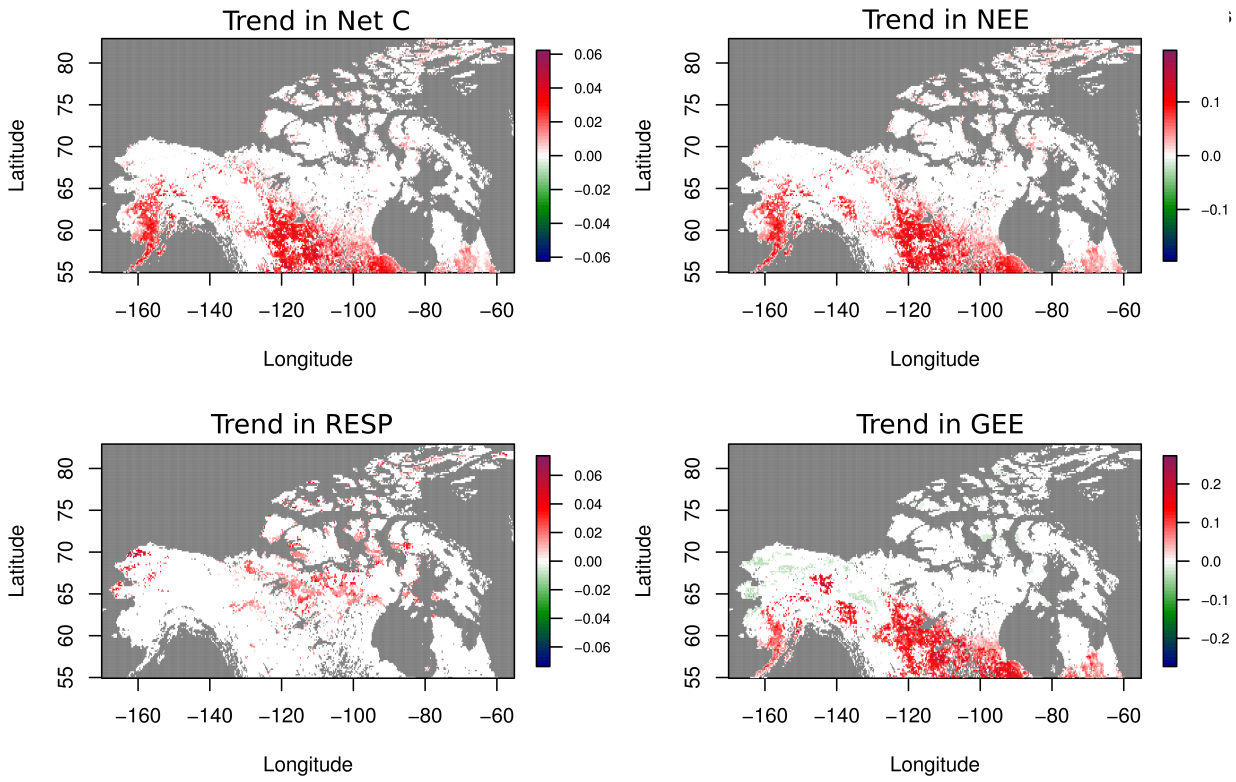

Figure 5.6: Sen's slope values, indicating the median change (2001–2012) in PolarVPRM estimates of mean annual NEE, respiration and GEE (in μmol/m^2/s), and mean annual net carbon exchange in (t C/ha). All Sen's slope values shown correspond to p-values<0.05.

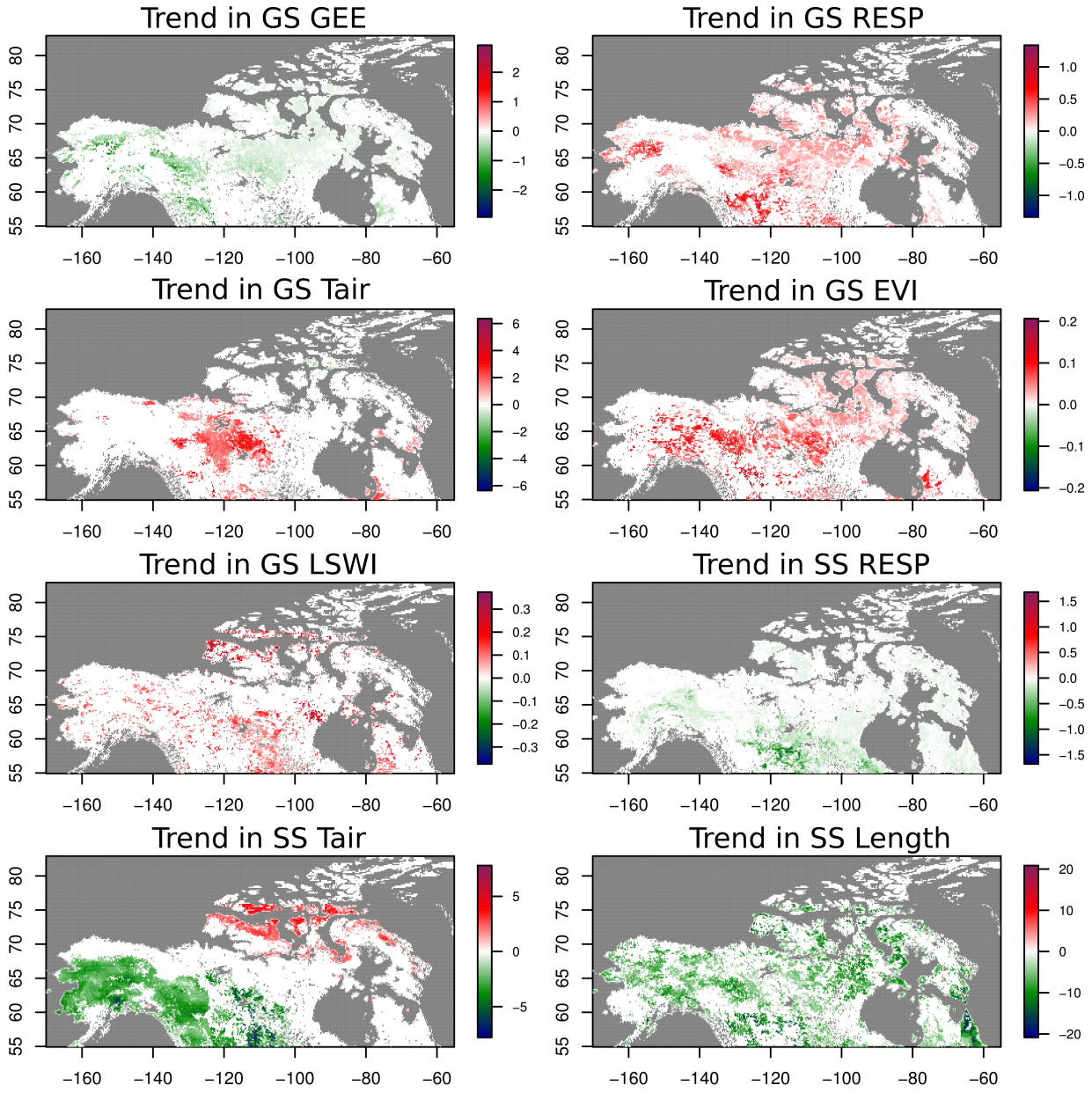

Figure 5.7: Sen's slope of median change (2001–2012) in PolarVPRM estimates of carbon cycle variables, and driver data. All variables are shown for either the growing season (GS, when SCA<50%) or snow season (SS, when SCA≥ 50%), and all values refer to the sums of non-zero values over these time periods. Values are only shown for locations at with a significant (p-value<0.05) change over time. NEE, RESP and GEE are all expressed in μmol/m^2/s, T_{air} is in °C, SS length is in days, and both EVI and LSWI are dimensionless (0-1).

Chapter 6

Conclusions

6.1 Summary

Substantial uncertainties regarding the high-latitude carbon cycle and its recent responses to climate change complicate efforts to understand the biospheric feedbacks between the climate system and the carbon cycle. These feedbacks will heavily influence the future intensity of climate change, and it is therefore crucial that models generate accurate estimates of the high-latitude carbon cycle. The central objectives of this thesis were to reduce uncertainty in model estimate of high-latitude NEE by representing polar influences on NEE, and to then examine the implications of these improved model estimates of high-latitude NEE for our current understanding of the magnitude and response of the high-latitude carbon cycle to recent biospheric changes (2001–2012).

PolarVPRM, a model for estimating high-latitude NEE, was developed by making several important changes to the existing Vegetation Photosynthesis Respiration Model (VPRM). Model inputs were selected on the basis of performing well over high-latitude regions, Arctic-specific vegetation classes were implemented and the influence of snow on NEE was explicitly represent. A literature review indicated that snow properties influence NEE, and outlined possible approaches to represent these influences using remote sensing observations [Chapter 2]. One approach involved using MODIS observations of fractional snow cover to represent the influence of snow on NEE. Analysis over a low Arctic site at Daring Lake, NWT, Canada indicated good agreement between local and remote sensing

observations of fractional snow cover. PolarVPRM was calibrated and run over paired calibration and validation sites using model formulations both with and without an explicit representation of snow. Findings from this approach showed that uncertainty in estimates of NEE could be reduced by delineating the snow and growing seasons according to fractional snow cover, such that growing season respiration could be calculated according to air temperature and snow season respiration could be calculated according to soil temperature [Chapter 3].

When Arctic vegetation classes were created for PolarVPRM using SYNMAP and CAVM, questions arose regarding 1) how well these vegetation classes captured distinctly different regions with the heterogeneous Arctic/sub-Arctic; and 2) the pan-Arctic associations between snow accumulation and growing season drivers of NEE (air temperature, soil moisture and vegetation). Preliminary analysis indicated that these relationships were non-linear, and that their shape varied according to the vegetation class and time period over which they were investigated [Chapter 4]. The ACE approach was therefore applied to further analyze these associations in order to determine whether regions undergoing greater rates of soil respiration (through greater snow accumulation) would also tend to have greater uptake of CO_2 during the growing season.

Findings from this chapter indicated that associations between snow and growing season processes observed at the pan-Arctic scale showed strong agreement with *in situ* observations of these same linkages. For instance, Arctic regions that tended to accumulate more snow tended to be warmer during the growing season, drier at the start and end of the snow season, and to contain more vegetation. Conversely, forested regions that accumulated more snow tended to be colder during the growing season and to have less vegetation. Results therefore indicated that the associations between snow and growing season influences were non-linear, and could not be generalized across vegetation class. Gaining accurate pan-Arctic estimates of year-round NEE would therefore require both the snow and growing season land surface influences on NEE to be well represented. As previous analysis had indicated that representing the influence of snow cover on rates of respiration improved model performance, the PolarVPRM model was created with the aforementioned vegetation classes and remote sensing approach to representing the influence of snow on respiration.

Overall, representing the influence of fractional snow cover on NEE using remote sensing observations of fractional snow cover reduced uncertainty in model estimates of NEE [Chapter 5]. Validation of the PolarVPRM model indicated good agreement between model estimates and eddy covariance measurements of NEE, and found that the main source of errors in PolarVPRM estimates of NEE arose from strong differences in the associations between GEE and the amount of inputted shortwave radiation, resulting in underestimates

of GEE at both validation sites. Model inter-comparison indicated that PolarVPRM estimates of mean daily and monthly NEE fit more closely against eddy covariance observations than estimates of mean daily and monthly NEE by two existing models: CarbonTracker and FLUXNET Multi-Tree Ensemble. PolarVPRM estimates of NEE therefore appear to be adequate in light of even larger uncertainties in other existing models.

To understand the implications discovered by this newly developed model, inter-annual variability and trends over time were assessed in PolarVPRM estimates of high-latitude North American NEE. PolarVPRM output indicated a net decline in the uptake of carbon by North American ecosystems north of 55°N between 2001–2012, shifting high-latitude ecosystems from a net carbon sink to a very weak net carbon source. Although tundra vegetation displays a green-up and increase in photosynthetic uptake in response to warmer air temperatures, conditions that are too warm hinder the capacity of boreal vegetation to conduct photosynthesis. Warmer air temperatures also encourage greater rates of respiration. These findings are in general agreement with *in situ* and remote sensing findings of changes in vegetation, but provide a unique contribution by estimating the net contribution of these shifts for the high-latitude carbon cycle.

6.2 Contributions

This research contributed several novel aspects to our understanding of the high-latitude carbon cycle. The first major contribution was in outlining specific strategies which could be used to represent snow season processes in model estimates of NEE using remote sensing observations [Chapter 2]. The second main contribution was in determining that uncertainty in model estimates of high-latitude NEE could be reduced by using a remote sensing approach to differentiate the snow and growing seasons, such that snow season respiration could be estimated as a function of soil temperature, and growing season respiration could be represented as a function of air temperature [Chapter 3]. The third major contribution of this research was the elucidation of spatial associations between snow and growing season drivers of NEE, and their dependence on the predominant vegetation class and the time period over which they are studied [Chapter 4]. Findings indicated variability, non-linearity and complexity in the associations between snow and growing season influences on NEE. It therefore became evident that representing snow season influences on NEE could allow valuable, non-intuitive insights to be gained into the response of the high-latitude carbon cycle to changes in land surface conditions during the snow and growing seasons.

The final contribution of this research was in developing PolarVPRM [Chapter 5], a model found to generate more accurate estimates of eddy covariance derived NEE than ex-

isting approaches. Using this model, inter-annual variability (2001–2012) in high-latitude North American estimates of the carbon cycle were analyzed in context of changing meteorological and land surface conditions. The high-latitude carbon cycle was therefore quantified, and insights were provided into the estimated influence of warming air temperatures on increasing rates of respiration and photosynthetic uptake over tundra regions, and diminishing growing season uptake of carbon over forests. PolarVPRM estimates indicated a net increase in CO_2 efflux over time that has led high-latitude regions to shift from a carbon sink to a weak carbon source. The majority of research contributions therefore arose in the process of developing PolarVPRM; however, the resulting model itself may be the most important contribution.

PolarVPRM estimates of the northern carbon cycle are being employed through collaboration with two ongoing research projects. Myung-Gwang Kim, a PhD student in Earth and Environmental Sciences at the University of Waterloo, is running the Stochastic Time-Inverted Lagrangian Transport (STILT) model to assess anthropogenic CO_2 fluxes over northern Canada, using PolarVPRM estimates of biospheric CO_2 fluxes (2005–2010). Likewise, NASA's Carbon in Arctic Reservoirs Vulnerability Experiment (CARVE) is using PolarVPRM estimates of NEE in combination with the STILT model to analyze airborne observations of CO_2 concentrations over Alaska (2012).

6.3 Limitations

The accuracy of model estimates are inherently limited by the quality of input data, and on the assumption that calibration sites are typical of the region from which they originate. Once sites were paired according to vegetation type, in each case, and then somewhat arbitrarily assigned as either calibration or validation. Error analysis revealed that vegetation at the site shows a smaller photosynthetic response to incoming photosynthetically active radiation than the vegetation at Barrow. PolarVPRM was calibrated over Atqasuk and run over Barrow as a validation site; Barrow GEE was therefore underestimated. At this time, it is not possible to determine which of these paired sites is more representative of high-latitude wetlands and barren vegetated regions across North America. PolarVPRM may therefore underestimate peak growing season GEE in wetland or vegetated barren tundra regions.

A major source of both known and unquantifiable errors in PolarVPRM arises due to the difficulty associated with collecting year-round observations of NEE at Arctic North American sites. Few eddy covariance observation sites exist at high-latitudes in North America, and most are clustered on the North Slope of Alaska. PolarVPRM is calibrated

and validated primarily over the northern Alaska. Of these sites, few collect observations throughout the snow season. When snow season observations are collected, these are characterized by large measurements uncertainties. Therefore, although comparisons of PolarVPRM output against July 2008 observations of NEE over northern Canada indicated good model fit, uncertainty in year-round estimates of NEE over the vast majority of the Canadian Arctic cannot presently be quantified with the existing eddy covariance observation network.

Furthermore, although a central focus of the PolarVPRM is on generating improved estimates of snow season NEE, complete characterizations of snowpack properties are not typically available at high-latitude eddy covariance sites. As a result, many of the complex associations between snowpack dynamics and NEE observed *in situ* cannot presently be simulated in regional estimates of NEE. A possibility may exist to instead represent these processes using calibration/validation across a variety of Eurasian sites in conjunction with observations from the Total Carbon Column Observing Network (TCCON), which may indicate one possible direction for future work.

6.4 Future work

Although most of the aforementioned limitations are the same impossible quandaries that make this work appealing and necessary, there exist a few possible directions for future improvements in PolarVPRM estimates of NEE. Future research directions will consist of calibrating and validating PolarVPRM across Eurasian FLUXNET sites. This will also allow insights to be gained into the pan-Arctic carbon cycle and its responses to climate change. These improvements could come about through model calibration according to high-latitude sites across Eurasia, thereby allowing high resolution pan-Arctic estimates of NEE. Model validation across Eurasia would also allow a better understanding of the source and magnitude of errors in PolarVPRM estimates of NEE. PolarVPRM estimates of pan-Arctic NEE could provide important insights into the response of the circumpolar carbon cycle to climate driven-shifts in snow and growing season land surface properties.

Future opportunities may exist to represent snow season influences such as snow accumulation and snowpack dynamics in PolarVPRM if greater availability of *in situ* observations of these properties become available. Findings from PolarVPRM indicated that the parameter describing the maximum temperature at which plants are able to carry out photosynthesis played an important role in describing the influence of warming air temperatures on NEE. Values for these parameters were set from literature. Future research

could therefore focus on improving the accuracy of these temperature thresholds for each vegetation class.

Possibilities may also exist in future for other researchers to use PolarVPRM output for a variety of applications. Regional-scale output from the PolarVPRM model will therefore be made available to researchers online (`www.polarvprm.com`) and through a listing on the Polar Data Catalogue (`www.polardata.ca`).

Appendix A

Appendices

A.1 List of Acronyms

NEE Net Ecosystem Exchange

NEP Net Ecosystem Production

GPP Gross Primary Production

GEE Gross Ecosystem Exchange

NPP Net Primary Production

$\mathbf{R}_h$ Heterotrophic Respiration

$\mathbf{R}_a$ Autotrophic Respiration

SWE Snow Water Equivalent

PAR Photosynthetically Active Radiation (400-700 nanometers)

LUE Light Use Efficiency

CAVM Circumpolar Arctic Vegetation Map

SYNMAP Synergistic Land Cover Product

CASA Carnegie-Ames-Stanford Approach

LPJ Lund-Potsdam-Jena Dynamic Global Vegetation Model

fAPAR Fraction of Absorbed Photosynthetically Active Radiation

SiB2 Simple Biosphere model

GCM General Circulation Model

LSWI Land Surface Water Index

NDVI Normalized Difference Vegetation Index

LAI Leaf Area Index

EVI Enhanced Vegetation Index

VPRM Vegetation Photosynthesis Respiration Model

MODIS NASA's Moderate Resolution Imaging Spectroradiometer

AMSR-E NASA's Advanced Microwave Scanning Radiometer for Earth Observing Systems

GloPEM Global Production Efficiency Model

NLDAS North American Land Data Assimilation System

NARR North American Regional Reanalysis

A.2 Description of GlobSnow SWE and NTSG land surface variables

The products compared in this study are derived from gridded Level 2A brightness temperature from the Advanced Microwave Scanning Radiometer for the Earth Observing System (AMSR-E). AMSR-E is a multichannel satellite passive microwave radiometer collecting observations at 6.925, 10.65, 18.7, 23.8 36.5 and 89.0 GHz (*Kawanishi et al.*, 2003). Passive microwave observations rely on estimates of microwave radiance, which increases proportionally with temperature and emissivity of a surface. Brightness temperature (T_b), the

variable of observation by passive microwave instruments, is a function of the product of kinetic temperature (T_k) and emissivity (ϵ): $T_b = T_k\epsilon$. T_b is equivalent to the physical temperature of a blackbody ($\epsilon = 1$) (*Jones et al.*, 2010).

AMSR-E T_b has been used previously to estimate snow water equivalent (*Kelly*, 2009), vegetation and soil moisture (*Njoku and Chan*, 2005). These approaches have continued improving in accuracy and global coverage, culminating in the recent release of the AMSR-E derived data sets analyzed in this study: NTSG land parameters by *Jones and Kimball* (2012) and GlobSnow SWE by *Luojus et al.* (2009). The following subsections describe the methodologies applied by the Finnish Meteorological Institute (FMI)-led consortium and the University of Montana's Numerical Terradynamic Simulation Group (NTSG) to calculate GlobSnow SWE and land surface variables, respectively. All data are calculated from AMSR-E brightness temperature observations acquired at 6.9, 10.7, 18.7, 23.8, 36.5 and 89.0 GHz twice daily with native resolutions varying inversely with frequency from 5 km to 60 km (*Jones and Kimball*, 2010a). NTSG and GlobSnow both use NSIDC Level 2A AMSR-E data, which resamples each frequency's native resolution to that of the 6.9 GHz frequency. The resulting product is on a 25 km grid (*Ashcroft and Wentz*, 2003) and use an EASE-Grid projection (*Knowles et al.*, 2010). GlobSnow snow water equivalent uses 18.7 and 36.5 GHz frequency data (*Luojus et al.*, 2009). Both the GlobSnow and AMSR-E air temperature datasets have been validated against in situ and AIRS/AMSU observations, respectively (*Jones et al.*, 2010). Analysis in this study made use of AMSR-E land surface variables version 1.2 (*Jones and Kimball*, 2012) and version 0.9.1 of GlobSnow SWE (*Luojus et al.*, 2009).

A.2.1 GlobSnow snow water equivalent (winter season)

The snow depth and quantity of snow can be estimated from passive microwave observations as a linear function of the difference between brightness temperatures at two frequencies, such as 18 GHz and GHz with horizontal polarization (*Chang et al.*, 1987). A new data set used for SWE estimates, GlobSnow, optimizes agreement between measured and simulated brightness temperature using forward simulation of different grain sizes.

GlobSnow SWE estimates (in mm) are calculated using AMSR-E 18.7 and 36.5 GHz data as well as meteorological data. Meteorological stations provide estimates of snow depth, which are filtered to remove spurious values and are then kriged between stations (*Takala et al.*, 2011). In the GlobSnow algorithm, regions with thin snowpacks, snowmelt or wet snow are masked out, as wet snow acts as a microwave emitter (*Armstrong and Brodzik*, 2001). Snow grain size is estimated through an inversion of AMSR-E observations using the

Helsinki University of Technology snow microwave emission model (*Pulliainen et al.*, 1999). Snow water equivalent is then calculated from snow depth through knowledge of snow density. Single fixed variables are used to estimate snowpack, soil and forest characteristics. Surface roughness and soil moisture are assumed to have the same value across the entire pan-Arctic, and forest cover effects are removed using vegetation transmissivity collected in winter (*Pulliainen*, 2006).

GlobSnow SWE has been validated for several northern sites, and was found to have a root mean squared error (RMSE) of 33 mm (*Luojus et al.*, 2009). GlobSnow SWE has been found to simulate *in situ* SWE more accurately than other SWE algorithms, especially over >100 mm snowpacks (*Luojus et al.*, 2010; *Takala et al.*, 2011; *Hancock et al.*, 2013). Overall, GlobSnow SWE has been found to perform well at estimating values of SWE up to 150 mm. Thicker snowpacks act as a source of emission rather than a scattering medium, which leads to SWE being underestimated (*Takala et al.*, 2011). Over Canadian tundra regions, this threshold has been observed at 130 mm (*Derksen et al.*, 2010). It is also important to note that passive microwave retrievals of SWE are only reliable over >15 mm snowpacks (*Solberg et al.*, 2009), as thin snowpacks are difficult to detect. Similarly, although specific modifications are made to the GlobSnow SWE algorithm to enable accuracy over forested regions, the amount of SWE recorded over densely forested regions can be underestimated (*Takala et al.*, 2011). GlobSnow estimates of SWE are therefore considered most reliable over the 15–150 mm range in forested regions without dense canopy cover, and over the 15–130 mm range over tundra regions.

A.2.2 NTSG air temperature (growing season)

The central goal in the creation of the NTSG land surface variable dataset was to gain accurate estimates of minimum and maximum air temperature (in Kelvin) at a height of 2 m using AMSR-E observations. The accuracy of NTSG air temperature estimates was improved by quantifying and removing the influence of vegetation, soil moisture and atmospheric water vapor on brightness temperature. Vegetation transmissivity and soil moisture variables were therefore extracted through this process (*Jones and Kimball*, 2010b).

Minimum air temperature is calculated according to morning retrievals, and maximum air temperature is calculated according to late afternoon retrievals. Both estimates carefully account for the effects of vegetation, soil moisture, fractional cover of open water on land, and atmospheric water vapor. The complete details regarding calculations of air temperature can be found in *Jones et al.* (2010). Air temperatures from meteorological stations were used for calibration (270 stations) and validation (273 stations) of resulting products, with these stations being assigned randomly. Comparisons indicated root

mean squared error (RMSE) values of 3.5 K between AMSR-E derived temperature and meteorological data. Larger errors were observed in regions with sparse vegetation, higher elevations and higher fractional cover of open water on land. Non-desert regions had RMSE values between 1 and 3.5 K, which shows better accuracy than previous approaches that had relied on carefully selected meteorological stations (*Jones et al.*, 2010). For the purpose of this project, daily air temperature was calculated as the daily average of maximum and minimum temperatures reported by *Jones et al.* (2010).

A.2.3 NTSG soil moisture (growing season)

The emissivity of soils depends largely on its dielectric properties. The real part of the dielectric constant increases as a function of soil moisture content. As a result, wetter soils have a diminished emissivity relative to drier soils (*Njoku and Kong*, 1977). Passive microwave observations are most sensitive to subsurface soil moisture at low ($\lesssim$3 GHz) frequencies, and at these low frequencies, the influences of vegetation and surface roughness is also limited (*Njoku and Kong*, 1977; *Njoku and Chan*, 2005).

The NTSG soil moisture product therefore relies primarily on the lowest AMSR-E frequency (6.9 GHz) to generate estimates of surface ($\leq$2 cm) soil moisture (*Jones and Kimball*, 2010a). Soil moisture is expressed as a dimension-free value ranging between 0–1. Soil moisture was found to be correlated with precipitation at meteorological stations in the Northern Hemisphere ($0.2 < r < 0.8$) (*Jones and Kimball*, 2010, updated 2011).

A.2.4 NTSG vegetation transmissivity (growing season)

Vegetation acts as an attenuating layer that diminishes the transmissivity of passive microwave radiation. The vegetation water content alters the dielectric properties of the landscape, such that there exists diminished emissivity over regions with greater vegetation water content (*Jackson and O'Neill*, 1990). Furthermore, the vegetation canopy layers influence scattering (*Jones and Kimball*, 2010a), generally resulting in increased scattering and diminished transmissivity over regions that have greater biomass, although the canopy structure (stem geometry, leaf orientation, angle distributions, spatial distribution, etc.) and type of vegetation also influence the surface roughness and scattering (*Njoku and Chan*, 2005; *Jensen*, 2007). The optical depth of vegetation can thus be defined according to the height of the attenuating layer (z_{top}) and the extinction with height ($k(z)$ in 1/m) (*Jones et al.*, 2010):

$$\tau = \int_0^{z_{\text{top}}} k(z)\mathrm{d}z. \tag{A.1}$$

Over a vegetated region with a single species and relatively constant surface roughness, the attenuating influence of vegetation, or vegetation optical depth (τ), can be estimated as a linear function of canopy water content (g in kg/m^2) using a species-specific parameter (b): $\tau = b \times g$ (*Jackson and O'Neill*, 1990). A similar description is used by *Jones et al.* (2010) to define the optical depth of Northern Hemispheric vegetation as a function of water content using a parameter α that expresses both the influences of roughness factors (h) and look angle (θ), as well as frequency and angular impacts on canopy extinction (b in m^2/kg):

$$\tau = \alpha g = bhg\sec(\theta). \tag{A.2}$$

Vegetation transmissivity to passive microwave radiation (t) can be expressed as the logarithmically scaled counterpart of vegetation optical depth: $t = \exp(-\tau)$. Vegetation transmissivity is calculated iteratively from a combination of inverted analytical expressions using AMSR-E inputs, emissivity and ratios, as detailed in *Jones et al.* (2010). Separate versions of the NTSG vegetation transmissivity product are available using inputs from the 6.9, 10.7 and 18.7 GHz channels. There is a great deal of similarity between these observations, and so only the 10.7 GHz channel is used in this analysis, just as in *Njoku and Chan* (2005).

Comparisons of this product with Moderate Resolution Imaging Spectroradiometer (MODIS) derived leaf area index, normalized difference vegetation index (NDVI) and enhanced vegetation index yielded correlations of up to 0.9 (*Jones et al.*, 2011). As the aforementioned MODIS products are typically used to estimate the vegetation health or quantity of aboveground biomass, it seems reasonable to assume that vegetation transmissivity likewise provides a relatively reliable estimate of the quantity of aboveground biomass.

References

Abramowitz, G., A. Pitman, and H. Gupta (2007), Systematic bias in land surface models, *Journal of Hydrometeorology*, *8*, 989–1001. 20

Adams, J., N. Bond, and J. Overland (2000), Regional variability of the Arctic heat budget in fall and winter, *Journal of Climate*, *13*, 3500–3510. 77

AMAP (2011), Snow, water, ice and permafrost in the Arctic (SWIPA), *Oslo: Arctic Monitoring and Assessment Programme (AMAP)*. 38, 39, 59

Amiro, B. (2010), Estimating annual carbon dioxide eddy fluxes using open-path analyzers for cold forest sites, *Agricultural and Forest Meteorology*, *150*, 1366–1372. 17, 54

Ananyan, A. (1970), Unfrozen water content in frozen clay at a temperature from -0.6°c to -40°c – -60°c, *Merzlotnye Issledovaniya*, *10*, 267–270. 19

Arft, A., et al. (1999), Responses of tundra plants to experimental warming: Meta-analysis of the international tundra experiment, *Ecological Monographs*, *69*(4), 491–511. 85

Armstrong, R., and M. Brodzik (2001), Recent northern hemisphere snow extent: A comparison of data derived from visible and microwave satellite sensors, *Geophysical Research Letters*, *28*(19), 3673–3676. 119

Ashcroft, P., and F. Wentz (2003), AMSR-E/Aqua L2A global swath spatially-resampled brightness temperatures (Tb) V001, *National Snow and Ice Data Center, Boulder, CO, digital media*. 119

Atwood, D., R. Guritz, R. Muskett, et al. (2007), DEM control in Arctic Alaska with ICESat laser altimetry, *IEEE Transactions on Geoscience and Remote Sensing*, *45*, 3710–3720. 32

Aurela, M., T. Laurila, and J. Tuovinen (2004), The timing of snow melt controls the annual CO_2 balance in a subarctic fen, *Geophysical Research Letters*, *31*(16), L16,119. 12, 13, 37, 39, 92

Ayres, E., J. Nkem, D. Wall, B. Adams, J. Barrett, B. Simmons, R. Virginia, and A. Fountain (2010), Experimentally increased snow accumulation alters soil moisture and animal community structure in a polar desert, *Polar Biology*, *33*(7), 897–907. 79

Bäckstrand, K., P. Crill, M. Jackowicz-Korczyñski, et al. (2010), Annual carbon gas budget for a subarctic peatland, Northern Sweden, *Biogeosciences*, *7*, 95–108. 17

Baker, I. (2005), SiB3 prognostic variables and equation set, *Available at, http, //bioda-vatmoscolostateedu/kraus/Papers/SiB/SiB3_eqns_masterpdf*. 14

Baker, I., L. Prihodko, A. Denning, et al. (2008), Seasonal drought stress in the Amazon: Reconciling models and observations, *Journal of Geophysical Research – Biogeosciences*, *113*, G00B01. 14, 20

Baldocchi, D. (2008), Breathing of the terrestrial biosphere, Lessons learned from a global network of carbon dioxide flux measurements, *Australian Journal of Botany*, *56*, 1–26. 14

Baldocchi, D., B. Hincks, and T. Meyers (1988), Measuring biosphere-atmosphere exchanges of biologically related gases with micrometeorological methods, *Ecology*, *69*(5), 1331–1340. 17

Bi, J., L. Xu, A. Samanta, Z. Zhu, and R. Myneni (2013), Divergent arctic-boreal vegetation changes between North America and Eurasia over the past 30 years, *Remote Sensing*, *5*(5), 2093–2112. 103

Billings, W., and H. Mooney (1968), The ecology of arctic and alpine plants, *Biological Reviews*, *43*, 481–529. 23, 24, 45

Björkman, M., E. Morgner, E. Cooper, et al. (2010), Winter carbon dioxide effluxes from Arctic ecosystems, An overview and comparison of methodologies, *Global Biogeochemical Cycles*, *24*, GB3010. 13, 16, 17, 28

Boesch, H., D. Baker, B. Connor, D. Crisp, and C. Miller (2011), Global characterization of CO_2 column retrievals from shortwave-infrared satellite observations of the orbiting carbon observatory-2 mission, *Remote Sensing*, *3*(2), 270–304. 16

Bokhorst, S., J. Bjerke, H. Tømmervik, et al. (2009), Winter warming events damage sub-Arctic vegetation, consistent evidence from an experimental manipulation and a natural event, *Journal of Ecology*, *97*, 1408–1415. 28, 39

Bokhorst, S., J. Bjerke, F. Bowles, et al. (2010), Impacts of extreme winter warming events on litter decomposition in a sub-Arctic heathland, *Soil Biology and Biochemistry*, *42*, 611–617. 13, 19, 20, 25, 28, 29, 45, 57

Bonan, G. (2002), *Ecological Climatology, Concepts and Applications*, New York, Cambridge University Press. 10, 21, 22, 28, 45, 68, 77, 78, 85

Bondeau, A., P. Smith, S. Zaehle, et al. (2007), Modelling the role of agriculture for the 20th century global terrestrial carbon balance, *Global Change Biology*, *13*, 679–706. 14, 20

Breiman, L., and J. Friedman (1985), Estimating optimal transformations for multiple regression and correlation, *Journal of the American Statistical Association*, *80*(391), 580–598. 64, 65, 66

Bréon, F., and P. Ciais (2010), Spaceborne remote sensing of greenhouse gas concentrations, *Comptes Rendus - Geoscience*, *342*(4-5), 412–424. 17

Buckeridge, K., and P. Grogan (2010), Deepened snow increases late thaw biogeochemical pulses in mesic low Arctic tundra, *Biogeochemistry*, *101*, 105–121. 13, 27, 28, 30, 38, 45, 59

Buckeridge, K., Y. Cen, D. Layzell, et al. (2010), Soil biogeochemistry during the early spring in low Arctic mesic tundra and the impacts of deepened snow and enhanced nitrogen availability, *Biogeochemistry*, *99*, 127–141. 13, 57

Burt, T., and D. Butcher (1985), Topographic controls of soil moisture distributions, *European Journal of Soil Science*, *36*(3), 469–486. 79

Callaghan, T., et al. (2011), The changing face of Arctic snow cover: A synthesis of observed and projected changes, *AMBIO: A Journal of the Human Environment*, *40*, 17–31. 71, 85

Campbell, J., M. Mitchell, P. Groffman, et al. (2005), Winter in northeastern North America: A critical period for ecological processes, *Frontiers in Ecology and the Environment*, *3*, 314–322. 17

Cao, Z., R. Stewart, and W. Hogg (2007), Extreme winter warming over the Mackenzie Basin, Observations and causes, *In, Woo M-K (ed) Cold Region Atmospheric and Hydrologic Studies, The Mackenzie GEWEX Experience*, *1*, 83–108. 39

Carstairs, A., and W. Oechel (1978), Effects of several microclimatic factors and nutrients on net carbon dioxide exchange in Cladonia alpestris (L) Rabh in the sub-Arctic, *Arctic and Alpine Research*, *10*(1), 81–94. 24, 45

Chang, A., J. Foster, M. Owe, et al. (1985), Passive and active microwave studies of wet snowpack properties, *Nordic Hydrology*, *16*, 57–66. 35

Chang, A., J. Foster, and D. Hall (1987), Nimbus-7 smmr derived global snow cover parameters, *Annals of Glaciology*, *9*(9), 39–44. 119

Chang, T., P. Gloersen, T. Schmugge, et al. (1976), Microwave emission from snow and glacier ice, *Journal of Glaciology*, *16*, 23–39. 33

Chapin, F. (1983), Direct and indirect effects of temperature on arctic plants, *Polar Biology*, *2*(1), 47–52. 103

Chapin III, F., and G. Shaver (1985), Individualistic growth response of tundra plant species to environmental manipulations in the field, *Ecology*, *66*(2), 564–576. 93

Chevallier, F., L. Feng, H. Bösch, P. Palmer, and P. Rayner (2010), On the impact of transport model errors for the estimation of CO_2 surface fluxes from GOSAT observations, *Geophysical Research Letters*, *37*(21), L21,803. 16

Christensen, C., N. Schmidt, and A. Michelsen (2012), High Arctic dry heath CO_2 exchange during the early cold season, *Ecosystems*, *15*, 1083–1092. 10, 13, 24

Christensen, J., B. Hewitson, A. Busuioc, et al. (2007), Regional Climate Projections, *In, Solomon S, Qin D, Manning M, and others (eds) Climate Change, 2007*. 38

Church, J. (1933), Snow surveying: its principles and possibilities, *Geographical Review*, *23*(4), 529–563. 83, 85

Colbeck, S. (1980), Thermodynamics of snow metamorphism due to variations in curvature, *Journal of Glaciology*, *26*, 291–301. 26

Coops, N., T. Black, R. Jassal, et al. (2007), Comparison of MODIS, eddy covariance determined and physiologically modelled gross primary production (GPP) in a Douglas-fir forest stand, *Remote Sensing of Environment*, *107*, 385–401. 20

Cox, P., R. Betts, C. Jones, et al. (2000), Acceleration of global warming due to carbon-cycle feedbacks in a coupled climate model, *Nature*, *408*, 184–187. 10

Cramer, W., D. Kicklighter, B. A, et al. (1999), Comparing global models of terrestrial net primary productivity (NPP): Overview and key results, *Global Change Biology*, *5*, 1–15. 10, 14, 16

Cramer, W., A. Bondeau, and F. Woodward (2001), Global response of terrestrial ecosystem structure and function to CO and climate change, Results from six dynamic global vegetation models, *Global Change Biology*, *7*, 357–373. 10, 39

Crane, R., and M. Anderson (1984), Satellite discrimination of snow/cloud surfaces, *International Journal of Remote Sensing*, *5*(1), 213–223. 30

D'Agostino, R., and M. Stephens (1986), *Goodness-of-fit techniques*, vol. 68, CRC. 73

Dai, Y., X. Zeng, R. Dickinson, et al. (2003), The common land model, *Bulletin of the American Meteorological Society*, *84*, 1013–1023. 14

Dankers, R., and S. De Jong (2004), Monitoring snow-cover dynamics in Northern Fennoscandia with SPOT VEGETATION images, *International Journal of Remote Sensing*, *25*(2933-). 31

Deems, J., S. Fassnacht, and K. Elder (2006), Fractal distribution of snow depth from LiDAR data, *Journal of Hydrometeorology*, *7*, 285–297. 32

Derksen, C., P. Toose, A. Rees, et al. (2010), Development of a tundra-specific snow water equivalent retrieval algorithm for satellite passive microwave data, *Remote Sensing of Environment*, *114*, 1699–1709. 34, 120

Dietze, M., R. Vargas, A. Richardson, et al. (2011), Characterizing the performance of ecosystem models across time scales: A spectral analysis of the North American Carbon Program site-level synthesis, *Journal of Geophysical Research*, *116*, G04,029. 14

Dozier, J. (1989), Spectral signature of alpine snow cover from the landsat thematic mapper, *Remote sensing of Environment*, *28*, 9–22. 46

Dozier, J., and T. Painter (2004), Multispectral and hyperspectral remote sensing of alpine snow properties, *Annual Review of Earth and Planetary Sciences*, *32*, 465–494. 31

Duguay, C., J. Green, C. Derksen, M. English, A. Rees, M. Sturm, and A. Walker (2005), Preliminary assessment of the impact of lakes on passive microwave snow retrieval algorithms in the arctic, in *62nd Eastern Snow Conference Proceedings*, pp. 223–228. 84

Elberling, B. (2007), Annual soil CO_2 effluxes in the High Arctic: The role of snow thickness and vegetation type, *Soil Biology and Biogeochemistry*, *39*, 646–654. 13, 21, 25, 26, 29, 33, 93

Elberling, B., and K. Brandt (2003), Uncoupling of microbial CO_2 production and release in frozen soil and its implications for field studies of Arctic C cycling, *Soil Biology and Biochemistry*, *35*(2), 263–272. 12, 13, 18, 19, 20, 92

Elberling, B., C. Nordstrøm, L. Grøndahl, et al. (2008), High-Arctic soil CO_2 and CH_4 production controlled by temperature, water, freezing and snow, *Advances in Ecological Research*, *40*, 441–472. 13, 28, 30, 45

Entekhabi, D., et al. (2010), The soil moisture active passive (smap) mission, *Proceedings of the IEEE*, *98*(5), 704–716. 35

Essery, R., and J. Pomeroy (2004), Vegetation and topographic control of wind-blown snow distributions in distributed and aggregated simulations for an arctic tundra basin, *Journal of Hydrometeorology*, *5*(5), 735–744. 81, 82

Euskirchen, E., A. McGuire, D. Kicklighter, et al. (2006), Importance of recent shifts in soil thermal dynamics on growing season length, productivity, and carbon sequestration in terrestrial high-latitude ecosystems, *Global Change Biology*, *12*, 731–750. 10

Euskirchen, E., M. Bret-Harte, G. Scott, et al. (2012), Seasonal patterns of carbon dioxide and water fluxes in three representative tundra ecosystems in northern Alaska, *Ecosphere*, *3*, 1–19. 13, 17, 24, 25, 38, 45, 95

Evans, B., D. Walker, C. Benson, E. Nordstrand, and G. Petersen (1989), Spatial interrelationships between terrain, snow distribution and vegetation patterns at an arctic foothills site in Alaska, *Ecography*, *12*(3), 270–278. 82

Fassnacht, S., and J. Deems (2006), Measurement sampling and scaling for deep montane snow depth data, *Hydrological Processes*, *20*, 829–838. 32

Fisher, J. B., et al. (In Preparation), The state of land surface model uncertainty for the Alaskan Arctic, *Journal of Geophysical Research*. 91

Fitzgibbon, J., and T. Dunne (1979), Characteristics of subarctic snowcover/les caractéristiques de la couverture de neige presque arctique, *Hydrological Sciences Journal*, *24*(4), 465–476. 82

Foster, J., C. Sun, J. Walker, et al. (2005), Quantifying the uncertainty in passive microwave snow water equivalent observations, *Remote Sensing of Environment*, *94*, 187–203. 33

Foster, J., D. Hall, J. Eylander, et al. (2011), A blended global snow product using visible, passive microwave and scatterometer satellite data, *International Journal of Remote Sensing*, *32*, 1371–1395. 31, 34, 35

Fox, A., B. Huntley, C. Lloyd, et al. (2008), Net ecosystem exchange over heterogeneous Arctic tundra, Scaling between chamber and eddy covariance measurements, *Global Biogeochemical Cycles*, *22*, GB2027. 13, 17

Frank, I., and S. Lanteri (1988), ACE: A non-linear regression model, *Chemometrics and intelligent laboratory systems*, *3*(4), 301–313. 64, 65, 66

Frei, A., and S. Lee (2010), A comparison of optical-band based snow extent products during spring over North America, *Remote Sensing of Environment*, *114*(9), 1940–1948. 31

Frei, A., M. Tedesco, S. Lee, J. Foster, D. Hall, R. Kelly, and D. Robinson (2012), A review of global satellite-derived snow products, *Advances in Space Research*, *50*(8), 1007–1029. 32

French, H., and A. Binley (2004), Snowmelt infiltration: Monitoring temporal and spatial variability using time-lapse electrical resistivity, *Journal of Hydrology*, *297*(1-4), 174–186. 79

Friedlingstein, P., L. Bopp, P. Ciais, et al. (2001), Positive feedbacks between future climate change and the carbon cycle, *Geophysical Research Letters*, *28*(8), 1543–1546. 10

Gatswirth, J., Y. Gel, and W. Miao (2009), The impact of Levene's test of equality of variances on statistical theory and practice, *Statistical Science*, *24*(3), 343–360. 71

Gel, Y. (2007), Comparative analysis of the local observation-based (LOB) method and the nonparametric regression-based method for gridded bias correction in mesoscale weather forecasting, *Weather and Forecasting*, *22*(6), 1243–1256. 64

Gelfan, A., J. Pomeroy, and L. Kuchment (2004), Modeling forest cover influences on snow accumulation, sublimation, and melt, *Journal of Hydrometeorology*, *5*(5), 785–803. 82, 83

Golding, D., and R. Swanson (1986), Snow distribution patterns in clearings and adjacent forest, *Water Resources Research*, *22*(13), 1931–1940. 82

Gould, W., D. Walker, and D. Biesboer (2003), Combining research and education: Bioclimatic zonation along a Canadian Arctic transect, *Arctic*, *56*(1), 45–54. 21

Goulden, M. L., J. W. Munger, S.-M. FAN, B. C. Daube, and S. C. Wofsy (1996), Measurements of carbon sequestration by long-term eddy covariance: Methods and a critical evaluation of accuracy, *Global change biology*, *2*(3), 169–182. 95

Gouttevin, I., M. Menegoz, F. Dominé, et al. (2012), How the insulating properties of snow affect soil carbon distribution in the continental pan-Arctic area, *Journal of Geophysical Research Biogeosciences*, *117*, G02,020. 15, 46

Gray, D., and D. Male (1981), *Handbook of Snow, Principles, Processes, Management & Use*, Pergamon Press. 22, 23, 26, 27, 28, 29, 34

Green, J., C. Kongoli, A. Prakash, M. Sturm, C. Duguay, and S. Li (2012), Quantifying the relationships between lake fraction, snow water equivalent and snow depth, and microwave brightness temperatures in an arctic tundra landscape, *Remote Sensing of Environment*, *127*, 329–340. 84

Grippa, M., L. Kergoat, T. L. Toan, N. Mognard, N. Delbart, J. L'Hermitte, and S. Vicente-Serrano (2005), The impact of snow depth and snowmelt on the vegetation variability over central Siberia, *Geophysical Research Letters*, *32*(21), L21,412. 82

Grogan, P., and F. Chapin III (1999), Arctic soil respiration, Effects of climate and vegetation depend on season, *Ecosystems*, *2*(5), 451–459. 13

Grogan, P., and S. Jonasson (2005), Temperature and substrate controls on intra-annual variation in ecosystem respiration in two subarctic vegetation types, *Global Change Biology*, *11*(3), 465–475. 13, 17

Grogan, P., and S. Jonasson (2006), Ecosystem CO_2 production during winter in a Swedish subartic region: The relative importance of climate and vegetation type, *Global Change Biology*, *12*, 1479–1495. 13, 22, 23, 24, 33

Grogan, P., A. Michelsen, P. Ambus, et al. (2004), Freeze-thaw regime effects on carbon and nitrogen dynamics in sub-Arctic heath tundra mesocosms, *Soil Biology and Biochemistry*, *36*, 641–654. 13, 28, 45, 57

Hall, D., and G. Riggs (2007), Accuracy assessment of MODIS snow products, *Hydrological Processes*, *21*, 1534–1547. 30, 31, 46

Hall, D., G. Riggs, and V. Salomonson (1995), Development of methods for mapping global snow cover using moderate resolution imaging spectroradiometer data, *Remote Sensing of Environment*, *54*, 127–140. 30, 49

Hall, D., J. Foster, D. Verbyla, et al. (1998), Assessment of snow-cover mapping accuracy in a variety of vegetation-cover densities in central Alaska, *Remote Sensing of Environment*, *66*, 129–137. 31

Hall, D., G. Riggs, V. Salomonson, N. DiGirolamo, and K. Bayr (2002), MODIS snow-cover products, *Remote sensing of Environment*, *83*(1), 181–194. 46

Hancock, S., R. Baxter, J. Evans, and B. Huntley (2013), Evaluating global snow water equivalent products for testing land surface models, *Remote Sensing of Environment*, *128*, 107–117. 120

Hardy, J., et al. (2001), Snow depth manipulation and its influence on soil frost and water dynamics in a northern hardwood forest, *Biogeochemistry*, *56*, 151–174. 79, 80, 81, 85

Hare, F. (1968), The Arctic, *Quarterly Journal of the Royal Meteorological Society*, *94*(402), 439–459. 71

Helfrich, S., D. McNamara, B. Ramsay, et al. (2007), Enhancements to, and forthcoming developments in the Interactive Multisensor Snow and Ice Mapping System (IMS), *Hydrological Processes*, *21*, 1576–1586. 31

Hilton, T., K. Davis, K. Keller, and N. Urban (2012), Improving terrestrial CO_2 flux diagnosis using spatial structure in land surface model residuals, *Biogeosciences Discussions*, *9*, 7073–7116. 49

Hinzman, L., et al. (2005), Evidence and implications of recent climate change in northern alaska and other arctic regions, *Climatic Change*, *72*(3), 251–298. 3, 103

Hopkinson, C., M. Sitar, L. Chasmer, et al. (2004), Mapping snowpack depth beneath forest canopies using airborne LiDAR, *Photogrammetric Engineering and Remote Sensing*, *70*, 323–330. 32

Humphreys, E., and P. Lafleur (2011), *Does earlier snowmelt lead to greater CO_2 sequestration in two low Arctic tundra ecosystems?*, vol. 38, L09703 pp. 13, 28, 45, 47, 59, 93, 94

Huntzinger, D., W. Post, Y. Wei, et al. (2012), North American Carbon Program (NACP) regional interim synthesis: Terrestrial biospheric model intercomparison, *Ecological Modelling*, *232*, 144–157. 14, 16, 20, 91

Jackson, T., and P. O'Neill (1990), Attenuation of soil microwave emission by corn and soybeans at 14 and 5 ghz, *IEEE Transactions on Geoscience and Remote Sensing*, *28*(5), 978–980. 121, 122

Janowicz, R., D. Gray, and J. Pomeroy (2003), Spatial variability of fall soil moisture and spring snow water equivalent within a mountainous sub-arctic watershed, in *Proceedings of the Eastern Snow Conference*, vol. 60, pp. 127–139. 79

Jeffries, M., T. Zhang, K. Frey, et al. (1999), Estimating late-winter heat flow to the atmosphere from the lake-dominated Alaskan North Slope, *Journal of Glaciology*, *45*, 315–324. 27

Jensen, J. (2007), *Remote Sensing of the Environment: An Earth Resource Perspective*, Pearson Prentice Hall. x, 42, 82, 121

Johnson, D., and M. Caldwell (1975), Gas exchange of four arctic and alpine tundra plant species in relation to atmospheric and soil moisture stress, *Oecologia*, *21*(2), 93–108. 93

Johnsson, H., and L.-C. Lundin (1991), Surface runoff and soil water percolation as affected by snow and soil frost, *Journal of Hydrology*, *122*(1-4), 141–159. 79, 80, 81

Jones, H., J. Pomeroy, T. Davies, et al. (1999), CO_2 in Arctic snow cover, Landscape form, in-pack gas concentration gradients, and the implications for the estimation of gaseous fluxes, *Hydrological Processes*, *13*, 2977–2989. 13, 17, 21, 27

Jones, L., and J. Kimball (2010a), A global daily record of land surface parameter retrievals from AMSR-E Version 11. 119, 121

Jones, L., and J. Kimball (2010, updated 2011), Daily Global Land Surface Parameters Derived from AMSR-E. 121

Jones, L., and J. Kimball (2012), *Daily Global Land Surface Parameters Derived from AMSR-E*, Boulder, Colorado USA: National Snow and Ice Data Center, digital media. 63, 119

Jones, L., C. Ferguson, J. Kimball, K. Zhang, S. Chan, K. McDonald, E. Njoku, and E. Wood (2010), Satellite Microwave Remote Sensing of Daily Land Surface Air Temperature Minima and Maxima From AMSR-E, *IEEE Journal of Selected Topics in Applied Earth Observations and Remote Sensing*, *3*(1), 111–123. 119, 120, 121, 122

Jones, L. A., and J. S. Kimball (2010b), Daily Global Land Surface Parameters Derived from AMSR-E, Digital media. 120

Jones, M., J. Kimball, K. McDonald, and L. Jones (2011), Utilizing satellite passive microwave remote sensing for monitoring global land surface phenology, *Remote Sensing of Environment*, *115*, 1102–1114. 122

Jung, M., K. Henkel, M. Herold, and G. Churkina (2006), Exploiting synergies of global land cover products for carbon cycle modeling, *Remote Sensing of Environment*, *101*(4), 534–553. 69, 93

Jung, M., M. Reichstein, A. Bondeau, et al. (2009), Towards global empirical upscaling of fluxnet eddy covariance observations: validation of a model tree ensemble approach using a biosphere model, *Biogeosciences*, *6*(10), 2001–2013. 96

Kane, D., L. Hinzman, C. Benson, and G. Liston (1991), Snow hydrology of a headwater arctic basin 1 physical measurements and process studies, *Water Resources Research*, *27*(6), 1099–1109. 80

Kappen, L. (1993), Plant activity under snow and ice with particular reference to lichens, *Arctic*, *46*, 297–302. 23

Kawanishi, T., et al. (2003), The Advanced Microwave Scanning Radiometer for the Earth Observing System (AMSR-E), NASDA's contribution to the EOS for global energy and water cycle studies, *IEEE Transactions on Geoscience and Remote Sensing*, *41*(2), 184–194. 118

Kelly, R. (2009), The AMSR-E snow depth algorithm: Description and initial results, *Journal of the Remote Sensing Society of Japan*, *29*(1), 307–317. 119

Khvorostyanov, D., G. Krinner, and P. Ciais (2008), Vulnerability of permafrost carbon to global warming Part I, Model description and role of heat generated by organic matter decomposition, *Tellus Series B*, *60*, 250–264. 19

Kim, S., J. van Zyl, K. McDonald, and E. Njoku (2010), Monitoring surface soil moisture and freeze-thaw state with the high-resolution radar of the Soil Moisture Active/Passive (SMAP) mission, in *2010 IEEE Radar Conference*, pp. 735–739, IEEE. 35

Knowles, K., M. Savoie, R. Armstrong, and M. Brodzik (2010), AMSR-E/Aqua daily EASE grid brightness temperatures, NSIDC. 119

Koven, C., B. Ringeval, P. Friedlingstein, et al. (2011), Permafrost carbon-climate feedbacks accelerate global warming, *Proceedings of the National Academy of Sciences*, *108*, 14,769–14,774. 19

Krinner, G., N. Viovy, N. De Noblet-Ducoudre, et al. (2005), A dynamic global vegetation model for studies of the coupled atmosphere-biosphere system, *Global Biogeochemical Cycles*, *19*, GB1015. 14, 20

Kucharik, C., J. Foley, C. Delire, et al. (2000), Testing the performance of a dynamic global ecosystem model: Water balance, carbon balance, and vegetation structure, *Global Biogeochemical Cycles*, *14*, 795–825. 15

Kwok, R., and G. Cunningham (2008), *ICESat over Arctic sea ice: Estimation of snow depth and ice thickness*, vol. 113, C08010 pp. 32

La Puma, I., T. Philippi, and S. Oberbauer (2007), Relating NDVI to ecosystem CO_2 exchange patterns in response to season length and soil warming manipulations in Arctic Alaska, *Remote Sensing of Environment*, *109*(2), 225–236. 13, 20

Lafleur, P., and E. Humphreys (2008), Spring warming and carbon dioxide exchange over low Arctic tundra in central Canada, *Global Change Biology*, *14*, 740–756. 3, 38, 47, 91, 94

Lafleur, P., T. Griffis, and W. Rouse (2001), Interannual variability in net ecosystem CO_2 exchange at the Arctic treeline, *Arctic, Antarctic, and Alpine Research*, *33*, 149–157. 13

Lafleur, P., E. R. Humphreys, V. L. St. Louis, M. C. Myklebust, T. Papakyriakou, L. Poissant, J. D. Barker, M. Pilote, and K. Swystun (2012), Variation in peak growing season net ecosystem production across the canadian arctic, *Environmental Science and Technology*. 96, 99

Lantz, T., S. Gergel, and S. Kokelj (2010), Spatial heterogeneity in the shrub tundra ecotone in the Mackenzie Delta region, Northwest Territories, *Implications for Arctic environmental change Ecosystems*, *13*, 194–204. 13

Larsen, K., A. Ibrom, S. Jonasson, et al. (2007a), Significance of cold-season respiration and photosynthesis in a subarctic heath ecosystem in Northern Sweden, *Global Change Biology*, *13*, 1498–1508. 12, 13, 23, 24, 92

Larsen, K., P. Grogan, S. Jonasson, et al. (2007b), Respiration and microbial dynamics in two subarctic ecosystems during winter and spring thaw: Effects of increased snow depth, *Arctic, Antarctic, and Alpine Research*, *39*, 268–276. 58

Laskowski, C. (2010), Seasonal, annual, and interannual carbon dynamics of a remote tussock tundra ecosystem in Ivotuk, Alaska, Ph.D. thesis, University of California Davis and San Diego State University. 47, 94

Lefsky, M., W. Cohen, G. Parker, et al. (2002), LiDAR remote sensing for ecosystem studies, *BioScience*, *52*, 19–30. 32

Lemoine, F., N. Zelensky, D. Chinn, et al. (2010), Towards development of a consistent orbit series for TOPEX, Jason-1, and Jason-2, *Advances in Space Research*, *46*, 1513–1540. 32

Levene, H. (1960), Robust testes for equality of variances, in *Contributions to Probability and Statistics*, Stanford University Press. 70

Levy, P., A. Grelle, A. Lindroth, et al. (1999), Regional-scale CO_2 fluxes over central Sweden by a boundary layer budget method, *Agricultural and Forest Meteorology*, *98*, 169–180. 20

Lin, J., C. Gerbig, S. Wofsy, et al. (2004), Measuring fluxes of trace gases at regional scales by Lagrangian observations, Application of the CO_2 Budget and Rectification Airborne (COBRA) study, *Journal of Geophysical Research: Atmospheres*, *109*, D15,304. 16

Lin, J., M. Pejam, E. Chan, et al. (2011), Attributing uncertainties in simulated biospheric carbon fluxes to different error sources, *Global Biogeochemical Cycles*, *25*. 14, 94, 95

Liston, G., and M. Sturm (2002), Winter precipitation patterns in arctic Alaska determined from a blowing-snow model and snow-depth observations, *Journal of Hydrometeorology*, *3*(6), 646–659. 81

Lovett, G., J. Cole, and M. Pace (2006), Is net ecosystem production equal to ecosystem carbon accumulation?, *Ecosystems*, *9*(1), 152–155. 12, 45

Lundberg, A., and S. Halldin (2001), Snow interception evaporation: Review of measurement techniques, processes, and models, *Theoretical and Applied Climatology*, *70*(1), 117–133. 82, 84

Luojus, K., J. Pulliainen, and C. Derksen (2009), Snow Water Equivalent (SWE) product guide, *Global Snow Monitoring for Climate Research*, *091/01*. 63, 119, 120

Luojus, K., J. Pulliainen, M. Takala, J. Lemmetyinen, C. Derksen, and L. Wang (2010), Snow Water Equivalent (SWE) product guide, Global Monitoring for Climate Research. 120

Luus, K. (2009), Analyzing pan-Arctic 1982–2006 trends in temperature and bioclimatological indicators (productivity, phenology and vegetation indices) using remote sensing, model and field data, Master's thesis, University of Waterloo, Waterloo, ON, Canada. xiv, 4

Luus, K., C. Duguay, R. Kelly, J. Lin, and Y. Gel (2010a), AMSR-E snow water equivalent associated with AMSR-E growing season soil moisture, vegetation opacity and air temperature over six arctic study sites (2003-2008), in *Proceedings of the 67th Eastern Snow Conference*. 1

Luus, K., J. Lin, J. McCaughey, H. Margolis, and R. Kelly (2010b), Estimating the influence of snow on net ecosystem exchange, in *AGU Fall Meeting Abstracts*, vol. 1, p. 0428. 5

Luus, K., R. Kelly, J. Lin, E. Humphreys, and P. Lafleur (2011), Influence of snow cover area on net ecosystem exchange during snowmelt at Daring Lake, NWT, in *Proceedings of the 68th Eastern Snow Conference*. 1

Luus, K., J. Lin, and R. Kelly (2012), Modeling the impacts of snow, soil and vegetation drivers on North American net ecosystem exchange north of 55-deg N, in *International Polar Year Conference*. 1

Luus, K., Y. Gel, J. Lin, R. Kelly, and C. Duguay (2013), Pan-arctic linkages between snow accumulation and growing season air temperature, soil moisture and vegetation, *Biogeosciences Discussions*, *10*, 1747–1791. 93

Luus, K., J. Lin, R. Kelly, and C. Duguay (In press), Subnivean Arctic & sub-Arctic net ecosystem exchange (NEE): Towards representing snow season processes in models of NEE using cryospheric remote sensing, *Progress in Physical Geography*. 46

Luus, K., R. Kelly, J. Lin, E. Humphreys, P. Lafleur, and W. Oechel (Submitted), Modeling the influence of snow cover on low Arctic net ecosystem exchange, *Environmental Research Letters Special Issue on Cryospheric Ecosystems*. 92, 93

Mahadevan, P., S. Wofsy, D. Matross, et al. (2008), A satellite-based biosphere parametrization for net ecosystem CO_2 exchange: Vegetation photosynthesis and respiration model (VPRM), *Global Biogeochemical Cycles*, *22*, GB2005. 14, 46, 49, 92, 94

Marushchak, M., I. Kiepe, C. Biasi, et al. (2012), Carbon dioxide balance of subarctic tundra from plot to regional scales, *Biogeosciences Discussions*, *9*, 9945–9991. 13

Masarie, K., et al. (2011), Impact of CO_2 measurement bias on CarbonTracker surface flux estimates, *Journal of Geophysical Research*, *116*, D17,305. 96

McGuire, A., J. Melillo, J. Randerson, et al. (2000), Modeling the effects of snowpack on heterotrophic respiration across northern temperate and high latitude regions: Comparison with measurements of atmospheric carbon dioxide in high latitudes, *Biogeochemistry*, *48*, 91–114. 15, 45

McGuire, A., S. Sitch, J. Clein, et al. (2001), Carbon balance of the terrestrial biosphere in the twentieth century: Analyses of CO_2, climate and land use effects with four process-based models, *Global Biogeochemical Cycles*, *15*, 183–206. 39

McGuire, A., C. Wirth, M. Apps, et al. (2002), Environmental variation, vegetation distribution, carbon dynamics and water/energy exchange at high latitudes, *Journal of Vegetation Science*, *13*, 301–314. 21

McGuire, A., R. S. E. MacDonald, et al. (2010), The carbon budget of the northern cryosphere region, *Current Opinion in Environmental Sustainability*, *2*, 231–236. 3, 10, 91

McGuire, A., et al. (2012), An assessment of the carbon balance of arctic tundra: Comparisons among observations, process models, and atmospheric inversions, *Biogeosciences*, *9*, 3185–3204. 13, 16, 29

Metcalfe, R., and J. Buttle (1998), A statistical model of spatially distributed snowmelt rates in a boreal forest basin, *Hydrological Processes*, *12*(1011), 1701–1722. 83, 84

Mikan, C., J. Schimel, and A. Doyle (2002), Temperature controls of microbial respiration in Arctic tundra soils above and below freezing, *Soil Biology and Biochemistry*, *34*, 1785–1795. 12, 13, 22, 25, 29, 45, 46, 54

Miller, C. E., and S. J. Dinardo (2012), CARVE: The Carbon in Arctic Reservoirs Vulnerability Experiment, in *IEEE 2012 Aerospace Conference*, pp. 1–17, IEEE. 98

Morgner, E., B. Elberling, D. Strebel, et al. (2010), The importance of winter in annual ecosystem respiration in the High Arctic: Effects of snow depth in two vegetation types, *Polar Research*, *29*, 58–74. 12, 13, 17, 23, 24, 28, 30, 38, 45, 92

Niang, M., J. Dedie, Y. Durand, et al. (2007), New inversion method for snow density and snow liquid water content retrieval using C-band data from ENVISAT/ASAR alternating polarization in alpine environment, *In, Proceeding of the ENVISAT symposium, 2007*, 23–27. 35

Njoku, E., and S. Chan (2005), Vegetation and surface roughness effects on AMSR-E land observations, *Remote Sensing of Environment*, *100*(2), 190–199. 119, 121, 122

Njoku, E., and J. Kong (1977), Theory for passive microwave remote sensing of near-surface soil moisture, *Journal of Geophysical Research*, *82*(20), 3108–3118. 121

Nobrega, S., and P. Grogan (2007), Deeper snow enhances winter respiration from both plant-associated and bulk soil carbon pools in birch hummock tundra, *Ecosystems*, *10*, 419–431. 13, 19, 23, 24, 38

Nobrega, S., and P. Grogan (2008), Landscape and ecosystem-level controls on net carbon dioxide exchange along a natural moisture gradient in Canadian low Arctic tundra, *Ecosystems*, *11*, 377–396. 13

Nowinski, N., L. Taneva, S. Trumbore, and J. Welker (2010), Decomposition of old organic matter as a result of deeper active layers in a snow depth manipulation experiment, *Oecologia*, *163*(3), 785–792. 13, 39, 82

Oberbauer, S., and P. Miller (1979), Plant water relations in montane and tussock tundra vegetation types in Alaska, *Arctic and alpine research*, pp. 69–81. 93

Oberbauer, S., G. Starr, and E. Pop (1998), Effects of extended growing season and soil warming on carbon dioxide and methane exchange of tussock tundra in Alaska, *Journal of Geophysical Research D, Atmospheres*, *103*, 29,075–29,082. 13, 39

Oechel, W. C., H. Kwon, R. Zulueta, J. Verfaillie, G. Kinoshita, J. Kimball, F. Heinsch, and S. Running (2005), Spatial and temporal variability of carbon flux on the north slope of Alaska: A study of the Barrow-Atqasuk-Ivotuk region, in *8th Conference on Polar Meteorology and Oceanography*. 98

Oelbermann, M., M. English, and S. Schiff (2008), Evaluating carbon dynamics and microbial activity in Arctic soils under warmer temperatures, *Canadian Journal of Soil Science*, *88*, 31–44. 13, 22, 45, 54

Olsson, P., M. Sturm, C. Racine, et al. (2003), Five stages of the Alaskan Arctic cold season with ecosystem implications, *Arctic, Antarctic and Alpine Research*, *35*, 74–81. 13, 22, 25, 29, 45

Öquist, G., and N. Huner (2003), Photosynthesis of overwintering evergreen plants, *Annual Reviews of Plant Biology*, *54*, 329–355. 23, 24, 45

Overland, J., J. Adams, and N. Bond (1997), Regional variation of winter temperatures in the Arctic, *Journal of Climate*, *10*, 821–837. 77

Panikov, N. (2009), *Microbial activity in frozen soils*, 119–147 pp., In, Margesin R (ed) Permafrost soils. 16, 19

Panikov, N., P. Flanagan, W. Oechel, et al. (2006), Microbial activity in soils frozen to below -39°C, *Soil Biology and Biochemistry*, *38*, 785–794. 13, 18, 19, 20, 27

Papa, F., B. Legresy, N. Mognard, et al. (2002), Estimating terrestrial snow depth with the TOPEX/Poseidon altimeter and radiometer, *IEEE Transactions on Geoscience and Remote Sensing*, *40*, 2162–2169. 32

Paudel, K., and P. Andersen (2011), Monitoring snow cover variability in an agropastoral area in the Trans-Himalayan region of Nepal using MODIS data with improved cloud removal methodology, *Remote Sensing of Environment*, *115*, 1234–1246. 31

Peters, W., et al. (2007), An atmospheric perspective on North American carbon dioxide exchange: Carbontracker, *Proceedings of the National Academy of Sciences*, *104*(48), 18,925–18,930. 96

Pomeroy, J., and K. Dion (1996), Winter radiation extinction and reflection in a boreal pine canopy: measurements and modelling, *Hydrological Processes*, *10*(12), 1591–1608. 78

Pomeroy, J., R. Granger, A. Pietroniro, J. Elliott, B. Toth, and N. Hedstrom (1997), Hydrological pathways in the Prince Albert model forest, *Tech. rep.*, National Hydrology Research Institute Environment Canada, Saskatoon, Saskatchewan. 81, 83

Pomeroy, J., D. Gray, K. Shook, B. Toth, R. Essery, A. Pietroniro, and N. Hedstrom (1999), An evaluation of snow accumulation and ablation processes for land surface modelling, *Hydrological Processes*, *12*(15), 2339–2367. 84

Pomeroy, J., D. Gray, N. Hedstrom, and J. Janowicz (2002), Prediction of seasonal snow accumulation in cold climate forests, *Hydrological Processes*, *16*(18), 3543–3558. 63, 84, 85

Prihodko, L., A. Denning, N. Hanan, et al. (2008), Sensitivity, uncertainty and time dependence of parameters in a complex land surface model, *Agricultural and Forest Meteorology*, *148*, 268–287. 20

Prokop, A. (2008), Assessing the applicability of terrestrial laser scanning for spatial snow depth measurements, *Cold Regions Science and Technology*, *54*, 155–163. 32

Pulliainen, J. (2006), Mapping of snow water equivalent and snow depth in boreal and subarctic zones by assimilating space-borne microwave radiometer data and ground-based observations, *Remote sensing of Environment*, *101*(2), 257–269. 120

Pulliainen, J., and M. Hallikainen (2001), Retrieval of regional snow water equivalent from space- borne passive microwave observations, *Remote sensing of Environment*, *75*, 76–85. 33

Pulliainen, J., J. Grandell, and M. Hallikainen (1999), HUT snow emission model and its applicability to snow water equivalent retrieval, *IEEE Transactions on Geoscience and Remote Sensing*, *37*(3), 1378–1390. 120

Pumpanen, J., H. Ilvesniemi, and P. Hari (2003), A process-based model for predicting soil carbon dioxide efflux and concentration, *Soil Sciences Society of America Journal*, *67*, 402–413. 15, 19

Ramsay, B. (1998), The interactive multisensor snow and ice mapping system, *Hydrological Processes*, *12*(10), 1537–1546. 31

Randerson, J., F. Hoffman, P. Thornton, et al. (2009), Systematic assessment of terrestrial biogeochemistry in coupled climate-carbon models, *Global Change Biology*, *15*, 2462–2484. 14, 20

Ranson, K., G. Sun, K. Kovacs, et al. (2004), Landcover attributes from ICESat GLAS data in Central Siberia, *In, IEEE Geoscience and Remote Sensing Symposium, Anchorage, USA*, *2*, 753–756. 32

Rees, A., C. Derksen, M. English, A. Walker, and C. Duguay (2006), Uncertainty in snow mass retrievals from satellite passive microwave data in lake-rich high-latitude environments, *Hydrological Processes*, *20*(4), 1019–1022. 84

Rees, A., J. Lemmetyinen, C. Derksen, J. Pulliainen, and M. English (2010), Observed and modelled effects of ice lens formation on passive microwave brightness temperatures over snow covered tundra, *Remote Sensing of Environment*, *114*(1), 116–126. 33

Riggs, G., and D. Hall (2004), *Snow mapping with the MODIS Aqua instrument*, 81–84 pp., In, Proceedings of the 61st Eastern Snow Conference, Portland, USA. 30

Riggs, G., and D. Hall (2011), MODIS snow and ice products, and their assessment and applications, *In, Ramachandran B, Justice CO and Abrams MJ (eds) Land Remote Sensing and Global Environmental Change, Remote Sensing and Digital Image Processing*, *11*, 681–707. 31, 46, 51

Rigor, I., R. Colony, and S. Martin (2000), Variations in surface air temperature in the arctic, *Journal of Climate*, *13*, 896–914. 77

Ritchie, J., and F. Hare (1971), Late-quaternary vegetation and climate near the arctic treeline of northwestern North America, *Quaternary Research*, *1*(3), 331–342. 71

Rosenthal, W., and J. Dozier (1996), Automated mapping of montane snow cover at subpixel resolution from the landsat thematic mapper, *Water Resources Research*, *32*(1), 115–130. 46

Rott, H., S. Yueh, D. Cline, et al. (2010), Cold regions hydrology high-resolution observatory for snow and cold land processes, *Proceedings of the IEEE*, *98*, 752–765. 34, 35

Rouse, W. (1984), Soil microclimate of tundra and forest, *Water Resources Research*, *20*(1), 67–73. 78

Royer, A., K. Goïta, J. Kohn, et al. (2010), Monitoring dry, wet, and no-snow conditions from microwave satellite observations, *IEEE Geoscience and Remote Sensing Letters*, *7*, 670–674. 35

Running, S., R. Nemani, F. Heinsch, et al. (2004), A continuous satellite-derived measure of global terrestrial primary production, *Bioscience*, *54*, 547–560. 20

Rutter, N., R. Essery, J. Pomeroy, et al. (2009), Evaluation of forest snow processes models (SnowMIP2), *Journal of Geophysical Research: Atmospheres*, *114*, D06,111. 37

Saito, K., S. Yamaguchi, H. Iwata, Y. Harazono, K. Kosugi, M. Lehning, and M. Shulski (2012), Climatic physical snowpack properties for large-scale modeling examined by observations and a physical model, *Polar Science*, *6*(1), 7995. 29

Schaefer, K., T. Zhang, L. Bruhwiler, et al. (2011), Amount and timing of permafrost carbon release in response to climate warming, *Tellus B*, *63*, 165–180. 3, 10, 91

Schlesinger, W., and J. Lichter (2001), Limited carbon storage in soil and litter of experimental forest plots under increased atmospheric CO_2, *Nature*, *411*, 466–469. 38

Schuur, E., J. Vogel, K. Crummer, et al. (2009), The effect of permafrost thaw on old carbon release and net carbon exchange from tundra, *Nature*, *459*, 556–559. 13, 18, 39, 103

Sellers, P., Y. Mintz, Y. Sud, et al. (1986), A simple biosphere model (SiB) for use within general circulation models, *Journal of the Atmospheric Sciences*, *43*, 505–531. 14

Serreze, M., and R. Barry (2005), *The Arctic climate system*, Cambridge University Press. 63, 71, 77, 79, 85

Shaver, G., F. Chapin III, and B. Gartner (1986), Factors limiting seasonal growth and peak biomass accumulation in Eriophorum vaginatum in Alaskan tussock tundra, *The Journal of Ecology*, pp. 257–278. 93

Shi, J. (2008), *Active Microwave Remote Sensing Systems and Applications to Snow Monitoring*, 19–49 pp., In, Liang S (ed) Advances in Land Remote Sensing, System, Modelling, Inversion and Application, Springer. 34, 35

Shinoda, M. (2001), Climate memory of snow mass as soil moisture over central Eurasia, *Journal of Geophysical Research*, *106*(D24), 33,393. 63, 79, 80

Sitch, S., B. Smith, I. Prentice, et al. (2003), Evaluation of ecosystem dynamics, plant geography and terrestrial carbon cycling in the LPJ dynamic global vegetation model, *Global Change Biology*, *9*, 161–185. 15

Sitch, S., A. McGuire, J. Kimball, et al. (2007), Assessing the carbon balance of circumpolar Arctic tundra using remote sensing and process modeling, *Ecological Applications*, *17*, 213–234. 14, 16, 63

Slaymaker, O., and R. Kelly (2007), *The Cryosphere and Global Environmental Change*, Blackwell Publishing. 27, 33

Smith, C., C. Burn, C. Tarnocai, and B. Sproule (1998), Air and soil temperature relations along an ecological transect through the permafrost zones of northwestern Canada, pp. 23–26. 78

Smith, N., S. Saatchi, and J. Randerson (2004), Trends in high northern latitude soil freeze and thaw cycles from 1988 to 2002, *Journal of Geophysical Research*, *109*, D12,101. 33

Solano, R., K. Didan, A. Jacobson, and A. Huete (2010), MODIS Vegetation Indices (MOD13) C5 users guide, *Terrestrial Biophysics and Remote Sensing Lab-The University of Arizona*. 93

Solberg, R., et al. (2009), Global Snow Monitoring for Climate Research-Design Justification File. 120

Solomon, S., D. Qin, M. Manning, Z. Chen, M. Marquis, K. Averyt, M. Tignor, and H. Miller (Eds.) (2007), *Contribution of Working Group I to the Fourth Assessment Report of the Intergovernmental Panel on Climate Change*, Cambridge University Press. 3

Staple, W., J. Lehane, and A. Wenhardt (1960), Conservation of soil moisture from fall and winter precipitation, *Canadian Journal of Soil Science*, *40*(1), 80–88. 80

Starr, G., and S. Oberbauer (2003), Photosynthesis of Arctic evergreens under snow: Implications for tundra ecosystem carbon balance, *Ecology*, *84*, 1415–1420. 21, 24

Stiles, W., and F. Ulaby (1980), The active and passive microwave response to snow parameters 1, *Wetness Journal of Geophysical Research*, *85*, 1037–1044. 34

Stow, D., et al. (2004), Remote sensing of vegetation and land-cover change in Arctic Tundra Ecosystems, *Remote Sensing of Environment*, *89*(3), 281–308. 103

Sturm, M. (1992), Snow distribution and heat flow in the Taiga, *Arctic and Alpine Research*, *24*, 145–152. 22, 23, 25

Sturm, M., J. Holmgren, and G. Liston (1995), A seasonal snow cover classification system for local to global applications, *Journal of Climate*, *8*(2), 1261–1283. 26, 63

Sturm, M., J. Holmgren, M. König, et al. (1997), The thermal conductivity of seasonal snow, *Journal of Glaciology*, *43*, 26–41. 15, 22, 27

Sturm, M., J. Holmgren, J. McFadden, et al. (2001a), Snow-shrub interactions in Arctic tundra, A hypothesis with climatic implications, *Journal of Climate*, *14*, 336–344. 38, 63, 81, 82

Sturm, M., R. Pielke Sr, and F. Chapin III (2001b), Interactions of shrubs and snow in arctic tundra: Measurements and models, in *Soil-vegetation-atmosphere Transfer Schemes and Large-scale Hydrological Models: Proceedings of an International Symposium (Symposium S5) Held During the Sixth Scientific Assembly of the International Association of*

Hydrological Sciences (IAHS) at Maastricht, The Netherlands, from 18 to 27 July 2001, vol. 270, p. 317, International Assn of Hydrological Sciences. 81

Sturm, M., D. Perovich, and J. Holmgren (2002), Thermal conductivity and heat transfer through the snow on the ice of the Beaufort Sea, *Journal of Geophysical Research*, *107*(C10), 8043. 27

Sullivan, P. (2010), Snow distribution, soil temperature and late winter CO_2 efflux from soils near the Arctic treeline in northwest Alaska, *Biogeochemistry*, *99*, 65–77. 13, 19, 22, 23, 24, 27, 33

Sullivan, P., J. Welker, S. Arens, et al. (2008), Continuous estimates of CO_2 efflux from Arctic and boreal soils during the snow-covered season in Alaska, *Journal of Geophysical Research: Biogeosciences*, *113*, G04,009. 12, 13, 21, 23, 37, 38, 46, 92

Sun, C., J. Walker, and P. Houser (2004), A methodology for snow data assimilation in a land surface model, *Journal of Geophysical Research*, *109*, D08,108. 34

Suzuki, K., J. Kubota, T. Ohata, and V. Vuglinsky (2006), Influence of snow ablation and frozen ground on spring runoff generation in the Mogot Experimental Watershed, southern mountainous taiga of eastern Siberia, *Nordic hydrology*, *37*(1), 21–29. 81

Svensson, B., and T. Callaghan (1988), Small-scale vegetation pattern related to the growth of Lycopodium annotinum and variations in its micro-environment, *Plant Ecology*, *76*, 167–177. 21

Takala, M., K. Luojus, J. Pulliainen, C. Derksen, J. Lemmetyinen, J. Kärnä, J. Koskinen, and B. Bojkov (2011), Estimating northern hemisphere snow water equivalent for climate research through assimilation of space-borne radiometer data and ground-based measurements, *Remote Sensing of Environment*, *115*(12), 3517–3529. 34, 119, 120

Tape, K., M. Sturm, and C. Racine (2006), The evidence for shrub expansion in northern alaska and the pan-arctic, *Global Change Biology*, *12*(4), 686–702. 3, 103

Tarnocai, C. (2006), The effect of climate change on carbon in Canadian peatlands, *Global and Planetary Change*, *53*, 222–232. 3, 10, 103

Thompson, C., A. McGuire, J. Clein, F. Chapin, and J. Beringer (2006), Net carbon exchange across the arctic tundra-boreal forest transition in Alaska 1981–2000, *Mitigation and Adaptation Strategies for Global Change*, *11*(4), 805–827. 47

Tieszen, L. (1974), Photosynthetic competence of the subnivean vegetation of an arctic tundra, *Arctic and Alpine Research*, *6*(3), 253–256. 13, 24

Tranquillini, W. (1964), The physiology of plants at high altitudes, *Annual Review of Plant Physiology*, *15*(1), 345–362. 82

Ulaby, F., and W. Stiles (1980), The active and passive microwave response to snow parameters 2: Water equivalent of dry snow, *Journal of Geophysical Research*, *85*, 1045–1049. 33

Verbyla, D. (2008), The greening and browning of Alaska based on 1982–2003 satellite data, *Global Ecology and Biogeography*, *17*(4), 547–555. 103

Vikhamar, D., and R. Solberg (2003), Subpixel mapping of snow cover in forests by optical remote sensing, *Remote Sensing of Environment*, *84*, 69–82. 31

Vourlitis, G., W. Oechel, A. Hope, et al. (2000), Physiological models for scaling plot measurements of CO_2 flux across an Arctic tundra landscape, *Ecological Applications*, *10*, 60–72. 13

Wagner, D. (2008), *Microbial communities and processes in Arctic permafrost environments*, 133–154 pp., In, Dion P and Nautiyal CS (eds) Microbiology of Extreme Soils, Soil Biology 13. 19

Wahren, C., M. Walker, and M. Bret-Harte (2005), Vegetation responses in Alaskan arctic tundra after 8 years of a summer warming and winter snow manipulation experiment, *Global Change Biology*, *11*(4), 537–552. 63

Walker, D., W. Billings, and J. De Molenaar (2001), Snow–vegetation interactions in tundra environments, *Snow ecology: an interdisciplinary examination of snow-covered ecosystems*, pp. 266–324. 82, 85

Walker, D., M. Raynolds, F. Daniëls, et al. (2005), The Circumpolar Arctic Vegetation Map, *Journal of Vegetation Science*, *16*, 267–282. x, xiv, 13, 40, 69, 93

Walker, M., D. Walker, J. Welker, et al. (1999), Long-term experimental manipulation of winter snow regime and summer temperature in Arctic and alpine tundra, *Hydrological Processes*, *13*, 2315–2330. 12, 13, 23, 85, 92

Walsh, J. E., W. L. Chapman, and D. H. Portis (2009), Arctic cloud fraction and radiative fluxes in atmospheric reanalyses, *Journal of climate*, *22*(9), 2316–2334. 94

Wang, D., and M. Murphy (2004), Estimating optimal transformations for multiple regression using the ACE algorithm, *Journal of data science*, *2*(4), 329–346. 64, 65

Wang, L., M. Sharp, R. Brown, et al. (2005), Evaluation of spring snow covered area depletion in the Canadian Arctic from NOAA snow charts, *Remote Sensing of Environment*, *95*, 453–463. 31

Wang, X., C. Wang, and G. Yu (2008), Spatio-temporal patterns of forest carbon dioxide exchange based on global eddy covariance measurements, *Science in China, Series D, Earth Sciences*, *51*(8), 1129–1143. 35

Wang, Z., R. Grant, M. Arain, et al. (2011), Evaluating weather effects on interannual variation in net ecosystem productivity of a coastal temperate forest landscape: A model intercomparison, *Ecological Modelling*, *222*, 3236–3249. 20

Wania, R., I. Ross, and I. Prentice (2009), Integrating peatlands and permafrost into a dynamic global vegetation model, *1 Evaluation and sensitivity of physical land surface processes Global Biogeochemical Cycles*, *23*. 15, 45

Wardle, P. (1968), Engelmann spruce (Picea engelmannii Engel.) at its upper limits on the front range, colorado, *Ecology*, *49*(3), 483–495. 82

Williams, M., and E. Ratsetter (1999), Vegetation characteristics and primary productivity along an arctic transect: implications for scaling-up, *Journal of Ecology*, *87*(885), 885–898. 79

Willis, W., C. Carlson, J. Alessi, and H. Haas (1961), Depth of freezing and spring run-off as related to fall soil-moisture level, *Canadian Journal of Soil Science*, *41*(1), 115–123. 80, 81, 85

Willmott, C., and K. Matsuura (2005), Advantages of the mean absolute error (MAE) over the root mean square error (RMSE) in assessing average model performance, *Climate Research*, *30*(1), 79. 51, 96

Wu, W., S. Wang, X. Xiao, et al. (2008), Modeling gross primary production of a temperate grassland ecosystem in Inner Mongolia, China, using MODIS imagery and climate data Science in China, *Series D, Earth Sciences*, *51*, 1501–1512. 20

Xiao, X., D. Hollinger, J. Aber, et al. (2004a), Satellite-based modeling of gross primary production in an evergreen needleleaf forest, *Remote Sensing of Environment*, *89*, 519–534. 20

Xiao, X., Q. Zhang, S. Boles, et al. (2004b), Mapping snow cover in the pan-Arctic zone, using multi-year (1998-2001) images from optical VEGETATION sensor, *International Journal of Remote Sensing*, *25*, 5731–5744. 31

Yang, Z.-L., R. Dickinson, A. Robock, et al. (1997), Validation of the snow submodel of the biosphere-atmosphere transfer scheme with Russian snow cover and meteorological observational data, *Journal of Climate*, *10*, 353–373. 39

Zeng, H., G. Jia, and H. Epstein (2011), Recent changes in phenology over the northern high latitudes detected from multi-satellite data, *Environmental Research Letters*, *6*(4), 045,508. 103

Zhang, T., and R. Armstrong (2001), Soil freeze/thaw cycles over snow-free land detected by passive microwave remote sensing, *Geophysical research letters*, *28*, 763–766. 33

Zhang, T., T. Osterkamp, and K. Stamnes (1996), Influence of the depth hoar layer of the seasonal snow cover on the ground thermal regime, *Water Resources Research*, *32*(7), 2075–2086. 23, 25, 26, 45

Zhang, Y., W. Chen, and D. Riseborough (2008), Transient projections of permafrost distribution in Canada during the 21st century under scenarios of climate change, *Global and Planetary Change*, *60*, 443–456. 39

Zhao, L., and D. Gray (1999), Estimating snowmelt infiltration into frozen soils, *Hydrological processes*, *13*(12-13), 1827–1842. 81

Zimov, S., I. Semiletov, S. Daviodov, et al. (1993), Wintertime CO_2 emission from soils of Northeastern Siberia, *Arctic*, *46*, 197–204. 13, 19, 22, 29, 45

Zimov, S., S. Davidov, Y. Voropaev, et al. (1996), Siberian CO_2 efflux in winter as a CO_2 source and cause of seasonality in atmospheric CO_2, *Climatic Change*, *35*, 111–120. 12, 13, 19, 25, 28, 34, 37, 45

Zona, D., W. Oechel, K. Peterson, R. Clements, K. PAW U, and S. Ustin (2010), Characterization of the carbon fluxes of a vegetated drained lake basin chronosequence on the Alaskan Arctic Coastal Plain, *Global Change Biology*, *16*(6), 1870–1882. 95

Zona, D., W. C. Oechel, J. H. Richards, S. Hastings, I. Kopetz, H. Ikawa, and S. Oberbauer (2011), Light-stress avoidance mechanisms in a Sphagnum-dominated wet coastal Arctic tundra ecosystem in Alaska, *Ecology*, *92*(3), 633–644. 95

Zwally, H., B. Shutz, W. Abdalati, et al. (2002), ICESat's laser measurements of polar ice, atmosphere, ocean, and land, *Journal of Geodynamics*, *34*, 405–445. 32